A NEW BEHAVIOR OF CHAOTIC ATTRACTORS

Nahed AOUF, Nader.BELGITH, Kais.BOUALLEGUE, Mohsen MACHOUT
1Department Electronic and Micro-Electronic Laboratory, Faculty of Sciences of Monastir, University of Monastir 5000, Tunisia.
(E-mail: nahedaouf@gmail.com)
2Department of Electrical Engineering, Higher Institute of Applied Sciences and Technology of Sousse, University of Sousse, Tunisia.
Cité Taffala (ISSAT), 4003 Sousse Tunisie,

Abstract

This paper presents a new behavior of chaotic attractor. Therefore,creating a chaotic attractor with bounded behavior is a theoretically very attractive and yet technically a quite challenging task.It is obviously significant to create more complicated multi chaotic attractor with bounded behavior, in both theory and engineering application. Simulation demonstrates the validity and feasibility of the proposed method.

Keywords: Chua attractor, Rössler attractor, bounded function with bounded support,bounded function with compact support.

1 Introduction

The behavior of chaotic attractor is very interesting nonlinear effect which has been competently studied during the last four decades [1]. It reaches many natural and artificial dynamic systems such as human heart, mechanical system, electronic circuits, etc [2]. There are so many classical attractors are known until now such us Lorenz , Rossler , Chua , Chen, and others... Our approach in this paper is to generate a new behavior of chaotic attractor using Chua attractor and Julia Process.

2 Julia's Process

In recent years, there have been a lot of developments in Julia sets, including qualitative characters, applications and controls. In this section, the use of algorithms inspired from Julia processes, will be presented. To generate Julia processes, some of the properties are well known:

- The Julia set is a repeller.

- The Julia set is invariant.
- An orbit on Julia set is either periodic or chaotic.
- All unstable periodic points are on Julia set.
- The Julia set is either wholly connected or wholly disconnected.
- All sets generated only with Julia sets combination has fractal structure[5].

Real and imaginary parts of the complex numbers are separately calculated.

$$\begin{cases} x_{i+1} = x_i^2 - y_i^2 + x_c \\ y_{i+1} = x_i y_i + y_c \end{cases} \tag{1}$$

The listing of algorithm P is as follows:

Algorithm 1 $(y_{i+1}, x_{i+1}) = P(\arctan(x_i), y_i)$

if $x_i < 0$ **then**
  $x_{i+1} = \sqrt{(\sqrt{((\arctan(x_i))^2 + (y_i)^2)} + \frac{\arctan(x_i)}{2})}$
  $y_{i+1} = \frac{y_i}{2x_{i+1}}$
end if
if $x_i = 0$ **then**
  $x_{i+1} = \sqrt{\frac{|y_i|}{2}}$
  if $x_i > 0$ **then**
    $x_{i+1} = \frac{y_i}{2y_{i+1}}$
  end if
  if $x_i < 0$ **then**
    $y_{i+1} = 0$
  end if
end if
if $x_i > 0$ **then**
  $y_{i+1} = \sqrt{(\sqrt{((\arctan(x_i))^2 + (y_i)^2)} - \frac{\arctan(x_i)}{2})}$
  $x_{i+1} = \frac{y_i}{2x_{i+1}}$
  if $y_i < 0$ **then**
    $y_{i+1} = -y_{i+1}$
  end if
end if

3 Rössler attractor

Rössler system was introduced in the 1970s as prototype equation with the minimum ingredients for continuous time chaos. This system is minimal for continuous chaos for at least three reasons: Its phase space has the minimal dimension three, its nonlinearity is minimal because there is a single quadratic term, and it generates a chaotic attractor with a single scroll, in contrast to the Lorenz attractor with has two scrolls.

$$M\begin{cases} \dot{z}_1 = -(z_2 + z_3) \\ \dot{z}_2 = z_1 + \alpha z_2 \\ \dot{z}_3 = (z_1 z_3 - \beta z_3 + \gamma z_1) \end{cases} \tag{2}$$

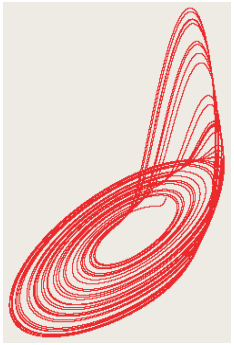

(a)

Figure 1: Rossler chaotic attractor

We apply the methodology cited in paper [4]. The number of scrolls are increased. Figure 7 shows behavior result of implementation.

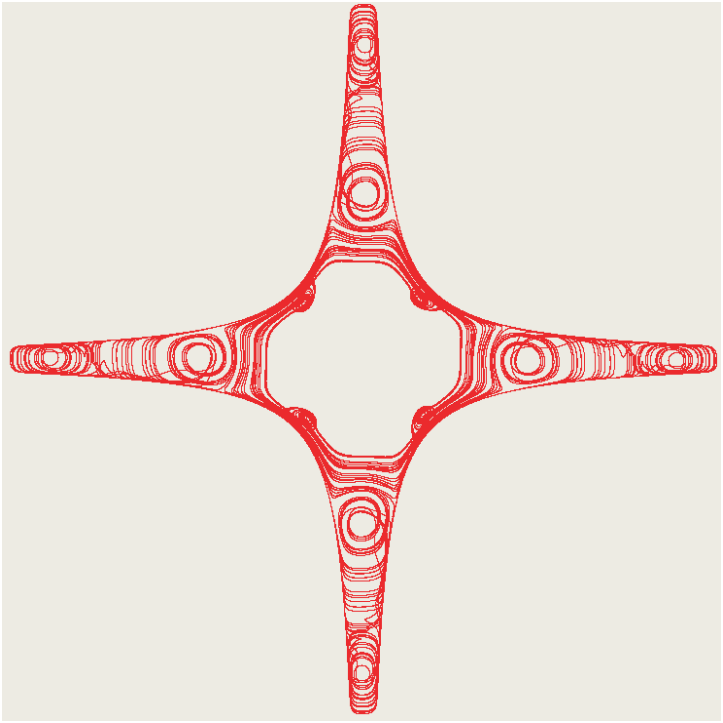

Figure 2: Behavior of bounded chaotic attractor

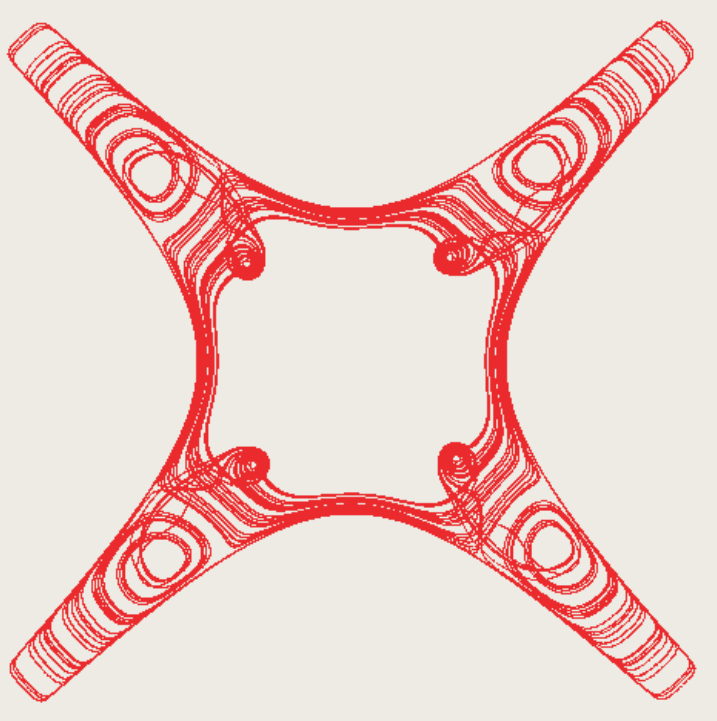

Figure 3: An other behavior of bounded chaotic attractor

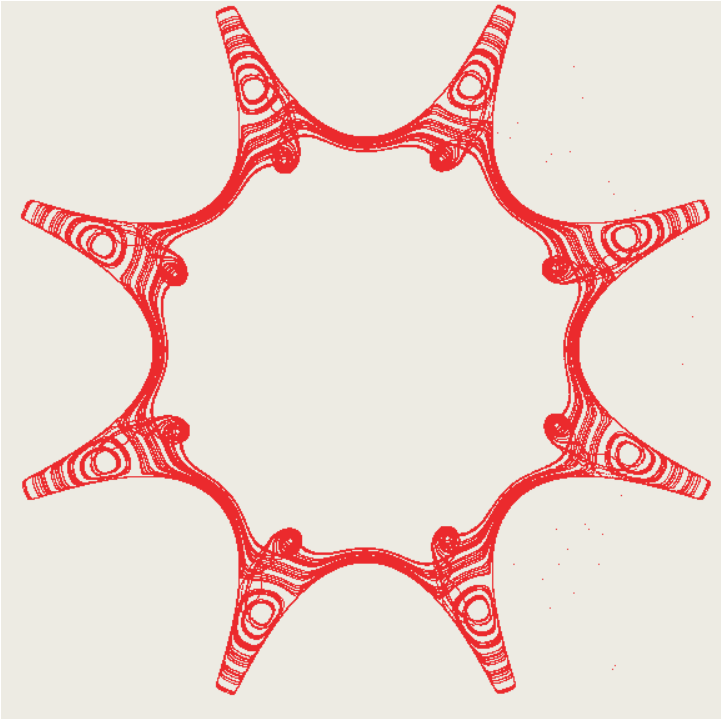

Figure 4: Chaotic attractor with scrolls bounded

4 Chua attractor

Chua's circuits, which were introduced by Leon Ong Chua in 1983, are simplest electric circuits operating in the mode of chaotic oscillations. different dynamic system had inspired from Chua circuit such as:

$$\begin{cases} \dot{x}_1 = x_2 \\ \dot{x}_2 = x_3 \\ \dot{x}_3 = a(-x_1 - x_2 - x_3 + f(x_1)) \end{cases} \tag{3}$$

where $\dot{x}$,$\dot{y}$ and $\dot{z}$ are the first time derivatives and a is a real parameter. Where $f(x_1)$ is a statured function as follows :

$$f(x) = \begin{cases} k, if x > 1 \\ kx, if |x| < 1 \\ -k, if x < -1 \end{cases} \tag{4}$$

5 Chaotic attractor generated by FPS

Let $\mathcal{E}$ be the complete metric unit, Φ a fractal processes system of $\mathcal{E}$ in $\mathcal{E}$ such as:

$$\mathcal{E} \to \mathcal{E}$$
$$\Phi{:}(f_1, f_2) \to (X_G, Y_G)$$

The fractal processes system Φ is represented by:

$$\Phi \left\{ \ (u_1, v_1) = P_J(\dot{x}_1 + \beta, \dot{x}_2 + \beta) \right. \tag{5}$$

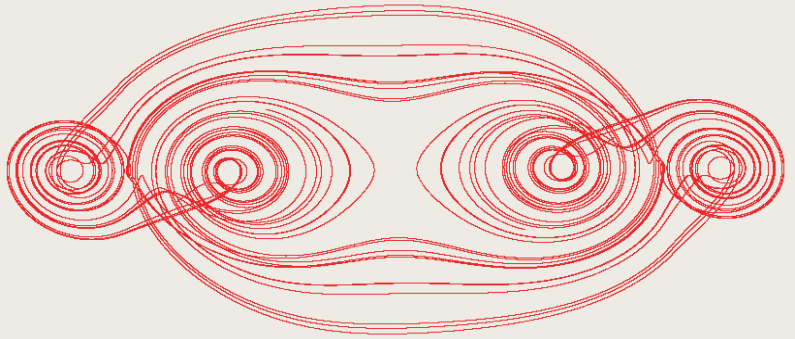

Figure 5: Chaotic attractor with four scrolls

5.1 Chaotic attractor with bounded function with bounded support

5.1.1 Example 1

We treat state of axis x by mathematical function, after implementation we obtain this results see 6.

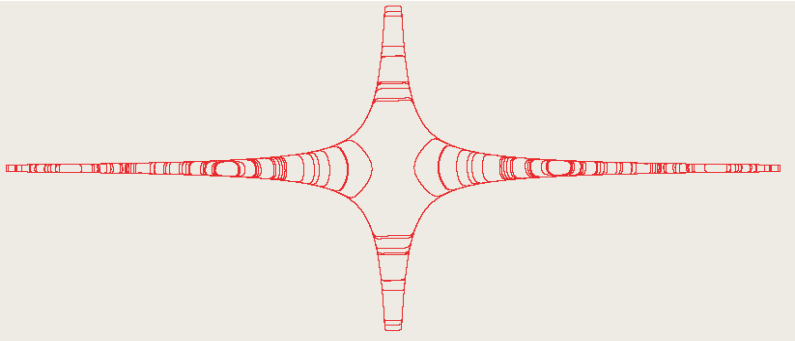

Figure 6: Behavior of bounded chaotic attractor

via changing the value of β the behavior of bounded chaotic attractor changed.

5.2 Chaotic attractor with bounded function with compact support

5.2.1 Example 2

We generate an other chaotic attractor by fractal processes system by the following equation:

$$\Phi \left\{ \ (u_1, v_1) = P_J(\dot{x}_1 + \beta, \dot{x}_2 + \beta) \right. \tag{6}$$

Simulation result illustrates in figure 7.

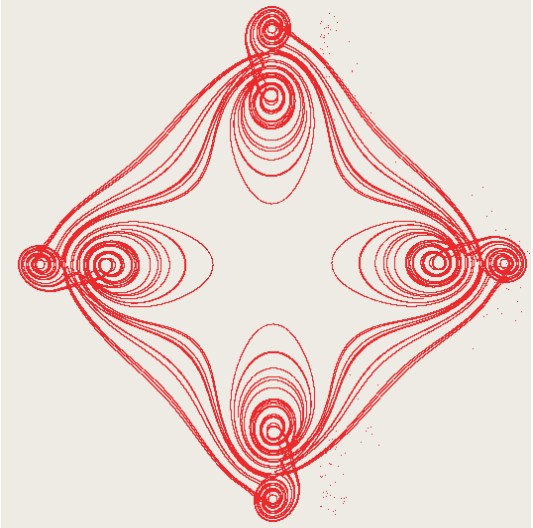

Figure 7: Chaotic attractor with eight scrolls

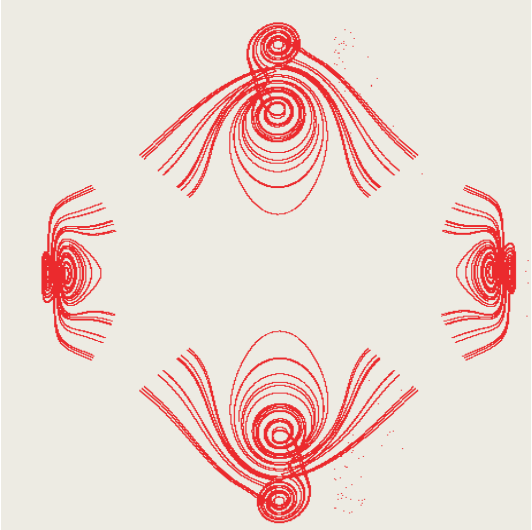

Figure 8: Bounded function with chaotic attractor

6 Conclusion

In this paper, we have proposed a new approach to generate behavior of bounded chaotic attractor. Numerical simulations, demonstrate the validity and feasibility of proposed method. The procedure mentioned in this paper has practical application in many disciplines.

References

[1] E.Ott Chaos in dynamical system Combridge University Press, Combridge 1993.

[2] Cafagna G. Grassi Int J Biffurcation Chaos 13 (2003) 2889.

[3] EE. Mohmoud Dynamics and synchronization of a new hyperchaotic complex Lorenz system, Math Computation Model 55(2012) 1951-1962.

[4] K.Bouallegue, A. Chaari, A. Toumi, Multi-scroll and multi-wing chaotic attractor generated with Julia process fractal,Chaos, Solitons & Fractals $2011; 44 : 79 - 85$

[5] Stephen.Lynuch, Dynamical Systems with Applications using Mathematica, Birkh¨auser Boston, 2007,ISBN-13:978 ? 0 ? 8176 ? 4482 ? 6.

HYPERCHAOS SET BY FRACTAL PROCESSES SYSTEM

Salah NASR[1,+],Nahed AOUF[2], Kais BOUALLEGUE[3],Hassen MEKKI[4],Mohsen Machhout [2].
[1]

1[+]CEM Lab, National Engineering School of Sfax, BP-1173, 3038 Sfax, Tunisia
2Department Electronic and Micro-Electronic Laboratory, Faculty of Sciences of Monastir, university of Monastir 5000, Tunisia. 3Department of Electrical Engineering. Higher Institute of Applied Sciences and Technology of Sousse, Tunisia
4 National Engineering School of Sousse, Sousse, Tunisia

Abstract.

This paper presents a new class of hyper chaotic attractor. This hyperchaos is a set of chaotic attractors with different number of scrolls. It has different behavior forms either separated or not with or without other nested chaotic attractors. This class of systems is constructed by using fractal processes system (FPS). For each parameter value which is treated by process that is presented in the FPS generates a new behavior and increases the number of scrolls. Therefore,creating a multi chaotic attractors with nested ones is a theoretically very attractive and yet technically a quite challenging task.It is obviously significant to create more complicated multi chaotic attractor and multi hyper-chaotic attractor, in both theory and engineering application. Simulation demonstrates the validity and feasibility of the proposed method.

Keywords: Multi-chaotic attractor, hyper chaotic attractor, fractal processes.

1 Introduction

Chaotic system has became a popular research area around the world after the first three-dimensional chaotic system was discovered by Lorenz, and many new chaotic systems have been proposed (i.e., Chen system, Lü system, Liu system)[3]

Recently, exploiting chaotic dynamics in high-tech and industrial engineering applications has attracted much interest, wherein more attention has been focused on creating chaos effectively[4].

Compared with the simple chaotic attractors, multi chaotic attractors can provide more complex dynamic behaviors, more adjustability and more encryption parameters. These properties indicate that multi- chaotic attractors have a general potential applications to communications, cryptography and many other fields.

Many methods have been used to construct a hyperchaotic system and several hyper chaotic have been discovered in high dimensional dynamics such as Hyperchaotic Rössler system [6], hyperchaotic Chua's circuit [7] and hyperchaotic Lorenz system [8]. Our approach is regarded as a new class of hyper chaos.

The rest of the paper is organized as follows: In section 2, We describe generation of multi chaotic attractors separated and non separated with the same behavior. In section 3 introduce an another generation of multi chaotic attractors with different form of behavior.

Finally ,in section 4 we conclude this paper by providing a summary of the above finding.

2 Chaos with the same form of behavior

We recall the structure of fractal processes system described in paper [10]. Here, we present a structure of a system of fractal processes by associating multiple fractal processes in a cascading manner. This structure starts with a set of initial conditions, a number of fractal processes, and a set of transformations.

Let $\mathcal{E}$ be the complete metric unit, Φ a system of fractal processes in $\mathcal{E}$ such as:

$$\begin{gathered}\mathcal{E} \to \mathcal{E} \\ \Phi{:}(x_i, y_i) \to (x_m, y_m)\end{gathered}$$

[1] **Corresponding author**
E-mail address: nasrsalah-tun@hotmail.fr

8th CHAOS Conference Proceedings, 26-29 May 2015
Henri Poincaré Institute, Paris France

The fractal processes system Φ is represented by:

$$\Phi \begin{cases} (x_0, y_0) \\ (x_{i+1}, y_{i+1}) = P_1(\alpha x_i + \gamma, \beta y_i + \lambda) \\ (x_{i+2}, y_{i+2}) = P_2(x_{i+1}, y_{k+1}) \\ (x_{i+3}, y_{i+3}) = T_1(x_{i+2}, y_{i+2}) \\ (x_{i+4}, y_{i+4}) = P_3(x_{i+3}, y_{i+3}) \\ \vdots \\ (x_{j+1}, y_{j+1}) = T_k(x_{j-1}, y_{j-1}) \\ \vdots \\ (x_m, y_m) = P_{m-k}(x_{m-1}, y_{m-1}) \end{cases} \tag{1}$$

The dynamics of the system of fractal processes is controlled by the assignment of x_{i+1} to x_i and of y_{i+1} to y_i.

$$\begin{cases} x_i \leftarrow x_{i+1} \\ y_i \leftarrow y_{i+1} \end{cases} \tag{2}$$

The system (1) is a combination of different transformations and different processes. It consists of m equations and k transformations, so $m - k$ processes for n iterations where the first iteration is (x_0, y_0).

We give different examples using FPS to show and validate our approach.

2.1 Chaos with separated chaotic attractors

In this paper, we use two classical chaotic attractors the first one we take Lorenz attractor in the second we choose Chua attractor. We recall the structure of the two chaotic attractors.

The Lorenz system [2]has become one of paradigms in the research of chaos, and is described by where x_1, x_2 and x_3 are system states and σ, ρ and β

$$M \begin{cases} \dot{z}_1 = \sigma(z_2 - z_1) \\ \dot{z}_2 = \rho z_1 - z_2 - z_1 z_3 \\ \dot{z}_3 = (z_1 z_2 - \beta z_3) \end{cases} \tag{3}$$

And the second is Chua's circuits[**?**], which were introduced by Leon Ong Chua in 1983, are simplest electric circuits operating in the mode of chaotic oscillations. different dynamic system had inspired from Chua circuit such as:

$$\begin{cases} \dot{x}_1 = x_2 \\ \dot{x}_2 = x_3 \\ \dot{x}_3 = a(-x_1 - x_2 - x_3 + f(x_1)) \end{cases} \tag{4}$$

where $\dot{y}_1$,$\dot{y}_2$ and $\dot{y}_3$ are the first time derivatives and a is a real parameter. Where $f(y_1)$ is a statured function as follows :

$$f(x) = \begin{cases} k, if x > 1 \\ kx, if |x| < 1 \\ -k, if x < -1 \end{cases} \tag{5}$$

2.2 Chaos with same behavior of separated chaotic attractors

Consider the following Φ a fractal processes system :

Let $\mathcal{E}$ be the complete metric unit, Φ a fractal processes system of $\mathcal{E}$ in $\mathcal{E}$ such as:

$$\mathcal{E} \rightarrow \mathcal{E}$$
$$\Phi{:}(f_1, f_2) \rightarrow (X_G, Y_G)$$

The fractal processes system Φ is represented by:

$$\Phi \begin{cases} (u_1, v_1) = P_J(\dot{z}_3 + \arctan(\dot{x}_1), \dot{x}_1 + \arctan(\dot{z}_3)) \\ (u_2, v_2) = P_J(\dot{z}_2 + \beta_1, \dot{z}_2) \\ (X_G, Y_G) = P_J(u_1 - \alpha u_2, v_1 - \alpha v_2) \end{cases} \tag{6}$$

Figure 1 shows eight chaotic attractors with the same behavior. Each chaotic attractor contains two scrolls one from Lorenz attractor and the other from Chua attractor.

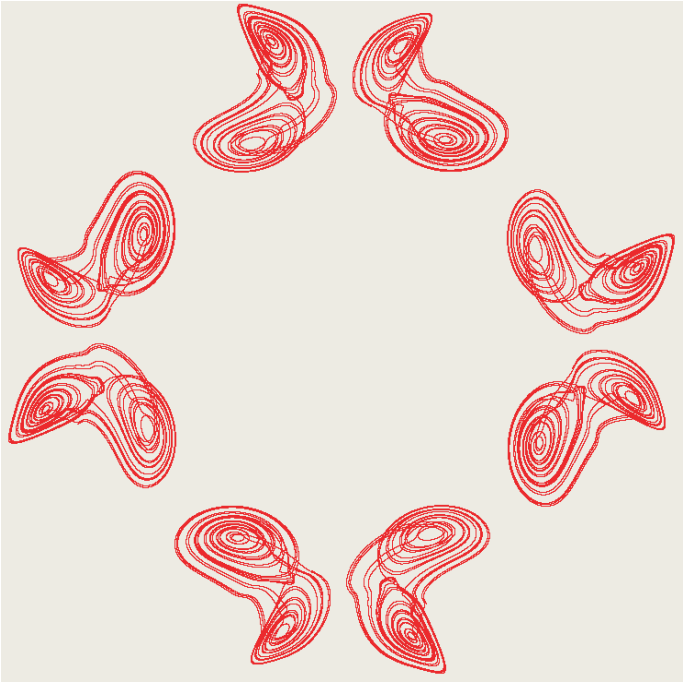

(a)

Figure 1: Chaotic attractors separated with the same form of behavior

2.3 Chaos with same behavior of non separated chaotic attractors

In this subsection, we take Rössler system were introduced in the 1970s as prototype equation with the minimum ingredients for continuous time chaos. This system is minimal for continuous chaos for at least three reasons: Its phase space has the minimal dimension three, its nonlinearity is minimal because there is a single quadratic term, and it generates a chaotic attractor with a single scroll, in contrast to the Lorenz attractor with has two scrolls. Rössler system is described as follows:

$$M \begin{cases} \dot{y}_1 = -(y_2 + y_3) \\ \dot{y}_2 = y_1 + \alpha y_2 \\ \dot{y}_3 = (y_1 y_3 - \beta y_3 + \gamma y_1) \end{cases} \tag{7}$$

Let $\mathcal{E}$ be the complete metric unit, Φ a fractal processes system of $\mathcal{E}$ in $\mathcal{E}$ such as:

$$\mathcal{E} \to \mathcal{E}$$
$$\Phi{:}(f_1, f_2) \to (X_G, Y_G)$$

The fractal processes system Φ is represented by:

$$\Phi \begin{cases} (u_1, v_1) = P_J(\dot{y}_1 + \beta_1, \dot{y}_2 + \beta_2) \\ (p_1, q_1) = P_J(\dot{y}_1 - \beta_1, \dot{y}_2 - \beta_2) \\ (m_1, n_1) = P_J(u_1 - \alpha p_1, v_1 - \alpha q_1) \\ (m_2, n_2) = P_J(m_1, n_1) \\ (m_3, n_3) = T(m_2, n_2) \\ (m_4, n_4) = P_J(m_3 + 4, n_3) \\ (m_5, n_5) = P_J(m_3 - 4, n_3 + 1) \\ (X_G, Y_G) = P_J(m_4 - \arctan(m_5/3) + 2, n_4 + \arctan(1.5 n_5)) \end{cases} \tag{8}$$

Figure 2 shows result of implementation. These behavior of chaotic attractors contain multi level of scales.

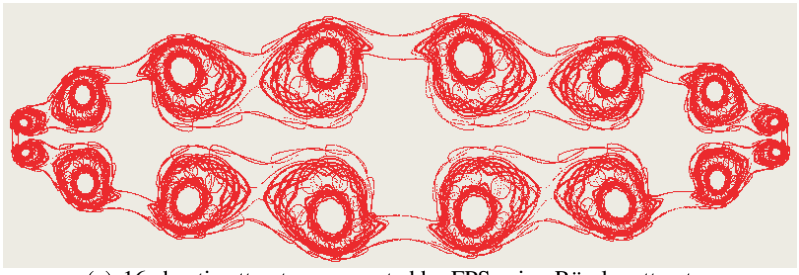

(a) 16 chaotic attractors generated by FPS using Rössler attractors

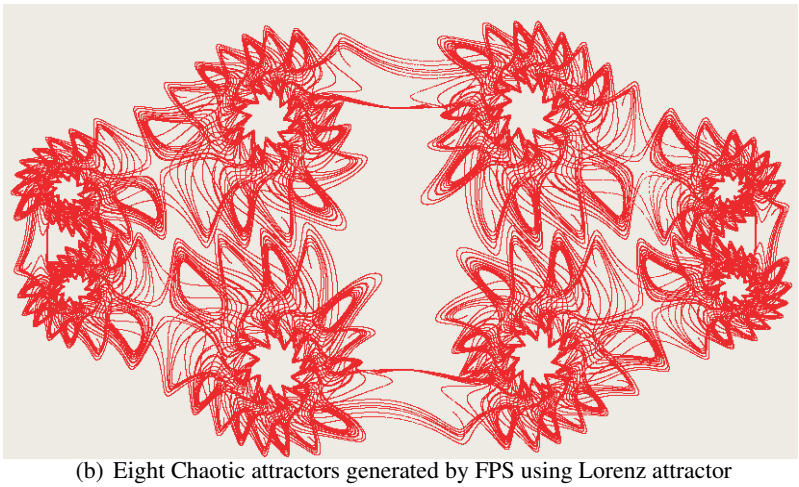

(b) Eight Chaotic attractors generated by FPS using Lorenz attractor

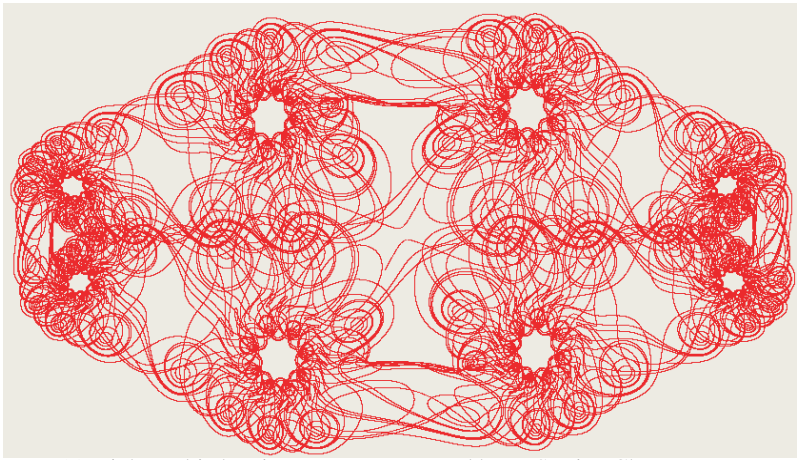

(c) Eight multi chaotic attractors generated by FPS using Chua attractor

Figure 2: HyperChaos Contains Eight linked chaotic attractors with same behavior

3 Chaos with the different form of behavior

3.1 Chaos with two behavior of chaotic attractors

A new chaotic attractors with two forms of behavior is established by the following Fractal Processes System:

Let $\mathcal{E}$ be the complete metric unit, Φ a fractal processes system of $\mathcal{E}$ in $\mathcal{E}$ such as:

$$\begin{gathered}\mathcal{E} \to \mathcal{E} \\ \Phi{:}(f_1, f_2) \to (X_G, Y_G)\end{gathered}$$

The fractal processes system Φ is represented by:

$$\Phi \begin{cases} (u_1, v_1) = P_J(\dot{x}_1 + \arctan(\dot{x}_1), \dot{x}_2 + \arctan(\dot{x}_2)) \\ (u_2, v_2) = (1 - u_1, 1 - v_1) \\ (p_1, q_1) = P_J(\dot{z}_2 + \beta, \dot{z}_3 - \beta) \\ (p_2, q_2) = (\alpha_1 p_1(1 - p_1), \alpha_2 q_1(1 - q_1)) \\ (m_1, n_1) = P_J(u_1 - p_1, v_1 - q_1) \\ (r_1, s_1) = P_J(\dot{x}_1 - \beta_1, \dot{x}_2 - \beta_2) \\ (X_G, Y_G) = P_J(r_1 - \rho m_1 + \lambda, s_1 - \rho n_1) \end{cases} \tag{9}$$

Figure 3 shows 8 chaotic attractors alternated with two forms of behavior.

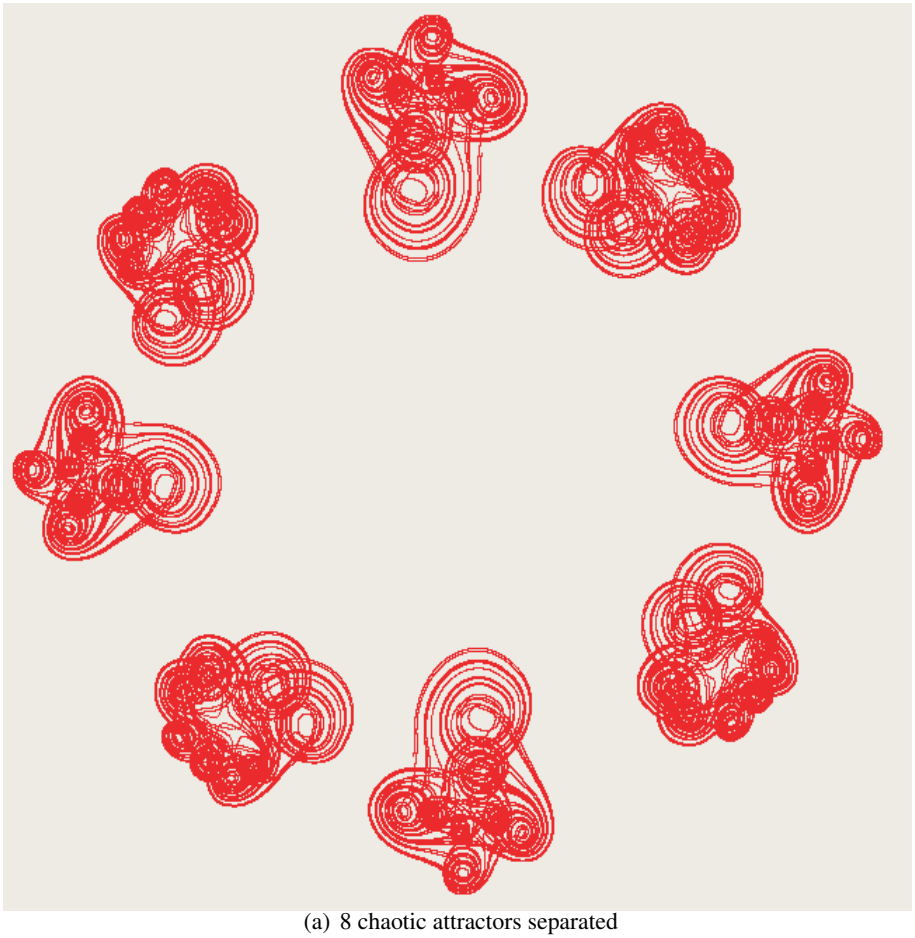

(a) 8 chaotic attractors separated

(b) First behavior chaotic attractors

(c) Second behavior chaotic attractors

Figure 3: Chaos with two behavior of chaotic attractors

3.2 Chaos with three behavior of chaotic attractors with four times

Let $\mathcal{E}$ be the complete metric unit, Φ a fractal processes system of $\mathcal{E}$ in $\mathcal{E}$ such as:

$$\begin{gathered}\mathcal{E} \to \mathcal{E} \\ \Phi{:}(f_1, f_2) \to (X_G, Y_G)\end{gathered}$$

The fractal processes system Φ is represented by:

$$\Phi \begin{cases} (u_1, v_1) = P_J(\dot{x}_1 + \arctan(\dot{x}_1), \dot{x}_2 + \arctan(\dot{x}_2)) \\ (u_2, v_2) = P_J(\dot{z}_2 + \beta_1, \dot{z}_3) \\ (u_3, v_3) = P_J(u_1 - 2u_2 + \beta_2, v_1 - v_2) \\ (p_1, q_1) = P_J(\dot{z}_2 + \beta_3, \dot{z}_3) \\ (p_2, q_2) = P_J(u_1 - 2p_1, v_1 - q_1) \\ (X_G, Y_G) = P_J(u_3 - 2p_2, v_3 - 2q_2) \end{cases} \tag{10}$$

Fractal processes system contains two different chaotic attractors the first one we choose Chua attractor noted with x the other Lorenz attractor noted with z. Implementation of fractal processes system shows result in figure

Figure 4 shows the result of implementation, It contains multi chaotic attractors with fractal and multi fractal scrolls.

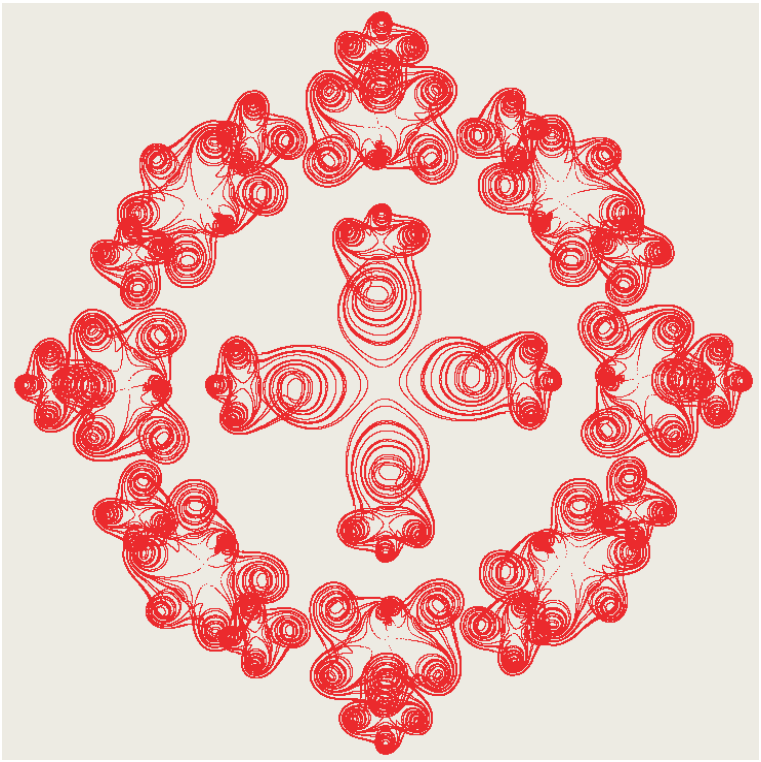

(a)

Figure 4: Chaotic attractors with three forms of behavior

Figure5 illustrates the three forms of behavior of chaotic attractors with fractal scrolls.

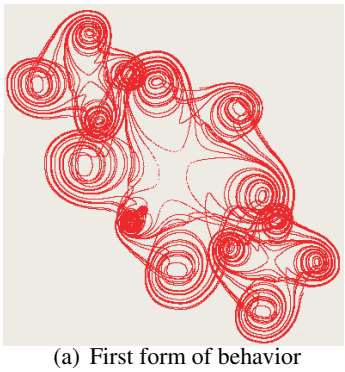

(a) First form of behavior

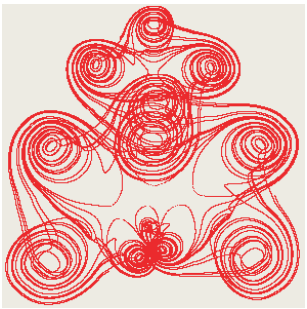

(b) Second form of behavior

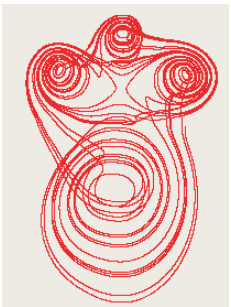

(c) Third form of behavior

Figure 5: Three forms of behavior of chaotic attractors

3.3 Chaos with nested and three behavior of chaotic attractors

Let $\mathcal{E}$ be the complete metric unit, Φ a fractal processes system of $\mathcal{E}$ in $\mathcal{E}$ such as:

$$\begin{array}{c} \mathcal{E} \to \mathcal{E} \\ \Phi{:}(f_1, f_2) \overset{479}{\to} (X_G, Y_G) \end{array}$$

The fractal processes system Φ is represented by:

$$\Phi \begin{cases} (u_1, v_1) = P_J(\dot{x}_1 + \arctan(\dot{x}_1), \dot{x}_2 + \arctan(\dot{x}_2)) \\ (u_2, v_2) = P_J(\dot{z}_2 + \beta_1, \dot{z}_3 - \beta) \\ (u_3, v_3) = P_J(u_1 - \alpha u_2 + \beta_2, v_1 - v_2) \\ (p_1, q_1) = P_J(\dot{z}_2 + \beta_3, \dot{z}_3) \\ (p_2, q_2) = P_J(u_1 - \alpha p_1, v_1 - q_1) \\ (X_G, Y_G) = P_J(u_3 - 2p_2, v_3 - 2q_2) \end{cases} \tag{11}$$

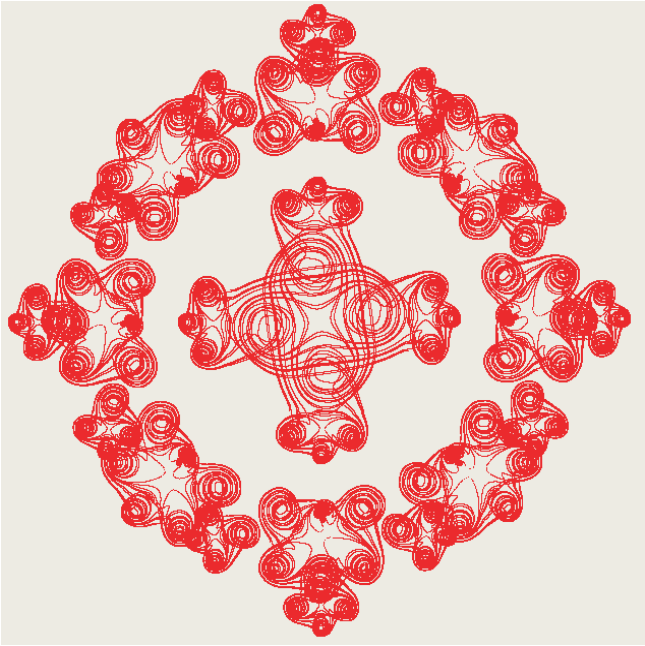

(a)

Figure 6: Chaotic attractors separated within nested chaotic attractors

3.4 Chaos with four behavior of chaotic attractors

Let $\mathcal{E}$ be the complete metric unit, Φ a fractal processes system of $\mathcal{E}$ in $\mathcal{E}$ such as:

$$\mathcal{E} \to \mathcal{E}$$
$$\Phi{:}(f_1, f_2) \to (X_G, Y_G)$$

The fractal processes system Φ is represented by:

$$\Phi \begin{cases} (u_1, v_1) = P_J(\dot{x}_1 + \arctan(\dot{x}_1), \dot{x}_2 + \arctan(\dot{x}_2)) \\ (u_2, v_2) = P_J(\dot{z}_2 + \beta_1, \dot{z}_3) \\ (u_3, v_3) = P_J(u_1 - \alpha u_2 + \beta_2, v_1 - v_2) \\ (p_1, q_1) = P_J(\dot{z}_2 + \beta_3, \dot{z}_3) \\ (p_2, q_2) = P_J(u_1 - 2p_1, v_1 - q_1) \\ (X_G, Y_G) = P_J(u_3 - 2p_2 + \beta_4, v_3 - 2q_2) \end{cases} \tag{12}$$

Figure 7shows result of implementation.

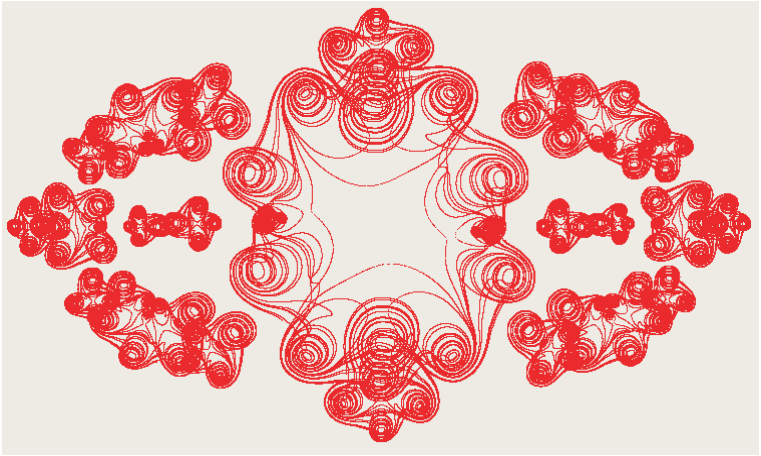

(a)

Figure 7: Chaotic attractors with four behavior forms

4 Conclusion

In this paper, different techniques of generating a new classes of chaos attractors by Chua attractor with fractal and multi fractal behavior. Many of them are new and interesting in both theory and engineering application. Moreover, many of them have some novel properties, therefore deserve further investigation in the future. Some numerical simulation results are provided to show the effectiveness of the method proposed in this work.

References

[1] Chua, L. O., Komuro, M. & Matsumoto, T. [1986]"The double scroll family,"*IEEE Trans. Circuits Syst* **33**, pp. 1072–1118.

[2] E.N. Lorenz, Deterministic nonperiodic flow, J. Atmos. Sci. $20(1963)130-141$.

[3] Xianming.Wu, Yigang.He,Wenxin.Yu,Baiqiang.Yin, A New Chaotic attractor and Its synchronization implementation. Circuit Syst. Sig. Process. DOI 10.1007/s00034-014-9946-7

[4] Guanghui.Sun,MaoWang.Lilian Huang.Liqun Shen, Generating Multi-Scroll Chaotic Attractors via Switched Fractional Systems.Circuits Syst.Sig.Process $30, 1183-1195(2011)$

[5] E.Ott Chaos in dynamical system Combridge University Press, Combridge 1993.

[6] E.O Rössler, Phys.Lett A 71(1979) 155.

[7] Cafagna G. Grassi Int J Biffurcation Chaos 13 (2003) 2889.

[8] EE. Mohmoud Dynamics and synchronization of a new hyperchaotic complex Lorenz system, Math Computation Model 55(2012) 1951-1962.

[9] K.Bouallegue, A. Chaari, A. Toumi, Multi-scroll and multi-wing chaotic attractor generated with Julia process fractal,Chaos, Solitons & Fractals $2011; 44 : 79-85$

[10] K.Bouallegue, Gallery of Chaotic Attractors Generated by Frcatal Network, Int J Biffurcation Chaos $(25)1(2015)1530002$. DOI $10.1142/S0218127415300025$.

Statistics of Chaos

David C. Ni

Dept. of Mathematical Research, Direxion Technology
9F, No. 177-1, Ho-Ping East Rd., Sec 1, Daan District, Taipei, Taiwan, R.O.C.

Abstract. In a previous effort, we demonstrated that transition to chaos being related to symmetry broken of the divergent sets in fractal forms of complex momentum-and-angular-momentum plane, which are constructed by an extended Blaschke product (EBP).

In the recent efforts, we demonstrated root computation via iteration of EBP. Using newly developed algorithms, we iterate the EBP and have mapped the convergent sets in the domains to the disconnected solution sets in the codomains. We demonstrated that solution sets showing various forms of canonical distributions and found counter examples of Fundamental Theorem of Algebra (FTA).

In this paper, we further extend the root-computation algorithms to the transition regions of chaos in the domains and the mapped codomains. We characterize the solution sets and explore the methodologies and the related theories to the modelling of physical phenomena, such as formation of galaxy cluster and stellar system.

Keywords: Nonlinear Lorentz Transformation, Nonlinear Relativity, Blaschke Equation, Fractal, Iterated solutions, Chaos, Statistics, dynamical systems.

1 Introduction

Contemporary models for N-body systems are mainly extended from temporal, two-body, and mass point representation of Newtonian mechanics. Other mainstream models include 2D/3D Ising models constructed from the lattice structures. These models have been encountering on-going debates in statistics. We were motivated to develop a new construction directly from complex-variable N-body systems based on the extended Blaschke functions (EBF)[1], which represent a non-temporal and nonlinear extension of Lorentz transformation on the complex plane – the normalized momentum-angular-momentum space. A point on the complex plane represents a normalized state of momentum and angular momentum (or phase) observed from a reference frame in the context of the theory of special relativity. This nonlinear representation couples momentum and angular momentum through real-imaginary equation of complex number.

The limited convergent sets in the domains and the corresponding codomains demonstrated hierarchical structures and topological transitions depending on

8th CHAOS Conference Proceedings, 26-29 May 2015, Henri Poincaré Institute, Paris France

parameter space. Among the transitions, continuum-to-discreteness transitions, nonlinear-to-linear transitions, and phase transitions manifest this construction embedded with structural richness for modelling broad categories of physical phenomena. In addition, we have recently developed a set of new algorithms for solving EBF iteratively in the context of dynamical systems. The solution sets generally follow the Fundamental Theorem of Algebra (FTA), however, exceptional cases are also identified. Through iteration, the solution sets show a form of $\sigma + i$ $[-t, t]$, where σ and t are the real numbers, and the $[-t, t]$ shows canonical distributions.

As in the previous paper [2,3,4,5,6,7], we introduce an angular momentum to the EBF, and for the degree of EBF, n, is greater than 2, we observed that the fractal patterns showing lags as shown in Fig. 9(a). As angular momentum increases, the divergent sets (fractal patterns) are connected to the adjacent sets and diffuse as shown in Fig. 9(a). As iteration further increasing, subsequently all convergent sets will become null set, which we define as chaotic state in this paper. The main effort hereby is to extend the solution iteration algorithm to the transition regions, where the domains and codomains becoming chaotic state. Particularly, we characterize the convergent sets in the codomain near the chaotic transition. The related theories and methodologies manifest a new paradigm for modeling chaos. As an example of efforts on the applications of modeling the physical phenomena, we apply the observations to the theories of formation of galaxy clusters and stellar systems.

2 Construction of functions and equations

2.1. Functions and Equations

Given two inertial frames with different momentums, u and v, the observed momentum, u', from v-frame is as follows:

$$u' = (u - v) / (1 - vu/c^2) \tag{1}$$

We set $c^2 = 1$ and then multiply a phase connection, $exp(i\psi(u))$, to the normalized complex form of the equation (1) to obtain the following:

$$(u'/u) = exp(i\psi(u))(1/u)[(u-v)/(1-uv)] \tag{2}$$

We hereby define a generalized complex function as follows:

$$f_{B_i}(z,m)= z^{-1} \Pi^m C_i \tag{3}$$

And C_i has the following forms:

$$C_i = exp(g_i(z))[(a_i-z)/(1-\bar{a}_i z)] \tag{4}$$

Where z is a complex variable representing the momentum u, a_i is a parameter representing momentum v, $\bar{a}_i$ is the complex conjugate of a complex number a_i and m is an integer. The term $g_i(z)$ is a complex function assigned to $\Sigma^p 2p\pi iz$ with p as an integer. The degree of $f_B(z,m) = P(z)/Q(z)$ is defined as Max{deg P, deg Q}. The function f_B is called an extended Blaschke function (EBF). The extended Blaschke equation (EBE) is defined as follows:

$$f_B(z,m) - z = 0 \tag{5}$$

2.2. Domains and Codomains

A domain can be the entire complex plane, C_∞, or a set of complex numbers, such as $z = x+yi$, with $(x^2 + y^2)^{1/2} \leqq R$, and R is a real number. For solving the EBF and EBE, a function f will be iterated as:

$$f^n(z) = f \circ f^{n-1}(z), \tag{6}$$

Where n is a positive integer indicating the number of iteration. The function operates on a domain, called domain. The set of $f^n(z)$ is called mapped codomain or simply a codomain. In the figures, the regions in black color represent stable Fatou sets containing the convergent sets of the concerned equations and the white (i.e., blank) regions correspond to Julia sets containing the divergent sets, the complementary sets of Fatou sets on C_∞ in the context of dynamical systems.

2.3. Parameter Space

In order to characterize the domains and codomains, we define a set of parameters called parameter space. The parameter space includes six parameters: 1) z, 2) a, 3) $exp(gi(z))$, 4) m, 5) *iteration*, and 6) *degree*. In the context of this paper we use the set {z, a, $exp(gi(z))$, m, *iteration*, *degree*} to represent this parameter space. For example, {a}, is one of the subsets of the parameter space.

2.4. Domain-Codomain Mapping

On the complex plane, the convergent domains of the EBFs form fractal patterns of with limited-layered structures (i.e., Herman rings), which demonstrate skip-symmetry, symmetry broken, chaos, and degeneracy in conjunction with parameter space [7]. Fig. 1 shows a circle in the domain is mapped to a set of twisted figures in the codomain. We deduce that the mapping related to the tori structures in conjunction with EBFs.

Fig. 2 shows two types of fractal patterns in the domains. These patterns are plots at different scales. In order to demonstrate these figures, we reverse the color tone of Fatou and Julia sets, namely, the black areas are the divergent sets.

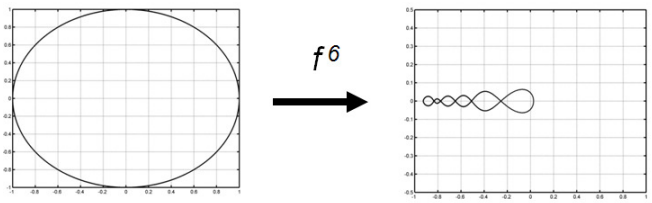

Fig. 1. Domain-Codomain mapping of a unit circle.

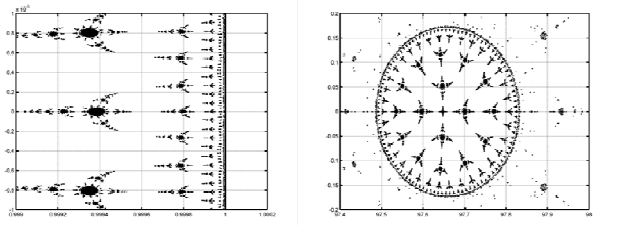

Fig. 2. Fractal Patterns of the divergent sets in the domains.

3 Transitions

3.1. Nonlinear to Linear Transitions

Fig. 3 shows the Fatou sets of domains with different degrees and values of parameter $\{a\}$. Fig. 3 (a) through (d) show that the Fatou sets are quite topologically different for different degrees, from $f_B(z,1)$, the linear equation to $f_B(z,4)$. When the value of $\{a\}$ increases from 0.1 to 0.8.

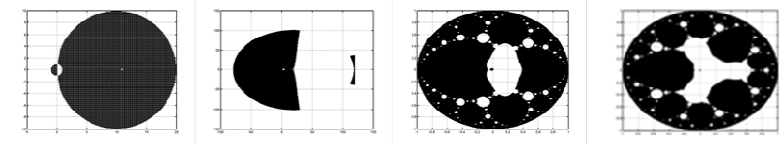

(a) $f_B(z,1)$, $a=0.1$ (b) $f_B(z,2)$, $a=0.1$ (c) $f_B(z,3)$, $a=0.1$ (d) $f_B(z,4)$, $a = 0.1$

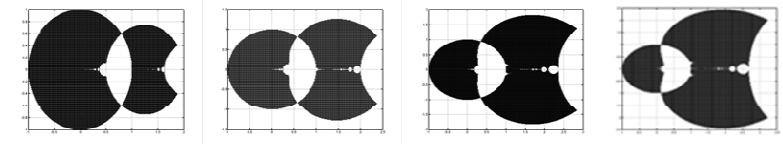

(e) $f_B(z,1)$, $a=0.8$ (f) $f_B(z,2$, $a=0.8$ (g) $f_B(z,3)$, $a=0.8$ (h) $f_B(z,4)$, $a = 0.8$

Fig. 3. Convergent sets of $f_B(z,1)$, $f_B(z,1)$, $f_B(z,1)$, and $f_B(z,1)$ with values of $\{a\}$ at *0.1* and *0.8* respectively.

The Fatou sets show topologically similar with minor variations as shown from fB(z,1), the linear equation to fB(z,4) or even at higher degrees as in Fig. 3 (e) through (h). We call this phenomenon as nonlinear-to-linear transition.

3.2. Continuum to Discrete Transitions

When the value of $\{a\}$ approaches to unity, the topological patterns of Fatou sets in the domains demonstrate an abrupt or quantum-type transition from the connected sets to the discrete sets. The discrete sets show Cantor-like pattern when mapping onto real axes on the complex plane, nevertheless, these sets are not Cantor sets by definition [6, 7, 8, 9].

The transition of EBF occurs between $a = 1 - 10^{-16}$ and $a = 1 - 10^{-17}$. Fig. 4 shows this type of topological transition. Fig. 4(a) through 4(d) shows the nonlinear-to-linear degeneracy, and 4(e) shows the Cantor-like pattern at all degrees once the transition occurs. Here, we define $\Delta = 1 - a$.

Fig. 5 shows another discreteness-to-continuum transition around a pole in original domains based on the parameter {*degree*}. Fig. 6 shows continuum-to-discreteness transitions in mapped domain based on the parameter {*iteration*}. These transitions demonstrate a fabric tori structure of EBF.

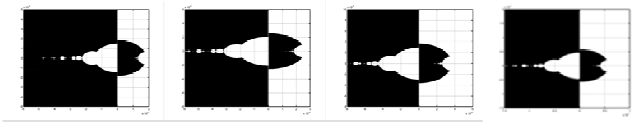

(a) $f_B(z,1)$ (b) $f_B(z,2)$ (c) $f_B(z,3)$ (d) $f_B(z,10)$

All with $\Delta \sim 10^{-16}$

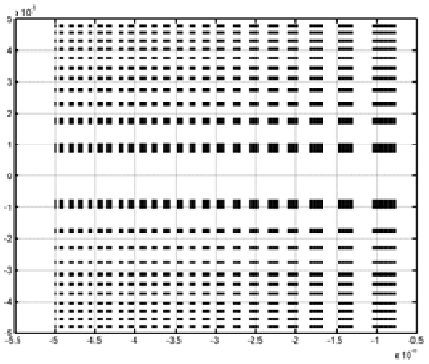

(e) $f_B(z,m)$, $\Delta = 10^{-17}$

Fig. 4. Connected sets transit to discrete Cantor-like sets for all $f_B(z,m)$ *at* $\Delta = 10^{-17}$ in the domains.

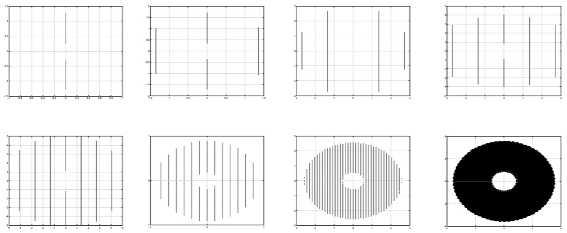

Fig. 5. Discreteness to continuum transitions around a pole of EBF as value {*degree*} increases in the domains.

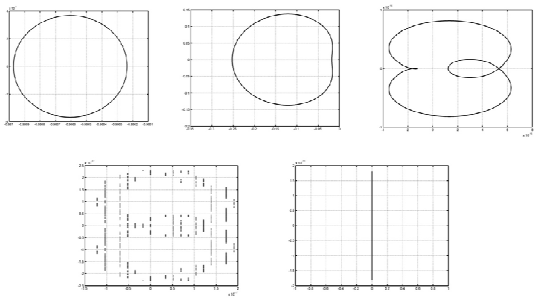

Fig. 6. Continuum to discreteness transitions as value {*iteration*} increases in the domains.

3.3. Topological Transitions

Fig. 7 shows a mapping from the convergent Fatou sets of the domain to the codomain. We examine the plots of three different values: absolute, real, and imaginary on the complex plane. The plots of absolute and real values show a modular pattern with 90 degree rotation. These sets are symmetrical to the y-axis, comparing to the x-axis symmetry of the Fatou sets of the domain. The plots of imaginary values demonstrate conjugate symmetry to the y-axis. Fig. 8 further shows this special feature with different values of *{a}*.

Using the color bar (with $z = 0$ at center of the bar) on the right side of individual figures in Fig. 8, we observe the relationship of $z(-x, y) = -z(x, y)$, as so-called conjugate symmetry. From perspective of angular momentum, the indication of this conjugate symmetry is related to the conversation law.

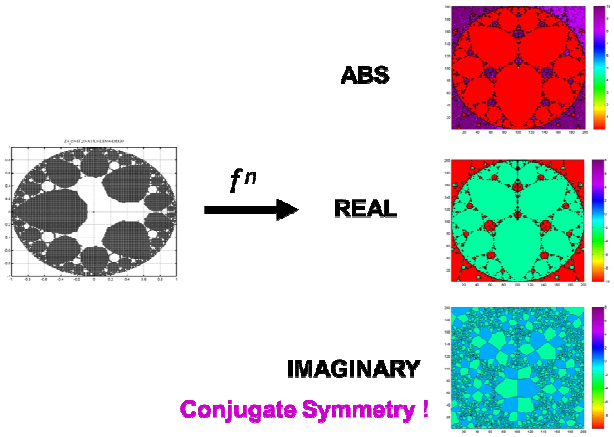

Fig. 7. Separation of Real and Imaginary values in the Domains

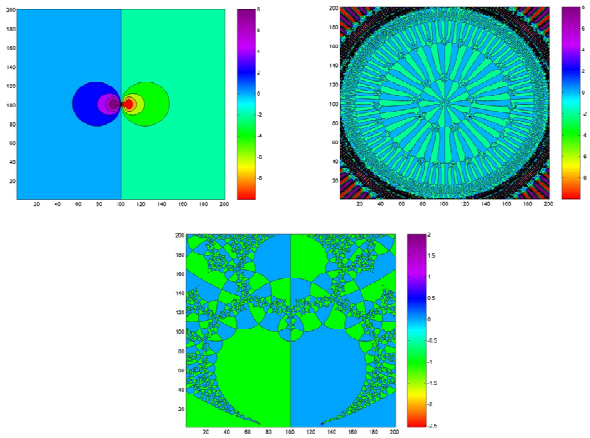

Fig. 8. Three patterns of conjugate symmetry at different values of *{a}*.

3.4. Chaotic Transitions

In the following, the convergent sets are colored in blue for those on the upper half of the complex plane, while those sets in red color are on the lower half. By doing so, we are able to examine the mappings in more details.

When an additional angular momentum applied to EBF as equation 7 below:

$$a = 0.1(\cos\theta + \sin\theta) \quad \text{with } degree = 4 \tag{7}$$

In Fig. 9(a), each layer or level of fractals, namely, the divergent sets will be lagged more as the value θ increases, and subsequently connected to the adjacent divergent sets, and eventually diffuse and become null sets for value of {*degree*} is greater than 2 as shown in Fig. 9(a). For value of {*degree*} is *1* or *2*, as shown in Fig. 9(b), this type of diffusion will not occur as shown in Fig. 9(b) [3, 4].

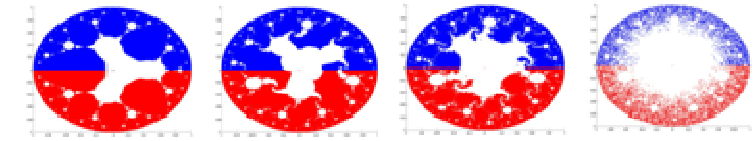

(a) degree = 4

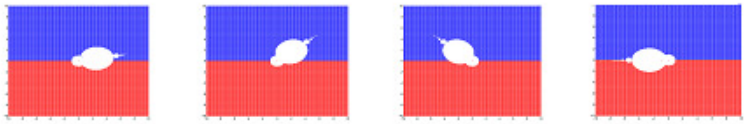

(b) degree = 1 or 2

Fig. 9. Additional angular momentum applied to convergent sets

4 EBF Solutions via Iteration

4.1. Solution sets in Domain and Codomain

As shown in Fig. 10, a new set of iteration algorithms are adopted for solving EBFs, and the discrete sets in the codomain demonstrate fixed-point-like solution sets.

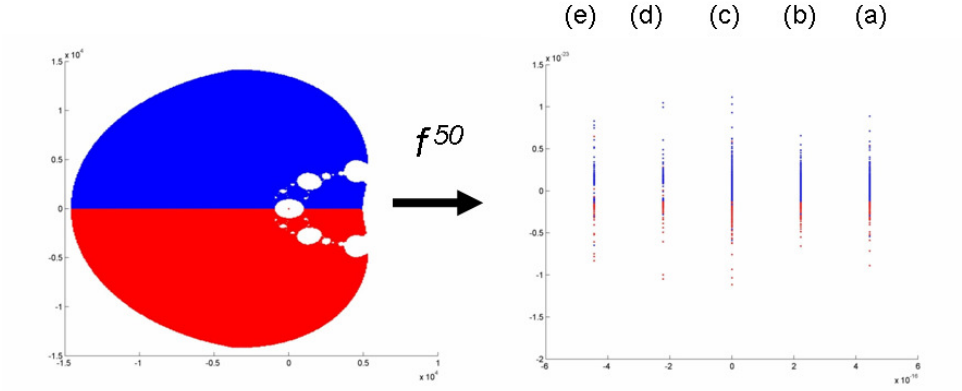

(a) Domain (b) Codomain

Fig. 10. Iterated sets of EBF for $a = 0.1$ and $degree = 3$ at scale of 10^4 as the domain (10(a)) mapping to the convergent set (a), (b), (c), (d) and (e) in the codomain (10(b)) showing violation of FTA.

As Fundamental Theorem of Algebra (FTA) asserts that the number of solution sets is equal to the degree of EBF, however, we found cases of FTA violation as shown in Fig. 10 [10].

For the individual convergent sets shown in Fig. 10 (b) in the codomain, we can examine closely which sets in the domain are mapping from as shown in Fig. 11. These figures demonstrate a deterministic perspective against the uncertainty of mapping and may fundamentally change the definition of probability in the context of statistics.

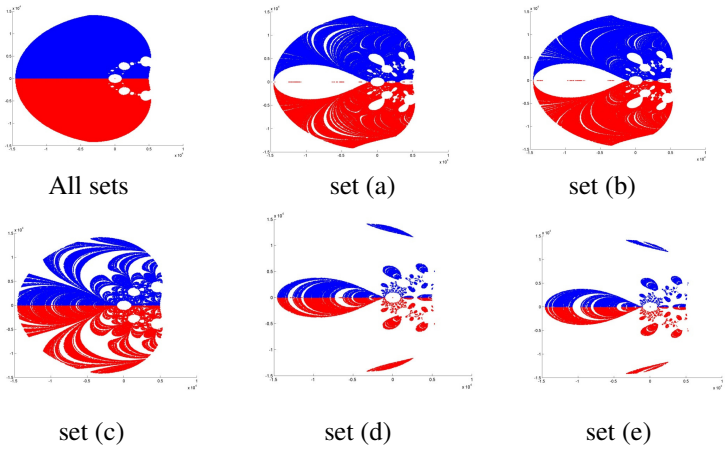

Fig. 11. The individual sets in domain (10(a)) corresponding to the convergent set (a), (b), (c), (d) and (e) in the codomain (10(b)).

Fig. 12 shows solutions by iteration for 7^{th} degree and 12^{th} degree EBFs, the numbers of solution sets are as FTA asserts. The solution sets show that the individual sets with specific real values are with spread-out imaginary sets demonstrating various distributions.

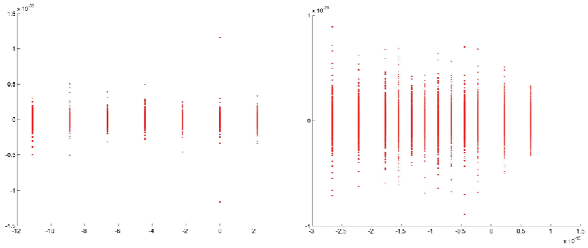

(a) $f_B(z,7)$ *(b)* $f_B(z,12))$

Fig. 12. Two solution plots with two different values of *{degree}*.

4.2. Distributions

For the individual convergent sets as shown in Fig. 10 (b), we further plot the distributions of real and imaginary point sets with a designated partition as shown in Fig. 13. The plot at bottom of Fig.13 shows the weights of individual sets, while the plot on the right side of Fig. 13 shows overall distribution along the imaginary part, the angular momentum or phase [8, 9].

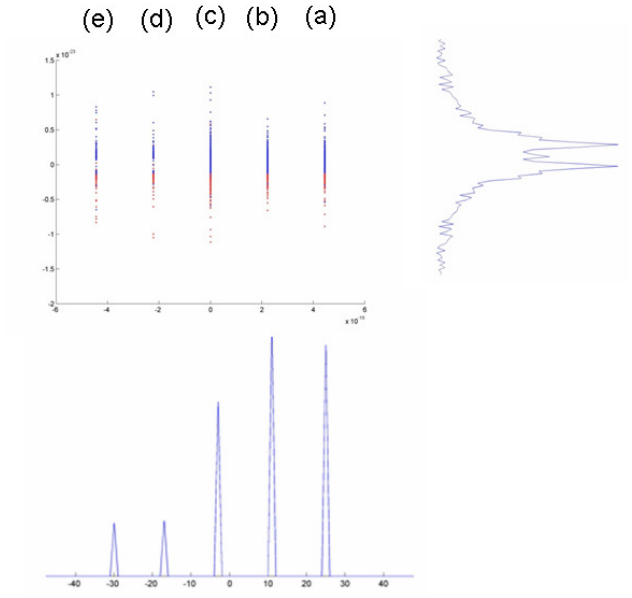

Fig. 13. Distribution plots of convergent sets in the codomain as in Fig. 10(b).

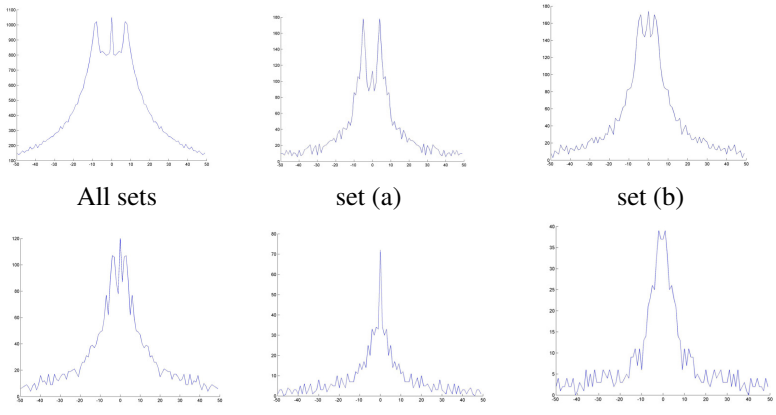

Fig. 14. Distribution plots of individual convergent sets in the codomain.

Further, we plot the distributions of the all and individual sets in Fig. 10 and Fig. 11 as shown Fig. 14. These distributions demonstrate 1-peak, 2-peak, and 3-peak distributions with different peak values. These distributions demonstrate scaling invariant to the parameter *{iteration}*.

At different scales of hierarchical convergent sets as same parameter space as in Fig. 10, the convergent sets in codomain demonstrate similar FTA violation, but the distributions are different. Fig. 15 shows that when scale changed from 10^4 to 10^{-4} , the distribution is more a quantum-mechanics distribution as in Fig. 15(b).

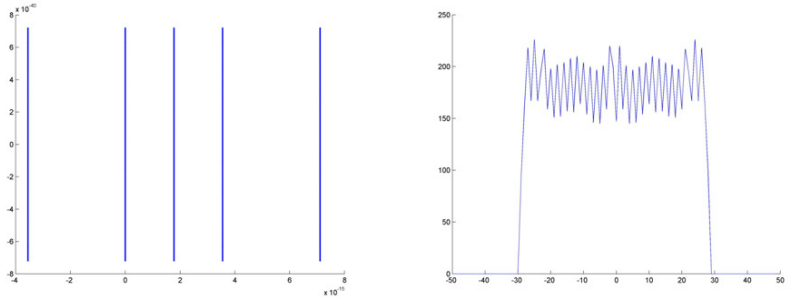

(a) Convergent sets in codomain (b) Distribution

Fig. 15. The convergent sets for $a = 0.1$ and $degree = 3$ at scale of 10^{-4} comparing with that in Fig. 10 and Fig. 13.

5 Pre-Chaos Sets in Domains and Codomains

Applying the methods described in the section 4 to the convergent sets in chaotic transitions described in section 3.4, we can examine closely the convergent sets in the codomains.

5.1. Near the chaotic transitions

As described in equation (7) in section 3.4., we have the following parameters as in equation (8):

$$a = 0.2\,(\cos(75*\pi/180) + \sin(75*\pi/180)) \quad \text{with } degree = 3 \quad (8)$$

As the value θ increases and the convergent sets approaching to the chaotic transitions, two divergent sets are both diffusing to the sub-fractal sets and demonstrate a balanced diffusion. Subsequently, the sets converge slowly and present a hierarchical structure of several layers, which are viable for the modelling of observed phenomena in the nature.

Fig. 16 shows the plots the distributions of the convergent sets in the codomain of equation (8).

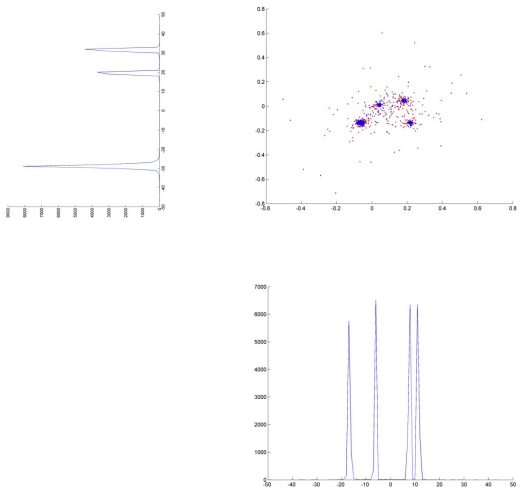

Fig. 16. The distributions of convergent sets for $a = 0.2$, $\theta=(75*\pi/180)$ and $degree = 3$ in the codomain.

Fig. 17 shows three distribution plots corresponding to the imaginary values (left set in Fig. 16) in details. The symmetry showing in Fig. 14 is broken.

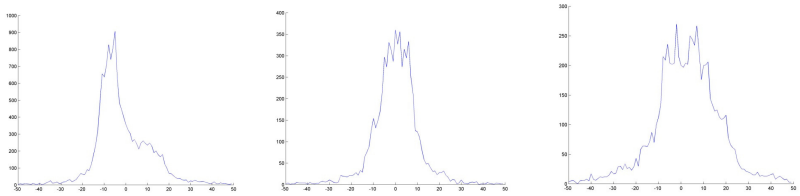

Fig. 17. The distributions of imaginary values of the convergent sets for $a = 0.2$, $\theta=(75*\pi/180)$ and $degree = 3$ in the codomain.

Fig. 18 shows four distribution plots corresponding to real values (bottom set in Fig. 16) in details. Both distribution sets of the real and imaginary values are not symmetrical, nevertheless, they are canonical distributions. The important ideas from these plots for the theoretical constructions are that in the chaotic transitions, the values of momentum and angular momentum are in limited discrete groups. This observation manifests that we can model the turbulence, chaos, and related phenomena more straightforward in momentum-angular-

momentum space than those in temporal space. In the following section, we will further extend this construction based on hierarchical structures.

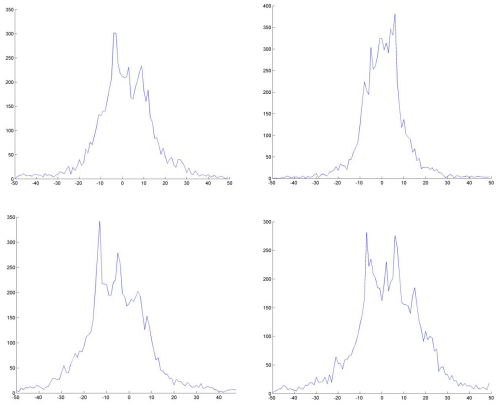

Fig. 18. The distributions of real values of the convergent sets for $a = 0.2$, $\theta=(75*\pi/180)$ and $degree = 3$ in the codomain.

5.2. Hierarchical Structures

The convergent sets in Fig. 16 have more internal structures as we examine in details. In the following, we study another set of parameters in equation (9) as below:

$$a = 0.1\ (\cos(120*\pi/180) + \sin(120*\pi/180)\ )\ \text{ with } degree = 3 \quad (9)$$

The convergent sets in codomain as shown in Fig. 19(a) are further expanded in Fig. 19(b).

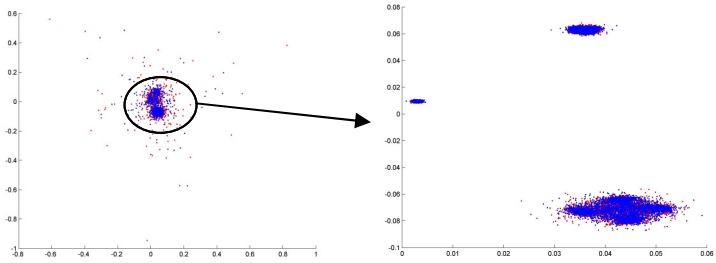

(a) Convergent sets in codomain (b) Expanded the circled area in (a)

Fig. 19. The distributions of the convergent sets for $a = 0.1$, $\theta=(120*\pi/180)$ and $degree = 3$ in the codomain.

We further expand the plot the three convergent groups of Fig. 19(b) to three individual plots as shown in Fig. 20. Then we select one of four sub-groups in Group 1 as shown Fig. 20(a), and expand one more level (2^{nd} level) down to show the convergent sets as in Fig. 21.

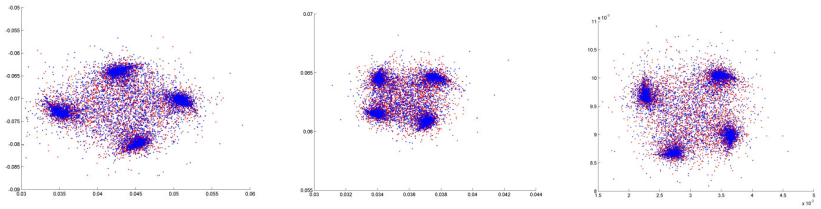

(a) Group 1 (b) Group 2 (c) Group 3

Fig. 20. The 1^{st} -level expanded distributions of the convergent sets for $a = 0.1$, $\theta=(120*\pi/180)$ and $degree = 3$ in the codomain.

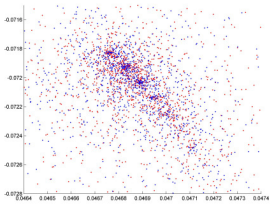

Fig. 21. The 2^{nd} -level expanded distributions of the convergent sets for $a = 0.1$, $\theta=(120*\pi/180)$ and $degree = 3$ in the codomain.

Although we are studying in the momentum-angular-momentum space, we can still see the richness of this construction for modeling physical phenomena, such as formation of galaxy cluster and stellar system, statistics related to Boltzmann Equations and Navier-Stokes equation.

As an example of modeling the formation of our stellar system, we can adopt the momentum-angular-momentum groups shown in Fig. 21 to the formation of individual planets from flattening disk of the solar nebular system.

Conclusions

In this paper, we explore the chaotic transition based on the mathematical construction of the extended Blaschke product (EBP), which can be claimed as foundation of Nonlinear Relativity. We present the domain-codomain mapping

in the context of dynamical systems, and elaborate the convergent sets of solution to chaotic transition.

We can summarize our study as follows:

- The solution sets of chaotic transitions are discrete, simple, hierarchical, and slowly convergent in the momentum space comparing with those in temporal space.
- The solution sets of pre-chaos demonstrate discrete distributions and potentially provide models for formation and structure of galaxy cluster, Boltzmann Equation, Navier-Stokes equations, among other studies.
- The complex functions with conjugate forms produce root counts higher than that of FTA asserts.

We will further investigate this mathematical construction to the modeling of chaos in the future.

References

1. W. Blaschke, Eine Erweiterung des Satzes von Vitali, "über Folgen analytischer Funktionen" Berichte Math.-Phys. Kl., Sächs. Gesell. der Wiss. Leipzig , No. 67, pp. 194–200, 1915.
2. D. C. Ni and C. H. Chin, "$Z^{-1}C_1C_2C_3C_4$ System and Application", Proceedings of TIENCS workshop, Singapore, August 1-5, 2006.
3. D. C. Ni and C. H. Chin, Symmetry Broken in Low Dimensional N-body Chaos, Proc. of Chaos 2009 Conference, Chania, Crete, Greece, pp. 53 (Abstract), June 1-5, 2009.
4. D. C. Ni and C. H. Chin, Symmetry Broken in low dimensional N-Body Chaos, CHAOTIC SYSTEMS: Theory and Applications (ed. by C. H. Skisdas and I. Domotikalis), pp. 215-223, 2010
5. D. C. Ni, "Chaotic Behavior Related to Potential Energy and Velocity in N-Body Systems", Proceedings of 8th AIMS International Conference on Dynamical Systems, Differential Equations and Applications, May 25-28, 2010, Dresden, Germany, pp. 328.
6. D. C. Ni and C. H. Chin, "Classification on Herman Rings of Extended Blaschke Equations", Differential Equations and Control processes, Issue No. 2, Article 1, 2010. (http://www.neva.ru/journal/j/EN/numbers/2010.2/issue.html).
7. D. C. Ni, "Numerical Studies of Lorentz Transformation", Proceeding of 7th EASIAM, Kitakyushu, Japan, June 27-29, 2011, pp. 113-114.
8. D. C. Ni, "Statistics constructed from N-body systems", Proceeding of World Congress, Statistics and Probability, Istanbul, Turkey, July 9-14, 2012, pp. 171.
9. D. C. Ni, "Phase Transition Models based on A N-Body Complex Statistics", Proceedings of the World Congress on Engineering 2013 (WCE 2013), Vol I, pp. 319-323, , July 3 - 5, 2013, London, U.K.
10. D.C. Ni, "A Counter Example of Fundamental Theorem of Algebra: Extended Blaschke Mapping", Proceedings of ICM 2014, August 13-August 21, Seoul, Korea, 2014.

From chaotic motion to Brownian motion. A survey and some connected problems

Gabriel V. Orman and Irinel Radomir

Department of Mathematics and Computer Science "Transilvania" University of Braşov, 500091 Braşov, Romania
(E-mail: ogabriel@unitbv.ro)

Abstract. In this paper we shall refer to the passing from chaotic motion to Brownian motion. To this end a review of some aspects concerning the Markovian nature of the Brownian path is presented. We discuss about some interesting results regarding to the 3-dimensional Brownian motion in connection with the Markov process in a generalized sense and the k-dimensional Brownian motion in connection with the Dirichlet problem. Then, we shall refer to some special connected studies.

Keywords: stochastic calculus, Markov processes, Markov property, Brownian motion, convergence.

1 Introduction

Let us imagine a chaotic motion of a particle of colloidal size immersed in a fluid. Such a chaotic motion of a particle is called, usually, *Brownian motion* and the particle which performs such a motion is referred to as a *Brownian particle*. Such a chaotic perpetual motion of a Brownian particle is the result of the collisions of particle with the molecules of the fluid in which there is.

But this particle is much bigger and also heavier than the molecules of the fluid which it collide, and then each collision has a negligible effect, while the superposition of many small interactions will produce an observable effect.

On the other hand, for a Brownian particle such molecular collisions appear in a very rapid succession, their number being enormous. For a so high frequency, evidently, the small changes in the particle's path, caused by each single impact, are too fine to be observable. For this reason the exact path of the particle can be described only by statistical methods.

Used especially in Physics, Brownian motion is of ever increasing importance not only in Probability theory but also in classical Analysis. Its fascinating properties and its far-reaching extension of the simplest normal limit theorems to functional limit distributions acted, and continue to act, as a catalyst in random analysis. As some authors remarks too, the Brownian motion reflects a perfection that seems closer to a law of nature than to a human invention.

Brownian motion was frequently explained as due to the fact that particles were alive.

We remind that Poincaré thought that it contradicted the second law of Thermodynamics.

8th CHAOS Conference Proceedings, 26-29 May 2015, Henri Poincaré Institute, Paris France

Today we know that this motion is due to the bombardament of the particles by the molecules of the medium. In a liquid, under normal conditions, the order of magnitude of the number of these impacts is of 10^{20} per second. It is only in 1905 that kinetic molecular theory led Einstein to the first mathematical model of Brownian motion. He began by deriving its possible existence and then only learned that it had been observed.

A completely different origin of mathematical Brownian motion is a game theoretic model for fluctuations of stock prices due to L. Bachélier from 1900.

In the sequel we shell refer shortly to his vision. At the same time we shall discuss some aspects regarding the Markovian nature of the Brownian path, the 3-dimensional Brownian motion in connection with a Markov process in a generalized sense and the extension to the k-dimensional Brownian motion. Finally, we shall refer shortly to some special connected studies.

2 The Markovian nature of the Brownian path

In his thesis (*Théorie de la spéculation*, Ann. Sci. École Norm. Sup. 17, 21-86, 1900) Bachélier found some solutions of the type $\psi(x)$. He derived the law governing the position of a single grain performing a 1-dimensional Brownian motion starting at $a \in \mathbf{R^1}$ at time $t = 0$:

$$P_a[x(t) \in db] = g(t, a, b)db \qquad (t, a, b) \in (0, +\infty) \times \mathbf{R^2}, \tag{1}$$

where g is the source (Green) function

$$g(t, a, b) = \frac{e^{-\frac{(b-a)^2}{2t}}}{\sqrt{2\pi t}} \tag{2}$$

of the problem of heat flow:

$$\frac{\partial u}{\partial t} = \frac{1}{2}\frac{\partial^2 u}{\partial a^2} \qquad (t > 0). \tag{3}$$

Bachélier also pointed out the Markovian nature of the Brownian path expressed in

$$\begin{aligned} P_a[a_1 \le x(t_1) < b_1,\, a_2 \le x(t_2) < b_2,\, \cdots,\, a_n \le x(t_n) < b_n] = \\ = \int_{a_1}^{b_1}\int_{a_2}^{b_2}\cdots\int_{a_n}^{b_n} g(t_1,\, a,\, \xi_1)\, g(t_2 - t_1, \xi_1, \xi_2)\cdots \\ \cdots g(t_n - t_{n-1},\, \xi_{n-1},\, \xi_n)\, d\xi_1\, d\xi_2 \cdots d\xi_n, \quad 0 < t_1 < t_2 < \cdots t_n \end{aligned} \tag{4}$$

and used it to establish the law of maximum displacement

$$P_0\left[\max_{s \le t} x(s) \le b\right] = 2\int_0^b \frac{e^{-\frac{a^2}{2t}}}{\sqrt{2\pi t}}\, da \qquad t > 0,\ b \ge 0. \tag{5}$$

It is very interesting that A. Einstein, in 1905, also derived (1) from statistical mechanical considerations and applied it to the determination of molecular diameters (see his work *Investigations on the theory of the Brownian movement*, New York, 1956).

The Brownian motion can be defined as follows

Definition 2.1 *A continuous-time stochastic process* $\{B_t \,|\, 0 \leq t \leq T\}$ *is called a "standard Brownian motion" on* $[0, T)$ *if it has the following four properties:*

i $B_0 = 0$.

ii *The increments of* B_t *are independent; that is, for any finite set of times* $0 \leq t_1 < t_2 < \cdots < t_n < T$, *the random variables*

$$B_{t_2} - B_{t_1},\, B_{t_3} - B_{t_2},\, \cdots, B_{t_n} - B_{t_{n-1}}$$

are independent.

iii *For any* $0 \leq s \leq t < T$ *the increment* $B_t - B_s$ *has the normal distribution with mean* 0 *and variance* $t - s$.

iv *For all* ω *in a set of probability one,* $B_t(\omega)$ *is a continuous function of* t.

The Brownian motion can be represented as a random sum of integrals of orthogonal functions. Such a representation satisfies the theoretician's need to prove the existence of a process with the four defining properties of Brownian motion, but it also serves more concrete demands. Especially, the series representation can be used to derive almost all of the most important analytical properties of Brownian motion. It can also give a powerful numerical method for generating the Brownian motion paths that are required in computer simulation.

3 In short about the Markov process in the generalized sense

A Markov process can be defined as follows:

Definition 3.1 *A Markov process is a system of stochastic processes*

$$\{X_t(\omega), t \in T, \omega \in (\Omega, K, P_a)\}_{a \in S},$$

that is for each $a \in S$, $\{X_t\}_{t \in S}$ *is a stochastic process defined on the probability space* (Ω, K, P_a).

But it is not difficult to observe that a definition of a *Markov process* as in Definition 3.1 not correspond to many processes that are of a real interest. For this reason it is useful to obtain an extension of this notion. Such an extended notion has been proposed by K. Itô ([6]) and we shall refer to it shortly.

Let E be a separable Banach space with real coefficients and norm $||\cdot||$ and let also $L(E, E)$ be the space of all bounded linear operators $E \longrightarrow E$. It can be observed that $L(E, E)$ is a linear space.

Definition 3.2 *The collection of stochastic processes*

$$X = \{X_t(\omega) \equiv \omega(t) \in S,\, t \in T,\, \omega \in (\Omega, K, P_a)\}_{a \in S}$$

is called a "Markov process" if the following conditions are satisfied:

1) *the "state space"* S *is a complete separable metric space and* $K(S)$ *is a topological* σ*-algebra on* S;

2) *the "time internal" $T = [0, \infty)$;*

3) *the "space of paths" Ω is the space of all right continuous functions $T \longrightarrow S$ and K is the σ-algebra $K[X_t : t \in T]$ on Ω;*

4) *the probability law of the path starting at a, $P_a(H)$, is a probability measure on (Ω, K) for every $a \in S$ which satisfy the following conditions:*

4a) $P_a(H)$ *is $K(S)$-measurable in a for every $H \in K$;*

4b) $P_a(X_0 = a) = 1$;

4c) $P_a(X_{t_1} \in E_1, \cdots, X_{t_n} \in E_n) =$
$$\int \dots \int_{a_i \in E_i} P_a(X_{t_1} \in da_1) P_{a_1}(X_{t_2 - t_1} \in da_2) \dots$$
$$\dots P_{a_{n-1}}(X_{t_n - t_{n-1}} \in da_n) \qquad for \quad 0 < t_1 < t_2 < \dots < t_n.$$

According to Definition 3.2, X will be referred as a *Markov process in the generalized sense.*

Now let X be a Markov process in a generalized sense and let us denote by $\mathbf{B}$(S) the space of all bounded real $K(S)$-measurable functions. Also let us consider a function $f \in \mathbf{B}(S)$.

It is supposed that

$$E_a\left(\int_0^\infty |f(X_t)|dt\right) \tag{6}$$

is bounded in a. Therefore

$$Uf(a) = E_a\left(\int_0^\infty f(X_t)dt\right) \tag{7}$$

is well-defined and is a bounded $K(S)$-measurable function of $a \in S$.

The Uf is called *the potential* of f with respect to X. Having in view that $Uf = \lim_{\alpha \downarrow 0} R_\alpha f$, it is reasonable to write R_0 instead of U. Based on this fact, $R_\alpha f$ will be called *the potential of order α* of f.

Remark 3.1 *It is useful to retain that $R_\alpha f \in \mathbf{B}(S)$ for $\alpha > 0$; and generally $f \in \mathbf{B}(S)$ while $R_0 f (= Uf) \in \mathbf{B}(S)$ under the condition (6).*

Now the name *potential* is justified by the following theorem on *the 3-dimensional Brownian motion*

Theorem 3.1 *Let X be the 3-dimensional Brownian motion. If $f \in \mathbf{B}(S)$ has compact support, then f satisfies (6) and*

$$Uf(a) = \frac{1}{2\pi} \int_{R^3} \frac{f(b)db}{|b - a|} = \frac{1}{2\pi} \times Newtonian\ potential\ of\ t. \tag{8}$$

Let us denote by D a bounded domain in $R^n, n \geq 1$.

Definition 3.3 *A function g is called "harmonic" in D if g is C^∞ in D and if $\Delta g = 0$ (where C^∞ is the class of functions differentiable infinitely many times).*

Now let f be a continuous function defined on the boundary ∂D and let us denote by X a k-dimensional Brownian motion defined as follows

Definition 3.4 *The k-dimensional Brownian motion is defined on $S = R^k$ by the equality*

$$p_t(a, db) = (2\pi t)^{-\frac{k}{2}} e^{-\frac{|b-a|^2}{2t}} db = N_t(b-a)db,$$

where $|b-a|$ is the norm of $b-a$ in R^k.

Given a k-dimensional Brownian motion X, if there exists a solution g for the Dirichlet problem (D, f)[1], then

$$g(a) = E_a(f(X_\lambda)), \tag{9}$$

where $\lambda \equiv \lambda_D$ = exit time from D (that is to say $\lambda_D = inf\{t > 0 : X_t \notin D\}$, the hitting time of D^C).

In this context an interesting result is given in the following theorem

Theorem 3.2 *If D is a bounded domain and g is a solution of the Dirichlet problem (D, f), then*

$$g(a) = E_a(f(X_\lambda))$$

where $a \in D$ and $\lambda = \lambda_D$.

On the other hand, the Dirichlet problem (D, f) has a solution if ∂D is smooth as it is prooved in the following theorem

Theorem 3.3 *If ∂D is smooth, then*

$$g(a) = E_a(f(X_\lambda)),$$

where $\lambda = \lambda_D$ = exit time from D, is the solution of the Dirichlet problem (D, f).

Note 3.1 *The expression "∂D is smooth" means that ∂D has a unic tangent plane at each point x of ∂D and the outward unit normal of the tangent plane at x moves continously with x.*

4 A general survey of some special connected studies

Bachélier was unable to obtain a clear picture of the Brownian motion and his ideas were unappreciated at that time. This because a precise definition of the Brownian motion involves a measure on the path space, and it was not until 1909 when É. Borel published his classical memoir on Bernoulli trials (*Les probabilités*

[1]The Diriclet problem (D, f) is to find a continuous function $g = g_{_{D,f}}$ on the closure $\overline{D} \equiv D \cup \partial D$ such that g is harmonic in D and $g = f \circ g\, \partial D$.

dénombrables et leurs applications arithmétique Rend. Circ. Mat. Palermo 27, 1909, 247-271.

As soon as the ideas of Borel, Lebesgue and Daniell appeared, it was possible to put the Brownian motion on a firm mathematical foundation and this was achived by N. Wiener in 1923 (*Differential space*, J. Math. Phis. 2,1923, 131-174).

Many researchers were fascinated by the great beauty of the theory of Brownian motion and many results have been obtained in the last decades. As for example, among other things, in *Diffusion processes and their sample paths* by K. Itô and H.P. McKean, Jr., in *Theory and applications of stochastic differential equations* by Z. Schuss, or in *Stochastic approximation* by M.T. Wasan as in *Stochastic calculus and its applications to some problems in finance* by J.M. Steele. In this context one can consider also our book *Aspects of convergence and approximation in random systems analysis*.

As we have already emphasized a rigorous definition and study of (mathematical) Brownian motion requires measure theory.

Consider the space of *continuous* path $w : t \in [0, +\infty) \to \mathbf{R^1}$ with coordinates $x(t) = w(t)$ and let β be the smallest Borel algebra of subsets B of this path space which includes all the simple events

$$B = (w : a \leq x(t) < b), \quad (t \geq 0,\, a < b).$$

Wiener established the existence of non-negative Borel measures $P_a(B)$, $(a \in \mathbf{R}^1, B \in \beta)$ for which (4) holds. Among other things, this result attaches a precise meaning to Bachélier's statement that *the Brownian path is continuous*.

Paul Lévy (*Sur certain processus stochastiques homogènes*, Compositio Math. 7, 1939, pp. 283-339) found another construction of the Brownian motion and also gave a profound description of the fine structure of the individual Brownian path[2].

Lévy's results with several complements due to D.B. Ray (*Sojourn times of a diffusion process*, IJM 7, 1963, 615-630) and K. Itô & H.P. McKean Jr. (*Diffusion processes and their Sample Path*, Springer-Verlag Berlin heidelberg, 1956) are of a special attention to the standard Brownian *local time* (*la measure du voisinage* of P. Lévy):

$$\tau(t, a) = lim_{b \downarrow a} \frac{measure(s : a \leq x(s) < b,\, s \leq t)}{2(b - a)}. \tag{10}$$

Given a Sturm-Liouville operator

$$\mathcal{D}(c_2/2)D^2 + c_1 D, \quad c_2 > 0$$

on the line, the source (Green) function $p = p(t, a, b)$ of the problem

$$\frac{\partial u}{\partial t} = \mathcal{D}u, \quad t > 0 \tag{11}$$

share with the Gauss kernel g of (2) the properties:
(a) $0 \leq p$

[2]P. Lévy, *Processus stochastiques et mouvement brownien*, Paris, 1948

(b) $\int_{R^1} p(t,a,b)db = 1$
(c) $p(t,a,b) = \int_{R^1} p(t-s,a,c)p(s,c,b)dc, \;\; t > s > 0.$

Soon after the publication of Wiener's monograph (*Generalized harmonic ana-lysis*, Acta Math. 5, 1930, 117-258), the associated stochastic motions (diffusions) analogous to the Brownian motion ($\mathcal{D} = D^2/2$) made their debut. At a later date (1946) K. Itô (*On a stochastic integral equation*, Proc. Japan acad. 22, 1946, 32-35) proved that if

$$|c_1(b) - c_1(a)| + |\sqrt{c_2(b)} - \sqrt{c_2(a)}| < constant \times |b-a|, \tag{12}$$

then the motion associated with

$$\mathcal{D} = (c_2/2)D^2 + c_1 D$$

is identical in law to the "continuous" solution of

$$a(t) = a(0) + \int_0^t c_1(a)ds + \int_0^t \sqrt{c_2(a)}db \tag{13}$$

where b is a standard Brownian motion.

W. Feller took to lead in the next development. Given a Markovian motion with sample paths $w : t \to x(t)$ and probabilities $P_a(B)$ on a linear interval Q, the operators

$$H_t : f \to \int P_a[x(t) \in db]f(b) \tag{14}$$

constitute a *semi-group* :

$$H_t = H_{t-s}H_s, \;\; t \geq s \tag{15}$$

and as E. Hille (*Represenation of one-parameter semi-groups of linear tansformations*, PNAS 28, 1942, 175-178) and K. Yosida (*On the differentiability and the representation of one-parameter semi-group of linear operators*, J. Math. Soc. Japan 1, 1948, 15-21) proved,

$$H_t = e^{t\mathcal{D}}, \;\; t > 0 \tag{16}$$

with a suitable interpretation of the exponential, where $\mathcal{D}$ is the so-called *generator*.

We mention again the name of D. Ray to emphasize that he proved (*Stationary Markov processes with continuos path*, TAMS, 82, 1956, pp. 452-493) that if the motion is *strict Markov* (i.e. if it *starts afresh* at certain stochastic (Markov) times including that passage times $m_a = \min(t : x(t) = a)$, etc.), then the so-called *generator* $\mathcal{D}$ is *local* if and only if the motion has *continuous* sample paths, substantiating a conjecture of W. Feller.

Then by combining this with some other Feller's papers as

• W. Feller, *The paraboloc differential equations and the associated semi-groups of tansformaions*, AM 55, 1952, 468-519;

• W. Feller, *The general diffusion operator and positivity preserving semi-groups in one dimension*, AM 60, 1954, 417-436;

• W. Feller, *On second order differential operators*, AM 61, 1955, 90-105;

• W. Feller, *Generalized second order differential operators and their lateral conditions*, IJM 1, 1957, 456-504,

it is implied that the generator of a strict Markovian motion with continuous paths (diffusion) can be expressed as a *differential operator*

$$(\mathcal{D}u)(a) = \lim_{b \downarrow a} \frac{u^+(b) - u^+(a)}{m(a,b)}, \tag{17}$$

where m is a non-negative Borel measure positive on open intervals and, with a change of scale

$$u^+(a) = \lim_{b \downarrow a} (b-a)^{-1} \left[u(b) - u(a)\right],$$

except of certain singular points where $\mathcal{D}$ degenerates to a differential operator of degreee ≤ 1.

Finally we remark that E.B. Dynkin (*Continous one-dimensional Markov processes*, Dokl. Akad. Nauk SSSR, 105, 1955, 405-408) also arrived at the idea of a stict Markov process. He derived an elegant formula for $\mathcal{D}$ and used it to make a simple (proba-bilistic) proof of Feller's expression for $\mathcal{D}$.

At the same time we consider that the papers of R. Blumenthal - *An extended Markov property*, TAMS 85, 1957, 52-72, and G. Hunt - *Some theorems concerning Brownian motion*, TAMS 81, 1956, 294-319, as well as the monographs of E.B. Dynkin - *Principles of the theory of Markov random processes*, Moskow-Leningrad, 1959; and *Markov processes*, Moskow, 1963, must also to be mentioned in such a connection.q

Remark 4.1 *Many other details regarding to the topics just discussed, proofs and some related problems can be found in [6], [5], [1], [4], [21], [10], [22], [9], [15], [13].*

References

[1] Bharucha-Reid, A.T. Elements of the Theory of Markov Processes and Their Applications. Dover Publications, Inc., Mineola, New York, 1997.

[2] Gihman, I.I. and Skorohod, A.V. Stochastic Differential Equations. Spriger-Verlag, Berlin, 1972.

[3] Gnedenko, B.V. The Theory of Probability. Mir Publisher, Moskow, 1976.

[4] K. Itô. Selected Papers. Springer, 1987.

[5] K. Itô and H.P. McKean Jr. Diffusion Processes and their Sample Paths. Springer-Verlag, Berlin Heidelberg, 1996.

[6] Itô, K. Stochastic Processes. Edited by Ole E. Barndorff-Nielsen, Kenichi Sato. Springer, 2004.

[7] Kushner, H.J. and Yin, G.G. Stochastic Approximation Algorithms and Applications. Springer-Verlag New York, Inc., 1997.

[8] Øksendal, B. Stochastic Differential Equations: An Introduction with Applications. Sixth Edition. Springer-Verlag, 2003.

[9] Øksendal, B. and Sulem, A. Applied Stochastic Control of Jump Diffusions. Springer, 2007.

[10] P. Olofsson and M. Andersson. Probability, Statistics and Stochastic Processes, 2nd Edition. John Wiley & Sons, Inc., Publication, 2012.

[11] Orman, G.V. Lectures on *Stochastic Approximation Methods and Related Topics.* "Gerhard Mercator" University, Duisburg, Germany, 2001.

[12] Orman, G.V. Handbook of Limit Theorems and Stochastic Approximation. Transilvania University Press, Brasov, 2003.

[13] G.V. Orman. On Markov Processes: A Survey of the Transition Probabilities and Markov Property. In C. H. Skiadas and I. Dimotikalis, editors, *Chaotic Systems: Theory and Applications*, World Scientific Publishing Co Pte Ltd., 224-232, 2010.

[14] Orman, G.V. *On a Problem of Approximation of Markov Chains by a Solution of a Stochastic Differential Equation.* In: Christos H. Skiadas, Ioannis Dimotikalis and Charilaos Skiadas (Eds.) Chaos Theory: Modeling, Simulation and Applications. World Scientific Publishing Co Pte Ltd., 2011, 30-40.

[15] Orman, G.V. and Radomir, I. *New Aspects in Approximation of a Markov Chain by a Solution of a Stochastic Differential Equation.* Chaotic Modeling and Simulation (CMSIM) International Journal, 2012, 711-718.

[16] Orman, G.V. Aspects of convergence and approximation in random systems analysis. LAP Lambert Academic Publishing, 2012.

[17] Orman, G.V. and Radomir, I. *On Stochastic Calculus and Diffusion Approximation to Markov Processes*. In: Chaos and Complex Systems, Eds. S.G. Stavrinides, S. Banerjee, S.H. Caglar, M. Ozer, Springer-Verlag Berlin Heidelberg 2013, 239-244.

[18] Orman, G.V. Basic Probability Theory, Convergence, Stochastic Processes and Applications (to appear).

[19] Qi-Ming He. Fundamentals of Matrix-Analytic Methods. Springer New York, 2014.

[20] Steele, J. M. Stochastic Calculus and Financial Applications. Springer-Verlag New York, Inc., 2001.

[21] Stroock, D. W. Markov Processes from K. Itô Perspective. Princeton Univ. Press, Princeton, 2003.

[22] Schuss, Z. Theory and Application of Stochastic Differential Equations. John Wiley & Sons, New York, 1980.

[23] Wasan, M.T. Stochastic Approximation. Cambridge University Press, 1969.

An Analysis Study on Role of Chaos in Symmetric Encryption Algorithm

Fatih Özkaynak[1], Ahmet Bedri Özer[2]

[1] Fırat University, Department of Software Engineering, 23119 Elazig, Turkey
(E-mail: ozkaynak_fatih@hotmail.com)
[2] Fırat University, Department of Computer Engineering, 23119 Elazig, Turkey
(E-mail: bedriozer@firat.edu.tr)

Abstract. In this study, we examine randomness properties of chaos based cryptographic designs. The analysis studies show that chaotic outputs which are used as a source of randomness, successfully pass the standard statistical tests, but their cryptographic randomness properties are worse than any standard random function. With these results, suitability of digital chaos in new cryptologic designs should be re-evaluated by the chaotic cryptology literature.
Keywords: Chaos; Cryptography; Cryptographically randomness; Effect of computation precision; Digital chaos.

1 Introduction

Basic goal of modern cryptography is ensuring security of communication across an insecure medium such as Internet. In order to achieve this goal, modern cryptography supplies a protocol. Briefly, the modern cryptography is about constructing and analyzing protocols which overcome the influence of adversaries [1-4]. A protocol is a collection of programs. These programs tell each party how to behave. A protocol can be probabilistic. This means that it can make random choices. Therefore, pseudo random functions are central tools in the design of protocols. A pseudo random function is a family of functions with the property that the input-output behavior of a random instance of the family is "computationally indistinguishable" from that of a random function [1, 2].

Chaos theory has been developed to model complex behavior using quite simple mathematical models. Chaotic systems are the highly unpredictable and random-looking signals [5]. In theory, there is a relationship between chaos and cryptography. The main characteristics of chaotic dynamics (dependency on the initial conditions and control parameters, ergodicity, mixing) are connected to the requirements of cryptography (confusion and diffusion of information) [6, 7].

Although there are number of chaos based cryptologic system proposals in the literature, it is curious that the subject is quite far from mainstream cryptology literature [8, 9]. This is largely because of the misinterpretation of

8th CHAOS Conference Proceedings, 26-29 May 2015, Henri Poincaré Institute, Paris France

the relationship between chaos and cryptology sciences. Chief aim of the cryptology science is to design and analyze the protocols to provide secure communication. Theoretically even if it is possible to use the chaotic systems during protocol design stage, [10-19] when practical applications considered there are several deficient problems [20-27, 37].

This study analyses the effects of chaotic system behaviors over cryptography systems depending on computational precision, when definite chaotic systems are used as pseudo random processes during cryptologic protocol design. As the result of analyses it is revealed that, although chaotic outputs successfully pass the standard statistical tests but, their randomness properties are worse than any standard random function. With this result, it is shown that neither digital chaos is suitable for cryptologic designs nor the statistical test packages are cryptographically adequate.

The outline of the study is as follows. In the next section, we examine basic problems of chaos based cryptography. In section 3, we show that effect of computational precision in chaotic systems. In the section 4, we present the summary of the random mapping statistics. In Section 5, we demonstrate performance comparisons. Finally, we give concluding remarks.

2 Problems of Chaos Based Cryptography

In the cryptography, there are two development paradigms, namely cryptanalysis-driven design and proof-driven design [1-3]. Chaos based cryptography studies have been used cryptanalysis-driven design paradigm. This paradigm has worked something like this.

1. A cryptographic goal is recognized.
2. A solution is offered.
3. One searches for an attack on the proposed solution.
4. When one is found, if it is deemed damaging or indicative of a potential weakness, you go back to Step 2 and try to come up with a better solution. The process then continues.

There are some difficulties with the approach of cryptanalysis-drive design. The obvious problem is that one never knows if things are right, nor when one is finished! The process should iterate until one feels “confident” that the solution is adequate. But one has to accept that design errors might come to light at any time. Despite that problem, cryptanalysis-drive design process is still employable. However, the main problem of chaos based cryptographic designs is the usage of very simple statistical tests for cryptanalysis studies. For example, NPCR (number of pixels change rate), UACI (unified average changing intensity) and histogram analysis have been used for differential and linear cryptanalysis of almost all chaos based image encryption algorithms.

In addition to the problems arising from the analysis, the fact that the chaotic systems are realized on digital computers is another issue to be evaluated. While cryptologic designs use a finite set of integers as the workspace, chaotic systems use a set of real numbers [20]. As a result, simulations of chaotic systems on digital computers suffer from truncation and round-off errors. In consequence,

random behavior expected from chaos is replaced with periodical behavior which does not meet the confusion and diffusion requirements of the cryptologic designs. This effect is shown in detail in next section.

3 Effects of Computational Precision in Chaotic Systems

Data representation is one of the most important theoretical problems for the computers which are designed to process, control and store of data. Data types like integers, real numbers or strings can be infinite by nature. However, since computers only have finite computational capacity, numerical errors will arise depending on computational precision. These numerical errors cause different data values to be perceived as representing the same value. Pigeonhole principle which is one of the most powerful tools in computer science can be applied to show this problem theoretically. If there are more pigeons than holes they occupy, then at least two pigeons must be in the same hole.

> **Theorem:** (Pigeonhole Principle). If $|A| > |B|$, then for every total function $f: A \to B$, there exist two different elements of A that are mapped by f to the same element of B.

In the interval [0, 1], there are infinitely real numbers. Let's consider representing these numbers with 4 bits computational precision. In such case, the [0, 1] interval will be divided into 2^4-1=15 different intervals. The upper and lower limits of those 15 intervals will be as shown in Fig 1. This implies that all real numbers falling into same interval will be represented with a single value, for instance all real numbers between 0.0625 and 0.1250 will be represented as 0,0625, producing numerical errors in all computations. This type of numerical errors will affect the pseudorandom behavior of the chaotic system. To illustrate, a logistic map implemented on a computer with 4 bits computational precision and the resulting trajectories are shown in Fig. 2. Although there are 2^4-1=15 different intervals and theoretically it is expected to obtain 15 different trajectories, only 2 different trajectories are obtained.

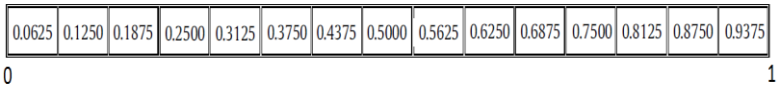

Fig. 1. Computation intervals for 4 bits computational precision

4 Properties of Random Mapping

Let f be a function, $f: X \to X$, where X denote the finite domain of size n and let F_n denote the collection of all functions where every function is equally likely to be chosen. So the sample space consists of n^n random mappings, in other words, the probability that a particular function (f) from F_n is chosen is $\frac{1}{n^n}$. Starting from a point $x_0 \in X$ and iteratively applying f, the following sequence is obtained;

$$\{x_0, f(x_0), f^2(x_0), \dots\} \quad (1)$$

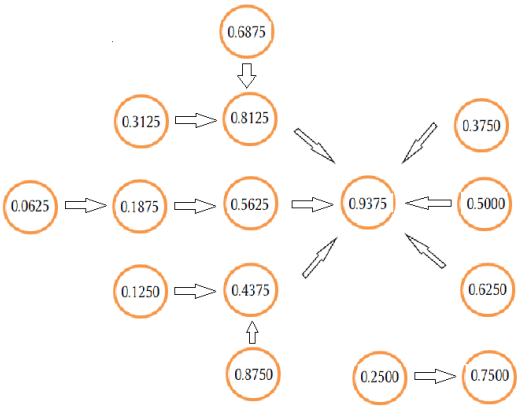

Fig 2. Trajectories of logistic map for 4 bits computational precision

The k^{th} iteration of f on X, where $0 \leq k \leq n$ will be $f^k(x_0) = f(f^{k-1}(x_0))$ where $f^0(x_0) = x_0$. For some $k \geq 0$ if $f^k(x_0) = y$ then we call y, a k^{th} image of x_0 in f. For $k < 0$, $f^k(x_0)$ may not exist, which we will call terminal nodes, (in other words, a node may have no inverse image) or may not be uniquely determined. A random mapping f can be represented by a functional graph. A functional graph of a function $f: X \to X$ is a directed graph whose nodes are the elements of X and whose edges are the ordered pairs $(x, f(x))$, for all $x \in X$.

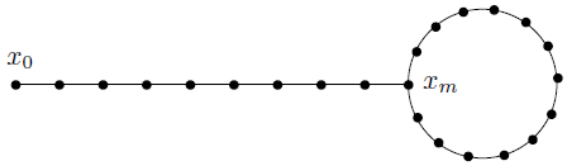

Fig. 3. Functional Graph

In Figure 3, the typical behavior of an iteration operation is given. Since the set X is finite, after some iterations, we will encounter a point that has occurred before. Let $f^m(x_0), 0 \leq m \leq n-1$ be the point that the iteration enters a loop. Then, $f^m(x_0) = f^k(f^m(x_0))$, k is the smallest positive integer which we call the cycle length. The path between x_0 and $f^m(x_0)$ is called the tail length. The sum of the tail length and cycle length is defined as the p-length.

Expected values of random mappings are widely studied in the literature. The results of the statistical behaviors of random mappings are summarized below [2, 28-31].

- Number of components: $\frac{\ln(n)}{2}$
- Number of terminal nodes: $e^{-1}n \cong 0.3679n$
- Number of image nodes: $(1-e^{-1})n \cong 0.6321n$
- Average cycle length: $\sqrt{\frac{\pi n}{8}} \cong 0.6267\sqrt{n}$
- Average tail length: $\sqrt{\frac{\pi n}{8}} \cong 0.6267\sqrt{n}$
- Average $p$length: $\sqrt{\frac{\pi n}{2}} \cong 1.2533\sqrt{n}$
- Average component size: $\frac{2n}{3}$
- Maximum cycle length: 0.78248 $\sqrt{n}$
- Maximum tail length: 1.73746 $\sqrt{n}$

5 Performance Comparisons of Chaos Based Randomness

One of the simplest and most studied chaotic system is the logistic map. In the many studies, logistic map has been studied as pseudo random number generator. The logistic map is given in Eq. (2).

$$x_{n+1} = a x_n (1 - x_n) \quad (2)$$

where $x_n \in (0,1)$ and a are the system variable and parameter, respectively, and n is the number of iterations. Thus, given an initial value x_n and a parameter a; the chaotic outputs are computed. For $0 \leq a \leq 1$ the trivial solution is the only fixed point. For $1 < a \leq 3$; we have a non-trivial fixed point. For $3 < a \leq 3.57$, the map exhibits the phenomenon of periodic doubling. For $3.57 < a \leq 4$, the map becomes chaotic.

Generating a pseudo random binary sequence from the orbit of the logistic map essentially requires mapping the state of the system to $(0,1)$. A simple way for turning a real number x_i to a discrete bit symbol z_i is simply by using a threshold function.

$$z_i = F(x_i) = \begin{cases} 0, & if\ x_i < c \\ 1, & otherwise \end{cases} \quad (3)$$

The output sequences of logistic map should be statistically indistinguishable from truly random sequences, therefore statistical analysis of logistic map are crucial. Analysis of logistic map is performed by producing a sample sequence, and evaluating this sequence by statistical randomness tests.

A statistical randomness test is developed to test a null hypothesis (H_0) which states the input sequence is random. The test takes a binary sequence as an input and "accepts" or "rejects" the hypothesis. Randomness tests are probabilistic and there are two types of errors. If the data is random and H_0 is

rejected type I error is occurred and if the data is nonrandom and H_0 is accepted type II error is occurred. The probability of a type I error is called the level of significance of the test and denoted by $\propto$. A statistical test produces a real number between 0 and 1 which is called p-value. If p-value > $\propto$ then H_0 is accepted, otherwise rejected.

A test suite is a collection of statistical randomness test that are designed to test the randomness properties of sequences. There are several test suites in the literature:

- The first collection of randomness tests were presented by Knuth in his famous book [32].
- CRYPT-X, a test suite developed in Queensland University of Technology [33].
- DIEHARD Test Suite was developed by Marsaglia and published in 1995 on a CDROM [34].
- TESTU01 is a recently designed test suite, which has two categories: Those that apply to a sequence of real numbers in (0, 1) and those designed for a sequence of bits [35].
- NIST Test Suite originally consisted of 16 tests [36]. The randomness tests in the suite are Frequency Test, Frequency Test within a Block, Runs Test, Test for the Longest Run of Ones in a Block, Binary Matrix Rank Test, Discrete Fourier Transform Test, Non-overlapping Template Matching Test, Overlapping Template Matching Test, Maurer's Universal Statistical Test, Lempel-Ziv Compression Test, Linear Complexity Test, Approximate Entropy Test, Cumulative Sums Test, Random Excursions Test, and Random Excursions Variant Test.

NIST Test Suite has been used in this study to assess randomness. The obtained results are shown in Table 1.

Calculated and expected values of random functions, obtained by using chaotic logistic map, are given in Table 2 for different computation precision values *n*. As can be seen from the table, calculated values are fewer than the expected values for chaos based random function. These results show that even though digital chaos based functions can pass the statistical tests, they are not fit to be used for cryptologic randomness

6 Conclusions

As a result of the analysis studies, it is determined that security of the chaos based cryptographic designs typically analyzed by using statistical tests alone. A common misconception, that the successful statistical test results are enough to analyze the security of a cryptologic system, is the most important problem in this area. To remove this misconception, the deficiencies of the statistical tests are investigated. It is revealed that, although chaotic outputs successfully pass the standard statistical tests their randomness properties are worse than any standard random function. Consequently, the question - whether numerical

chaos is really suitable for new cryptologic designs - should be re-evaluated by the chaotic cryptology literature.

Table 1 Results of SP 800-22 test for logistic map

Test	p-value	Logistic map
Approximate entropy	0.1554	pass
Block Frequency	0.4968	pass
Cumulative sums	0.889, 0.984	pass
FFT	0.1957	pass
Frequency	0.8556	pass
Linear complexity	0.8687	pass
Random excursions	0.2117…	pass
Random excursions variant	0.2067…	pass
Longest runs of ones	0.6153	pass
Overlapping template matching	0.6224	pass
Rank	0.3430	pass
Runs	0.8965	pass
Serial	0.672, 0.948	pass
Universal statistical	0.6508	pass

Table 2 Performance comparisons

Computation precisions		2^8	2^{10}	2^{16}	2^{23}
Maximum p-length	Expected value	20	40	320	2896
	Computed value	30	33	264	487
Component size	Expected value	4	5	8	11
	Computed value	4	4	6	7

References

[1]. M. Bellare, P. Rogaway, Introduction to modern cryptography, Course and lecture notes in cryptography, 2005.

[2]. A. J. Menezes, P. C. van Oorschot, S. A. Vanstone. Handbook of Applied Cryptography, CRC Press, Boca Raton, Florida, USA, 1997.

[3]. J. Katz, Y. Lindell, Introduction to modern cryptography: principles and protocols, Chapman & Hall, 2008.

[4]. C. Paar, J. Pelzl, Understanding Cryptography A Textbook for Student and Practitioners, Springer, 2010.
[5]. J. Sprott, Elegant Chaos Algebraically Simple Chaotic Flows. World Scientific, 2010.
[6]. J. M. Amigo, L. Kocarev, J. Szczapanski, Theory and practice of chaotic cryptography, Physics Letters A 366 (2007) 211-216.
[7]. G. Alvarez, S. Li, Some basic cryptographic requirements for chaos-based cryptosystems. International Journal of Bifurcation and Chaos 16/8 (2006) 2129–2151
[8]. E. Solak, Cryptanalysis of Chaotic Ciphers, in: L. Kocarev, S. Lian (Eds.), Chaos Based Cryptography Theory Algorithms and Applications, Springer-Verlag (2011) 227-256.
[9]. G. Alvarez, J. M. Amigo, D. Arroyo, S. Li, Lessons Learnt from the Cryptanalysis of Chaos-Based Ciphers, in: L. Kocarev, S. Lian (Eds.), Chaos Based Cryptography Theory Algorithms and Applications, Springer-Verlag (2011) 257-295.
[10]. X. Wang, W. Zhang, W. Guo, Jiashu Zhang, Secure chaotic system with application to chaotic ciphers, Information Sciences 221 (2013) 555-570.
[11]. A. Kanso, H. Yahyaoui, M. Almulla, Keyed hash function based on a chaotic map, Information Sciences 186/1 (2012) 249-264.
[12]. C. Chen, C. Lin, C. Chiang, S. Lin, Personalized information encryption using ECG signals with chaotic functions, Information Sciences 193 (2012) 125-140.
[13]. Z. Zhu, W. Zhang, K. Wong, H. Yu, A chaos-based symmetric image encryption scheme using a bit-level permutation, Information Sciences 181/6 (2011) 1171-1186.
[14]. .J. Fridrich, Symmetric ciphers based on two-dimensional chaotic maps, International Journal of Bifurcation and Chaos 8/6 (1998) 1259–1284.
[15]. C. Zhu, A novel image encryption scheme based on improved hyperchaotic sequences, Optics Communications 285/1 (2012) 29-37
[16]. H. Hu, L. Liu, N. Ding, Pseudorandom sequence generator based on Chen chaotic system, Computer Physics Communications 184 (2013) 765–768.
[17]. Q. Zhang, L. Guo, X. Wei, Image encryption using DNA addition combining with chaotic maps, Mathematical and Computer Modelling 52 (2010) 2028-2035.
[18]. N. Bigdeli, Y. Farid, K. Afshar, A robust hybrid method for image encryption based on Hopfield neural network, Computers and Electrical Engineering 38, pp.356–369, 2012.
[19]. L. Liu, Q. Zhang, X. Wei, A RGB image encryption algorithm based on DNA encoding and chaos map, Computers & Electrical Engineering, 38/5 (2012) 1240-1248.

[20]. F. Özkaynak, S. Yavuz, Security problems of pseudorandom sequence generator based on Chen chaotic system, Computer Physics Communications 184 (2013) 2178–2181.
[21]. F. Özkaynak, A. B. Özer, S. Yavuz, Cryptanalysis of a novel image encryption scheme based on improved hyperchaotic sequences, Optics Communications 285 (2012) 4946–4948.
[22]. F. Özkaynak, A. B. Özer, S. Yavuz, Cryptanalysis of Bigdeli algorithm using Çokal and Solak attack, International Journal of Information Security Science, 1/3 (2012) 79-81.
[23]. F. Özkaynak, A. B. Özer, S. Yavuz, (2012). Analysis of Chaotic Methods for Compression and Encryption Processes in Data Communication, 20th IEEE Signal Processing and Communications Applications Conference.
[24]. F. Özkaynak, A. B. Özer, S. Yavuz, (2013). Security Analysis of An Image Encryption Algorithm Based on Chaos and DNA Encoding, 21th IEEE Signal Processing and Communications Applications Conference.
[25]. E. Solak, C. Çokal , Algebraic break of image ciphers based on discretized chaotic map lattices, Information Sciences, 181/1 (2011) ,227-233
[26]. E. Solak, C. Çokal, O.T. Yildiz, T. Biyikoglu, Cryptanalysis of fridrich's chaotic image encryption. International Journal of Bifurcation and Chaos 20/5 (2010) 1405–1413.
[27]. F. Özkaynak, S. Yavuz, Analysis and improvement of a novel image fusion encryption algorithm based on DNA sequence operation and hyper-chaotic system, Nonlinear Dynamics: Volume, 78/2, 1311-1320, 2014.
[28]. P. Flajolet, A. M. Odlyzko, Random mapping statistics, In EUROCRYPT (1989) 329–354.
[29]. B. Harris, Probability distributions related to random mappings. The Annals of Mathematical Statistics 31/4 (1960) 1045–1062.
[30]. V. F. Kolchin. Random Mappings. Springer-Verlag, 1986.
[31]. J. Arney, E. A. Bender, Random mappings with constraints on coalescence and number of origins, Pacific J. Math. 103/2 (1982)269–294.
[32]. D. E. Knuth, Seminumerical Algorithms, volume 2 of The Art of Computer Programming, Addison-Wesley, 1981.
[33]. W. Caelli, E. Dawson, L. Nielsen, H. Gustafson, CRYPT–X statistical package manual, measuring the strength of stream and block ciphers, 1992.
[34]. G. Marsaglia, The Marsaglia random number CDROM including the DIEHARD battery of tests of randomness, 1996.
[35]. P. L'Ecuyer, R. Simard, Testu01: A c library for empirical testing of random number generators. ACM Trans. Math. Softw., 33/4 (2007) 22.

[36]. A. Rukhin, J. Soto, J. Nechvatal, M. Smid, E. Barker, S. Leigh, M. Levenson, M. Vangel, D. Banks, A. Heckert, J. Dray, S. Vo, A statistical test suite for random and pseudorandom number generators for cryptographic applications, 2001.
[37]. F. Özkaynak, Cryptographically secure random number generator with chaotic additional input, Nonlinear Dynamics, 78/3, 2015-2020, 2014.

Entropy Analysis with Lyapunov Exponents for Random Number Generators

Fatih Özkaynak[1], Ahmet Bedri Özer[2]

[1] Fırat University, Department of Software Engineering, 23119 Elazig, Turkey
(E-mail: ozkaynak_fatih@hotmail.com)
[2] Fırat University, Department of Computer Engineering, 23119 Elazig, Turkey
(E-mail: bedriozer@firat.edu.tr)

Abstract. Many applications require random numbers. Generating high quality random numbers is a very serious problem. It is quite easy to design a random number generator that will pass the statistical tests, but it is much more difficult to know where the randomness comes from and how much true randomness is there. Chaotic system is regarded as an important entropy source in the design of random number generator. The relationship between random number generator and chaotic dynamical systems is studied in this paper. The main contribution of this paper is that it gives an analysis method for entropy source in random number generators. Entropy describes the unpredictability of random number generators. In practice, calculation of entropy is hard, so Lyapunov exponent has been used as an unpredictability measure of entropy source. Proposed analysis method has been verified on a chaos based random number generator design, and fits to analysis of other RNG designs.
Keywords: Random number generator, Entropy, Lyapunov Exponent, Chaos.

1 Introduction

A random number generator (RNG) produces a sequence of random (or random-looking) numbers in a predetermined range, such as r_i∈{0,1} or r_i∈[0,1]. Random numbers have many applications: statistical physics, simulation, industrial testing and labeling, games, gambling, Monte Carlo methods, and cryptography [1, 2].

Generating high quality random numbers is a very serious problem. The random numbers should assume all admissible values with equal probability and should be independent from predecessors and successors. This characterizes an ideal RNG. In an ideal RNG, even with maximal knowhow and unlimited computational power an attacker has no better strategy blind guessing. Guessing n random bits costs 2^(n-1) trials in average. The guess work remains invariant in the course of the time. However, an ideal RNG is a mathematical construct. There are two basic categories of RNGs: True RNGs and Deterministic RNGs. It is quite easy to design a RNG that will pass the statistical tests, but it is much more difficult to know where the randomness comes from and how much true randomness is there [2-5].

The most striking feature of RNGs is the unpredictability of the past and future random numbers from some subsequent random numbers.

8th CHAOS Conference Proceedings, 26-29 May 2015, Henri Poincaré Institute, Paris France

Unpredictability is a consequence of the inherent instability of the entropy source. The unpredictability is related with sensitive dependence on initial seed value of RNG. The tiny deviations between the seed value of generators and every unobserved detail of the generators are important for generated random numbers [2, 5].

Chaos theory has been developed to model complex behavior using quite simple mathematical models. This theory has captured the attention of the scientific community for explaining and predicting the behavior of systems in the real world. Chaos is a deterministic and random-like process operating in nonlinear dynamic systems. Chaotic systems are not periodical and do not converge to a certain value despite being finite. The most important characteristic of chaotic systems is that they are highly dependent on the initial conditions and control parameters. Orbits of chaotic signals have highly unpredictable and random-looking nature. Mathematically, chaos is randomness of a simple deterministic dynamical system [6, 7].

Since 1990's many researchers have used chaotic systems as a source of entropy in the design of RNGs [5, 7-9, 12]. Apparently the characteristics of chaotic dynamics can be connected to the requirements of RNG. This work is focused on interaction between chaos and RNG. However, this interaction have been examined a different point of view. If chaotic systems can be applied to design of RNGs, chaos analysis methods are useful for analysis of RNGs. Therefore, the theory of dynamical systems can be helpful when analyzing the properties of RNG.

The main contribution of this paper is the analysis of RNG. This paper gives an analysis method for entropy source in RNG. Tools for detecting chaos are used for investigation of RNG's unpredictability. There are various methods for detecting chaos. In this paper, Lyapunov exponents are used to analyze of RNG. Proposed analysis method has been verified on a chaos based RNG designs, and fits to analysis of other RNG designs.

The paper is organized as follow: In Section 2, we briefly explain central aspects of Lyapunov exponents. A chaos based RNG design is showed in Section 3. In Section 4, we describe and analyze proposed test method for investigation of RNG's unpredictability. Finally, we give our concluding remarks.

2 Chaos Analysis Tools

A There are various methods for detecting chaos. These are time series analysis, phase portraits, Poincare maps, power spectrum, Lyapunov exponents, bifurcation diagram, Lyapunov dimension, correlation dimension, and etc. In this paper, we use Lyapunov exponents as tool for detecting chaos.

Lyapunov exponent is that diverge of two adjacent orbits in the phase space with nearby initial conditions. If separation of two adjacent orbits is very slow, then system is typical of predominantly periodic systems. If this separation is exponentially fast, then system has unpredictability. The properly averaged exponent of this increase is characteristic for the system underlying the data [6, 10].

Calculation of the Lyapunov exponent is conceptually simple since one only needs to follow two initially nearby trajectories and fit the logarithm of their separation to a linear function of time. The slope of the fit is the Lyapunov exponent. Let s_{n_1} and s_{n_2} be two points in state space with distance $\|s_{n_1} - s_{n_2}\| = \delta_0 \ll 1$. Denote by $\delta_{\Delta n}$ the distance some time Δn ahead between the two trajectories emerging from these points, $\delta_{\Delta n} = \|s_{n_1} - s_{n_2}\|$. Then λ is determined by Eq. (1) [6, 10].

$$\delta_{\Delta n} \cong \delta_0 e^{\lambda \Delta n},\ \delta_{\Delta n} \ll 1,\ \Delta n \gg 1 \quad (1)$$

If λ is positive, this means an exponential divergence of nearby trajectories with nearby initial conditions. A negative maximal Lyapunov exponent reflects the existence of a stable fixed point. Two adjacent orbits which approach the fixed point also approach each other exponentially fast. If the motion settles down onto a limit cycle, two adjacent orbits can only separate or approach each other slower than exponentially. In this case the maximal Lyapunov exponent is zero and the motion is called marginally stable. If a predominantly deterministic system is perturbed by random noise, on the small scales it can be characterized by a diffusion process, with n growing as n. Thus the maximal Lyapunov exponent is infinite. General characteristics of Lyapunov exponent is given in Table 1 [6, 10].

Table 1. General characteristics of Lyapunov exponent

Type of motion	**Maximal Lyapunov exponent**
stable fixed point	$\lambda < 0$
stable limit cycle	$\lambda = 0$
chaos	$0 < \lambda < \infty$
noise	$\lambda = \infty$

3 A Chaos Based RNG

Logistic map is one of the simplest and most studied nonlinear system in the design of RNGs. The logistic map is defined as Eq. (2).

$$f_\lambda(x) = f(\lambda, x) = \lambda x(1 - x) \quad (2)$$

Structure in Eq. (3) has been used to convert the iterations of a logistic map into binary digits is by defining a function $g: [0,1] \rightarrow \{0,1\}$.

$$B_i = g(x_i) = \begin{cases} 0, & if\ x_i < c \\ 1, & otherwise \end{cases} \quad (3)$$

where c is a threshold value taken to be 0.5 to ensure approximately equal distributions of 0's and 1's in the sequence B_i. Furthermore, for c = 0.5, the generated sequences have been demonstrated to possess good statistical distribution properties. The most comprehensive statistical test suite, NIST test suite [11], was applied to test such sequences, and the results turned out to be very satisfactory.

4. Definition of Analysis Methods

The most striking feature of chaos and RNGs is the unpredictability of the future despite a deterministic time evolution. The average error made when forecasting the outcome of a future measurement increases very rapidly with time, and in this system predictability is almost lost after only a few time steps. This unpredictability is a consequence of the inherent instability of the solutions, reflected by what is called sensitive dependence on initial conditions. The tiny deviations between the "initial conditions" of all the trajectories are blown up after a few time steps. A more careful investigation of this instability leads to two different concepts. One aspect is the loss of information related to unpredictability. This is quantified by the entropy. The other aspect is a simple geometric one, namely, that nearby trajectories separate very fast, or more precisely, exponentially fast over time.

If the random numbers are unpredictable, then the RNG also meets the knowledge of subsequences of random numbers shall not allow to compute predecessors or successors practically or to guess them with non-negligibly larger probability than without knowledge of these subsequences. This requirement is fulfilled if the conditional entropy per internal random number, or more precisely, the conditional entropy of the underlying random variables, is sufficiently large. Entropy quantifies the degree of uncertainty [2]. Let X denote a random variable that assumes values in a finite set $S = \{s_1, s_2, \ldots, s_n\}$. The entropy of X is given by Eq. (4).

$$H(X) = -\sum_{j=1}^{n} Prob(X = s_j) log_2(Prob(X = s_j)) \quad (4)$$

The most general definition of entropy is the Renyi entropy given by Eq. (5). If X is uniformly distributed on $S = \{0,1\}$ then $H_\alpha(X) = 1$ for each parameter α.

$$H_\alpha(X) = \frac{1}{1-\alpha} log_2 \sum_{j=1}^{n} Prob(X = s_j)^\alpha \quad (5)$$

Figure 1 is shown the varying of the n-gram conditional entropy with respect to the word length for the logistic map. The entropy per bit of a good RNG should be close to 1. High entropy level guarantees that the preceding or succeeding values cannot be guessed with a probability different from 0.5.

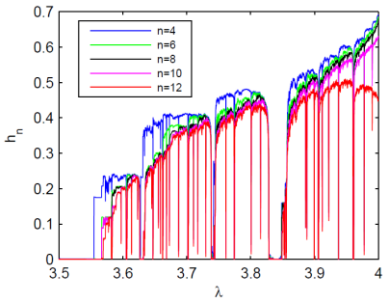

Fig. 1. n-gram conditional entropy with respect to the word length for the logistic map

Figure 2 illustrates x_n time series of logistic map when the initial condition $x_0 = 0.2$ and $\lambda = 3.9$, while Figure 3 illustrates y_n time series of logistic map when the initial condition $y_0 = x_0 + 10^{-8}$ and $\lambda = 3.9$. In Figure 4, we plot $\Delta_n = log|x_n - y_n|$. We see that for about the initial 30 iterations Δ_n increases more or less linearly until there is essentially no correlation left between x_n and y_n. In other words, an initial uncertainty in the state of the system of the order of 10^{-8} results after 30 time steps in a complete lack of knowledge of its behaviour. The rate at which uncertainty grows is given by the initial slope of the graph of $log|x_n - y_n|$ and corresponds to the largest Lyapunov exponent.

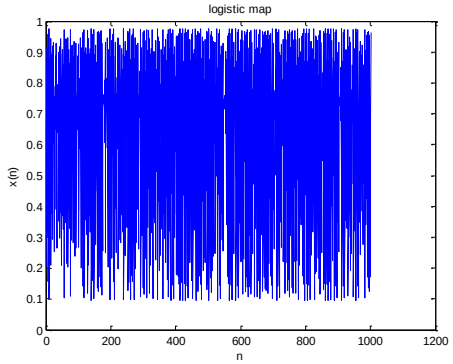

Fig. 2. x_n time series of logistic map when the initial condition x_0=0.2 and λ=3.9

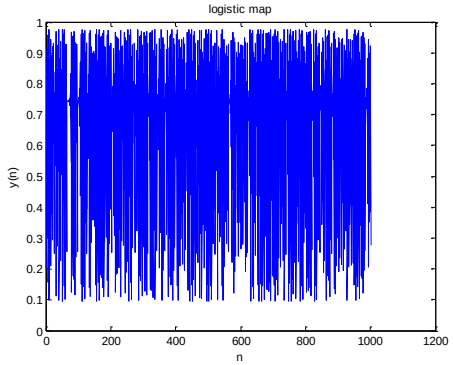

Fig. 3. y_n time series of logistic map when the initial condition $y_0=x_0+10^{-8}$ and λ=3.9.

Lyapunov exponent of logistic map is shown in Figure 5. Calculated Lyapunov exponents confirm that Lyapunov exponent connected with entropy measurements. Therefore, Lyapunov exponent can be used as analysis method for entropy source of RNG.

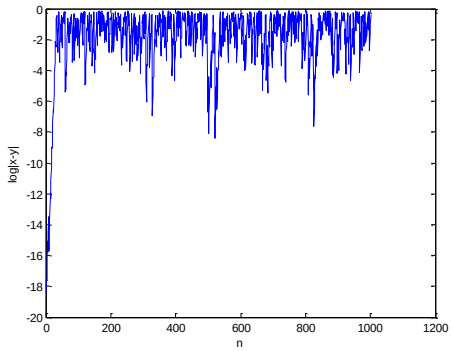

Fig. 4. $\Delta_n = log|x_n - y_n|$

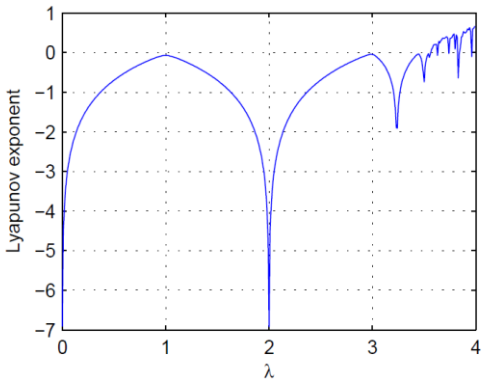

Fig. 5. Lyapunov exponent of logistic map

5. Conclusions

Suitability of RNG depends on the level of the generator's entropy. This level of entropy related to system dynamics. In this paper, we derive a relation between entropy and Lyapunov exponent. One can use this relation to determine, whether a given RNG is suitable for adequacy of entropy source or not. Proposed analysis method has been verified on a chaos based RNG designs, and fits to analysis of other RNG designs. In the future works, the theory of nonlinear dynamical systems can be providing new tools and quantities for the characterization of RNG.

References

1. A. J. Menezes, P. C. Oorschot, S. A. Vanstone. Handbook of Applied Cryptography, CRC Press, Boca Raton, Florida, USA, 1997.
2. W. Schindler: Random Number Generators for Cryptographic Applications. C .K. Koc (ed.): Cryptographic Engineering. Springer, Signals and Communication Theory, Berlin, 2009.

3. A. Savoldi, M. Piccinelli, P. Gubian, A statistical method for detecting on-disk wiped areas, Digital Investigation, 8/3–4 (2012) 194-214
4. P. Penrose, R. Macfarlane, W. J. Buchanan, Approaches to the classification of high entropy file fragments, Digital Investigation, 10/4 (2013) 372-384
5. F. Özkaynak, Cryptographically secure random number generator with chaotic additional input, Nonlinear Dynamics, 78/3, 2015-2020.
6. J. Sprott, Elegant Chaos Algebraically Simple Chaotic Flows. World Scientific, 2010.
7. L. Kocarev, S. Lian (Eds.), Chaos Based Cryptography Theory Algorithms and Applications, Springer-Verlag, 2011
8. L. Kocarev. G. Jakimoski, Pseudorandom bits generated by chaotic maps, IEEE Transactions on Circuits and Systems I: Fundamental Theory and Applications 50 (2003) 123-126.
9. T. Stojanovski, L. Kocarev, Chaos-based random number generators – Part I: Analysis, IEEE Transactions on Circuits and Systems I: Fundamental Theory and Applications 48 (2001) 281-288.
10. H. Kantz, T. Schreiber, Nonlinear Time Series Analysis 2nd Edition, Cambridge University Press, 2004.
11. A. Rukhin, J. Soto, J. Nechvatal, M. Smid, E. Barker, S. Leigh, M. Levenson, M. Vangel, D. Banks, A. Heckert, J. Dray, S. Vo, A statistical test suite for random and pseudorandom number generators for cryptographic applications, 2001.
12. F. Özkaynak, İ. H. Özdemir, A. B. Özer, Cryptographic Random Number Generator for Mobile Devices, 23th IEEE Signal Processing and Communications Applications Conference, 2015.

Simulation of Multidimensional Nonlinear Dynamics by One-Dimensional Maps with Many Parameters

Irina N. Pankratova[1] and Pavel A. Inchin[2]

[1] Institute of Mathematics and Mathematical Modeling, Dep. of Differential Equations, 050010 Pushkin str., 125, Almaty, Kazakhstan
(E-mail: inpankratova@gmail.com)
[2] Institute of Mathematics and Mathematical Modeling, Dep. of Differential Equations, 050010 Pushkin str., 125, Almaty, Kazakhstan
(E-mail: paul.inchin@yahoo.com)

Abstract. We propose a concrete class of discrete dynamical systems as nonlinear matrix models to describe the multidimensional multiparameter nonlinear dynamics. In this article we simulate the system asymptotic behavior. A two-step algorithm for the computation of ω-limit sets of the dynamical systems is presented. In accordance with the qualitative theory which we develop for this class of systems, we allocate invariant subspaces of the system matrix containing cycles of rays on which ω-limit sets of the dynamical systems are situated and introduce the dynamical parameters by which the system behavior is described in the invariant subspaces. As the first step of the algorithm, a cycle of rays which contains the ω-limit set of the system trajectory, is allocated using system matrix. As the second step, the ω-limit set of the system trajectory is computed using the analytical form of one-dimensional nonlinear Poincare map dependent on the dynamical parameters. The proposed algorithm simplifies calculations of ω-limit sets and therefore reduces computing time. A graphic visualization of ω- limit sets of n- dimensional dynamical systems, $n > 3$ is shown.
Keywords: Computer simulation, Nonlinear dynamics, Discrete dynamical systems, Dynamical parameters.

1 Introduction

To understand and analyse nonlinear multidimensional dynamics simple one-dimensional semi-dynamical systems with complicated dynamics and fairly complete qualitative description are used. These are, first of all, one-dimensional discrete dynamical systems, i.e. iterations of real one-dimensional maps. The first systematic results on one-dimensional discrete dynamical systems appeared in the early 60's and are linked to A.N. Sharkovskii [1]. Many properties of the dynamical systems are the direct result of the theories developed by A.N. Sharkovskii [2] and M. Feigenbaum [3]. A representative of this class of systems is the dynamical system generated by the one-dimensional logistic map

8^{th} *CHAOS Conference Proceedings, 26-29 May 2015, Henri Poicaré Institute, Paris France*

[4]. It was the first example of a complicated, chaotic behaviour of the system given by a simple nonlinear equation. Even though the properties of the one-dimensional logistic map are well studied, researchers continue referring to it as standard to check the many nonlinear phenomena [5]–[7]. However, up until now there is no well-developed qualitative theory available, which could be successfully applied in order to conduct a complete study of the multidimensional dynamical systems dependent on parameters. Therefore, it is appropriate to select concrete classes of the dynamical systems and to develop qualitative theories so as to be able to describe the properties and movements of the systems within these theories.

We focus our research on a concrete class of dynamical systems which represent a variant of generalization of one-dimensional discrete dynamical systems to the multidimensional multiparameter case. The systems are generated by a map in the form of the product of scalar and vector linear functions on compact sets of the real vector space. We propose the systems as nonlinear matrix models with limiting factors to describe the macro system dynamics, for example the dynamics of many group biological population in the presence of limited resources. In these models the scalar function plays a role of a limiting factor.

In recent years, the methods of computer simulation have become an essential tool in the study of the dynamical systems [8]–[10]. The modern computer capabilities make it possible to include in the system complicated nonlinear relationships between its variables and a large number of parameters. The presence of nonlinear relationships and multiparameter dependence reproduces in the model the phenomena which can be observed in actual experiments and which cannot be produced by splitting the system into separate components or reducing the number of parameters or variables. Thus, the improvement of current methods and the development of new ones for the dynamical system research are necessary and relevant [11,12]. In this case the quantitative research provides a theoretical basis for the algorithm constructions, and hence is particularly important.

We develop a qualitative theory for the class of the dynamical systems considered (see e.g. [13] and references there). The systems possess the obvious properties which are determined by the linear vector function (the system matix) and which do not depend on the scalar function. In particular, in vector space we allocate invariant subspaces containing cycles of rays of the system matrix, on which ω-limit sets of dynamical systems are situated. On the other hand, the complicated nonlinear dynamics of the systems can occur due to the scalar function. We study the system dynamics in the invariant subspaces containing cycles of rays using one-dimensional nonlinear Poincare maps and introduce the dynamical parameters by which the system behavior is described in the invariant subspaces. In this article we show the results of the simulation of the system asymptotic behavior and present an algorithm for the computation of ω-limit sets of the class of the dynamical systems considered. The algorithm consists of two steps of calculations in accordance with the qualitative theory. As the first step, a cycle of rays which contains the ω-limit set of the system trajectory is allocated using system matrix. The period of the cycle of rays, the number and values of the dynamical parameters by which the

system dynamics is described on the cycle of rays, are calculated as well. As the second step, the ω-limit set of the system trajectory is computed using one-dimensional nonlinear Poincare map dependent on the dynamical parameters. As a rule, these parameters differ from the system parameters and are unknown or not directly defined or computable [14]. The novelty of our research lies in the determination of the dynamical parameters and in the analytical form of one-dimensional nonlinear Poincare maps dependent on the dynamical parameters. We shall see below that the number of the dynamical parameters cannot be reduced without the loss of accuracy of the system behavior description, even when this number is greater than the number of the system parameters, i.e. entries of the system matrix.

2 Class of the dynamical systems

Let F be a map of the form [13]

$$F : \mathbb{R}^n \to \mathbb{R}^n, \;\; Fy = \Phi(y)Ay \tag{1}$$

where R^n is n- dimensional real vector-space, $\Phi(y)$ is a scalar function, A is a linear operator (a matrix of n-th order). Allocate set $\mathrm{X} \subseteq \mathbb{R}^n$ invariant under F i.e., $F : \mathrm{X} \to \mathrm{X}$. Map F in general is non invertible and generates in X a cyclic semi-group of maps $\{F^m\}$, $m \in Z_+$, which is called the dynamical system and is denoted by $\{F^m, \mathrm{X}, Z_+\}$. Set X is called phase space of the dynamical systems and specifies a set of valid states of the dynamical system, $Z_+ = \mathbb{N} \bigcup \{0\}$ is the set of nonnegative integers. Set $\{F^m y\}$ where y is fixed and m runs over Z_+, is called a trajectory of the point y. The dynamics of the system $\{F^m, \mathrm{X}, Z_+\}$ is understood as the process of transition from one state to another.

The dynamics of the system $\{F^m, \mathrm{X}, Z_+\}$ generally varies for different $\Phi(y)$. So, the systems $\{F^m, \mathrm{X}, Z_+\}$ are different too. But the systems possess similar properties which are determined by the linear operator A and do not depend on the function $\Phi(y)$. Therefore, the systems $\{F^m, \mathrm{X}, Z_+\}$ form one class of the dynamical systems.The elements of this class are, in particular, linear dynamical systems with $\Phi(y) = const$ and the dynamical system $\{f^m, \mathrm{X}, Z_+\}$ generated by the map f of the form [15]

$$f : \mathbb{R}^n \to \mathbb{R}^n, \;\; fy = (1 - \|y\|)Ay. \tag{2}$$

Here $\|\cdot\|$ is a vector norm in $\mathbb{R}^n$. If $n = 1$ then $A = \mu$ and we arrive at the well-known logistic map mentioned above

$$\psi_\mu : \mathbb{R}^1 \to \mathbb{R}^1, \quad \psi_\mu x = \mu(1 - x)x. \tag{3}$$

3 Mathematical models with limiting factors

We propose the class of the dynamical systems $\{F^m, \mathrm{X}, Z_+\}$ as mathematical models for describing the dynamics of model and real macro systems in the presence of limiting factors.

Let
n be a number of macro system's components,
$y \in \mathrm{X}$ be a vector of components' characteristics,
A be a matrix of components' interrelations and
$\Phi(y)$ be a limiting function (limiting factor).

Let X be a compact of the form

$$\mathrm{X} = \{y \in \mathbb{R}^n \mid y \geq 0, \ \ \|y\| \leq a\}, \quad a < \infty. \tag{4}$$

Here $y = (y_1, \ldots, y_n)' \geq 0$ means $y_i \geq 0$, $i = \overline{1,n}$ and is called a nonnegative vector. Note that X is invariant under F i.e., $F : \mathrm{X} \to \mathrm{X}$ if and only if [13]
1) $\Phi(y) \geq 0$ is continuous function on X,
2) $A = (a_{ij}) \geq 0$ ($a_{ij} \geq 0$, $i, j = \overline{1,n}$),
3) $\|A\| \leq aC^{-1}$ where $C = \max\limits_{y \in \mathrm{X}} \Phi(y)\|y\|$ and $\|A\|$ is a subordinate matrix norm for a matrix A based on the vector norm in $\mathbb{R}^n$.

Then the dynamical system $\{F^m, \mathrm{X}, Z_+\}$ describes the macro system's state changes over time m. For any nontrivial $\{F^m y\}$ we introduce a unit vector

$$e_m(y) = \|F^m y\|^{-1} F^m y \tag{5}$$

which is called a macro system structure and defines the ratio between components' characteristics at the time m. The state of macro system governed by the dynamical system $\{F^m, \mathrm{X}, Z_+\}$ (at the time m) we characterize by

$$S^m(y) = \{F^m y, e_m(y)\}. \tag{6}$$

The limiting factor concept was first coined in biology by Libig J. and generally, means a factor that restricts or constrains the dynamics of the system, process or phenomena. By using limiting factors, the state of the system is regulated.

On one hand, models given by the systems $\{F^m, \mathrm{X}, Z_+\}$ generalize in n- dimensional case many nonlinear one- and two-dimensional models widely used in practice. In particular, for describing the dynamics of n- group biological population with discrete generations in the presence of limited resources we propose the dynamical system generated by the map f of the form (2). In this representation y is a vector of densities of population age groups so, $\|y\| \leq 1$. If $n = 1$ then y is the total population density, $A \equiv \mu$ is the reproductive coefficient. The dynamical system $\{\psi_\mu^m, \mathrm{I}, Z_+\}$ in the interval $\mathrm{I}_1 = [0, 1]$ describes a mechanism of self-regulation of one-species biological population with limited resources [2].

On the other hand, models given by the systems $\{F^m, \mathrm{X}, Z_+\}$ generalize many matrix models, in particular, Leslie models both linear and nonlinear [16,17]. The last ones contain matrices A of the special form (Leslie matrix and its generalizations) and concrete limiting functions $\Phi(y)$.

4 Qualitative theory

We develop a qualitative theory for the class of the dynamical systems $\{F^m, \mathrm{X}, Z_+\}$ and apply the results of the theory in computer simulation of their dynamics.

Denote by $\omega_F y$ ω- limit set of the trajectory $\{F^m y\}$ (the set which attracts $\{F^m y\}$ when $m \to +\infty$). A ray passing through $y \in \mathbb{R}^n$, $y \neq 0$ is the set $\mathrm{cone}(y) = \{\alpha y \mid \alpha \geq 0\}$. By a system of p elements we mean a sequence of these elements, $p \in \mathbb{N}$. Then the system of distinct rays l_1, ..., l_p is called a cycle of rays of a linear operator A of period $p \in \mathbb{N}$ and is denoted by $\mathrm{L}_p = (l_1, ..., l_p)$ if

$$Al_k = l_{k+1}, \quad k = 1, \ldots, p-1, \quad Al_p = l_1.$$

As easy to see, that invariant sets of the system $\{F^m, \mathrm{X}, Z_+\}$ are contained in invariant subspaces of A. Denote $\ker A = \{y \in \mathbb{R}^n \mid Ay = 0\}$ and let

$$\mathcal{P}(A; p, \mu) = A^p - \mu^p E, \quad \mu \in \mathbb{C}.$$

We call the intersection $l \cap \mathrm{X}$ as a segment of ray l (ray segment). Denote by ϕ_μ map F when $n = 1$,

$$\phi_\mu x = \mu \Phi(x) x \tag{7}$$

where $x \in \mathrm{I_a} = [0, a]$. According to the qualitative theory there exist p, $q \in \mathbb{N}$, $\mu \in \sigma(A)$ such that any nontrivial ($\neq \{0\}$) $\omega_F y$ is located in some invariant subspace

$$\ker \mathcal{P}(A; p, \mu), \quad \mu^p > 0,$$

on a cycle of rays L_q where $\sigma(A)$ is a spectrum of A and q is a divisor of p, $1 \leq q \leq p$ [18]. More precisely, $\omega_F y \subseteq \mathrm{J_q} = \mathrm{L}_q \cap \mathrm{X} \subset \ker \mathcal{P}(A; p, \mu) \cap \mathrm{X}$ and $\mathrm{J_q}$ consists of q ray segments invariant under F^q. Without losing generality we agree $q = p$ and $\omega_F y \subseteq \mathrm{J}_p$. Then for the map F with $\Phi(\|y\|)$ map F^p represents in $\mathrm{J_p}$ as a superposition

$$F^p = \phi_{\mu_p} \circ \phi_{\mu_{p-1}} \circ \ldots \circ \phi_{\mu_1} \tag{8}$$

with some numbers $\mu_1 > 0, \ldots, \mu_p > 0$.

If to consider the system $\{F^m, \ker \mathcal{P}(A; p, \mu) \cap \mathrm{X}, Z_+\}$, then $\mu_1, \ldots, \mu_p$ turns into parameters. We call them dynamical parameters in contrast to the system parameters i.e. entries of the matrix A. Thus, in the whole X, the system dynamics is defined by the trajectory behavior in the sets $\ker \mathcal{P}(A; p, \mu) \cap \mathrm{X}$. So, by the parameters $\mu_1, \ldots, \mu_p$ the system dynamics is described in the whole X. Every ray segment of $\mathrm{J_p}$ is the one-dimensional Poincare section for the trajectories located in $\mathrm{J_p}$ and F^p is the one-dimensional first return (Poincare) map for the map F in each ray segment of $\mathrm{J_p}$. For the special form $\Phi(\|y\|)$ map F^p has analytical representation (8).

Denote by $e_1, \ldots, e_p$ the unit vectors directed along the ray segments of $\mathrm{J_p}$. We define $e_1, \ldots, e_p$ and $\mu_1, \ldots, \mu_p$ by the recurrent formulas. Let $p = 1$. Then $e_1 \geq 0$ is an eigen vector of the matrix $A \geq 0$ and there exists an eigen value $\mu > 0$ such as $Ae_1 = \mu e_1$. So, (8) takes the form

$$F = \phi_\mu. \tag{9}$$

Let $p > 1$ then $e_1 \geq 0$ is not an eigen vector of A, $\|e_1\| = 1$ and $e_2, \ldots, e_p$ are defined by the sequence

$$e_j = \|Ae_{j-1}\|^{-1} Ae_{j-1}, \quad j = \overline{2, p}. \tag{10}$$

Denote

$$\mu_j = \|Ae_j\|, \quad j = \overline{1,p}. \tag{11}$$

For the map F with different $\Phi(\|y\|)$, parameters $\mu_1, \ldots, \mu_p$ and vectors $e_1, \ldots, e_p$ are the same and their computation by the formulas (10)-(11) does not cause difficulties.

It should be noted that the dynamical parameters, their number and values depend on the location of the sets $\ker \mathcal{P}(A;p,\mu) \cap \mathrm{X}$ in X and J_p in $\ker \mathcal{P}(A;p,\mu) \cap \mathrm{X}$ and vary, as a rule, at the fixed entries of the matrix A. So, the dynamical parameters differ from the system parameters and identify the regions with different dynamics. Their number is less than or equal to p and may be very large, in particular, when $p > n^2$ at $n \geq 19$ [18]. According to (8) all parameters are involved in the representation of the map F^p so, their number cannot be reduced.

5 Computer simulation

We present computer simulation of multidimensional dynamics by the numerical realization of the models for the dynamics of biological population governed by the system $\{f^m, \mathrm{X}, Z_+\}$.

In the population model:
f is a map of the form (2): $fy = (1 - \|y\|)Ay$,
n is a number of population age groups,
y is a vector of densities of the age groups, $y \in \mathrm{X}$,
X is of the form (4) if $a = 1$ i.e.,

$$\mathrm{X} = \{y \in \mathbb{R}^n \mid y \geq 0,\ \|y\| \leq 1\},$$

A is a matrix of intergroup relations,
$\Phi(\|y\|) = 1 - \|y\|$ is a population size limiting function corresponding to the assumption of limited resources or available living space.

Let $\|y\| = \sum\limits_{1}^{n} y_i$ then the condition 3) for the invariance of X is as follows: $\|A\| = \max\limits_{j} \sum\limits_{i=1}^{n} a_{ij} \leq 4$. For any nontrivial $\{f^m y\}$ a unit vector $e_m(y) = \|f^m y\|^{-1} f^m y$ is an age structure of many-group population and defines the ratio between densities of age groups in total population density (at the time m). The state of the population governed by the dynamical system $\{f^m, \mathrm{X}, Z_+\}$ (at the time m) is $S^m(y) = \{f^m y, e_m(y)\}$.

According to the section 4, for any nonzero initial state $S^0(y)$, the structure of many-group population is asymptotically stabilized as p- periodic and is characterized by p vectors $e_1, \ldots, e_p$ defined by (10).

As to the population dynamics, we get that the many-group population model given by the dynamical system $\{f^m, \mathrm{X}, Z_+\}$ asymptotically has the same behavior as a family of one-species population models given by the one-dimensional systems $\{(\psi_{\mu_p} \circ \psi_{\mu_{p-1}} \circ \ldots \circ \psi_{\mu_1})^m, \mathrm{I}, Z_+\}$ where $\psi_{\mu_p} \circ \psi_{\mu_{p-1}} \circ \ldots \circ \psi_{\mu_1}$ is a superposition (8) with the map ψ_μ of the form (3) and $\mu_1, \ldots, \mu_p$ defined by (11).

Therefore, the population governed by the system $\{f^m, \mathrm{X}, Z_+\}$, has stabilized p- periodic structure at its final state, $p < \infty$ and densities of its age groups that change periodically or not. The same asymptotic behavior has the macro system governed by the system $\{F^m, \mathrm{X}, Z_+\}$ i.e., exactly p- periodic structure, $p < \infty$ and periodic or nonperiodic changes of its components' characteristics.

6 Method of one-dimensional superpositions

For correct determining cyclic ω-limit sets of large periods or chaotic ω-limit sets of the system $\{F^m, \mathrm{X}, Z_+\}$, we propose a computer method which we call as a method of one-dimensional superpositions. Let F be the map with a function $\Phi(\|y\|)$. The method implies calculations in two steps.

As the first step, a stable set J_p is determined for any nonzero $y \in \mathrm{X}$ using n- dimensional linear dynamical system $\{A^m, \mathrm{R}^n, Z_+\}$. At this step, period p is obtained and the unit vectors $\{e_1, \ldots, e_p\}$ along the rays of a cycle of rays L_p in which $\omega_F y$ is located, are computed by the matrix A. The number $1 \le t \le p$ and values of the dynamical parameters by which the trajectory dynamics in J_p is described, are computed as well. Here t is a divisor of p.

As the second step, set $\omega_F y$ is determined using the one-dimensional dynamical system $\{(\phi_{\mu_p} \circ \phi_{\mu_{p-1}} \circ \ldots \circ \phi_{\mu_1})^m, \mathrm{I}, Z_+\}$. At this step, the norm x of the projection of the vector y in the set J_p is obtained and a one-dimensional ω-limit set of the trajectory $\{(\phi_{\mu_p} \circ \phi_{\mu_{p-1}} \circ \ldots \circ \phi_{\mu_1})^m x\}$ is computed by the one-dimensional nonlinear Poincare map F^p with t parameters $\mu_1 > 0, \ldots, \mu_t > 0$. The points of this ω- limit set are coordinates of vectors which compose the part of $\omega_F y$ along the vector e_1.

The parts of $\omega_F y$ along the other vectors $e_2, \ldots, e_p$ are of the same type and structure and the vectors which compose these parts, are computed as well.

The method proposed simplifies calculations for large n and p for instance, $p > n^2$, $p > n^3$ and so on. Indeed, at first we detect the stable cyclic set J_p and later on we describe the trajectory dynamics in it. Using the method we compute any nontrivial set $\omega_F y$, in particular, we obtain the final state of many-group population for any nonzero initial state $S^0(y)$. The method also provides graphic visualization of ω- limit sets of n- dimensional dynamical systems $\{F^m, \mathrm{X}, Z_+\}$ at $n > 3$ and for large p.

The calculation algorithm for the computation of the set $\omega_F y$ and the final macro system state by the method of one-dimensional superpositions is as follows:

1. enter initial vector $y \ge 0$ and matrix $A \ge 0$ ($\|y\| < 1$, $\|A\| \le 4$);

1'. calculate eigen values and eigen vectors of matrix A;

2. calculate period p, vectors $e_1, \ldots, e_p$ of the set J_p and t distinct parameters $\mu_1, \ldots, \mu_t$ of the set $\{\mu_1, \ldots, \mu_p\}$ using (10), (11);

3. determine projection y' of vector y in the set $\mathrm{J_p}$ and calculate its norm $x = \|y'\|$;

4. obtain ω- limit set of the trajectory $\{\phi_{\mu_p} \circ \phi_{\mu_{p-1}} \circ \ldots \circ \phi_{\mu_1})^m x\}$ as some trajectory i.e.,

$$\omega_{\phi_{\mu_p} \circ \phi_{\mu_{p-1}} \circ \ldots \circ \phi_{\mu_1}} x = \{x_i^*\}_{i \ge 0}$$

where $x_i^* = (\phi_{\mu_p} \circ \phi_{\mu_{p-1}} \circ \ldots \circ \phi_{\mu_1})^i x^*$. After these calculations the iteration process stops;

5. The set $\omega_F y$ is a result of calculations done in step 4 and is the following set

$$\omega_F y = \{x^* e_1,\, (\phi_{\mu_1} x^*) e_2,\, (\phi_{\mu_2} \circ \phi_{\mu_1} x^*) e_3,\, (\phi_{\mu_3} \circ \phi_{\mu_2} \circ \phi_{\mu_1} x^*) e_4,\, \ldots,$$

$$(\phi_{\mu_{p-1}} \circ \ldots \circ \phi_{\mu_1} x^*) e_p,\, x_1^* e_1,\, \ldots\}.$$

So, vectors of $\omega_F y$ are of the form ue_i where $u \in \omega_{\phi_{\mu_p} \circ \phi_{\mu_{p-1}} \circ \ldots \circ \phi_{\mu_1}} x$, $i = \overline{1,p}$.

The final macro system state is a pair

$$S^*(y) = \{\omega_f y, E\} \quad \text{where } E = \{e_1, \ldots, e_p\}.$$

7 Examples

7.1 The dynamics of the Northern Spotted Owl

The algorithm for computing of the population dynamics is implemented in Matlab as a function with the following input data: n- dimensional initial vector $y \geq 0$ and matrix $A \geq 0$ of n order. The final state of the population is given as an output data in the form of two arrays of vectors.

Let us demonstrate this algorithm by simulating the dynamics of the Northern Spotted Owl. As an input data we use the real (3×3)- matrix A from article of Lamberson R., McKelvey R., at al. [19]. We would like to take into account limited resources for the population. For this purpose, in contrast to the linear model considered in [19], we propose nonlinear models given by the dynamical system $\{f^m, \mathrm{X}, Z_+\}$. In the models a proportional coefficient c is introduced as an input data to make the dynamics nontrivial.

Example 1. 1. enter a) $y = (0.1, 0.1, 0.1)'$,

b) $A = c \cdot \begin{pmatrix} 0 & 0 & 0.33 \\ 0.18 & 0 & 0 \\ 0 & 0.71 & 0.94 \end{pmatrix}$.

The elements in the top row of matrix A are fertility rates; the sub-diagonal elements are survival rates; nonzero diagonal element a_{ii} is the probability that females in stage i remain in the same stage next year;

c) $c = 3.1$ (almost maximum available value of c to fulfil $\|A\| \leq 4$);

2. vectors e_j of the set E with accuracy $\epsilon = 10^{-5}$ and parameters μ_j, $j = \overline{1,p}$, are computed. As a result, after 8 iterations, a convergence of the sequence of vectors $e_i(y)$ to E is obtained. The ultimate result is $p = 1$, $(n \times p)$- array $E = \{e\}$ and array $U = \{\mu\}$ where $e = (0.2402, 0.0440, 0.7159)'$, $\mu = 3.0491$;

3. given $x = 0.8$;

4. given accuracy $\epsilon = 10^{-5}$ for the trajectory $\{\psi_\mu^m x\}$ obtain $\omega_{\psi_\mu} x$ as a cycle of period 2 per 56 iterations,

$$\omega_{\psi_\mu} x = \{x^*, \psi_\mu x^*\} = \{0.5909, 0.7371\};$$

5. for the trajectory $\{f^m y\}$

$$\omega_f y = \{0.5909e, 0.7371e\} =$$

$$= \{(0.1419, 0.0260, 0.4230)', (0.1770, 0.0324, 0.5277)'\}.$$

The final population state is

$$S^*(y) = \{\omega_f y, E\} \quad \text{where } E = \{e\}$$

and is shown in Figure 1a.

Example 2. 1. enter a) $y = (0.1, 0.1, 0.1)'$,

b) $A = c \cdot \begin{pmatrix} 0 & 0 & 0.33 \\ 0.18 & 0 & 0 \\ 0 & 0.71 & 0 \end{pmatrix}$. In this model we suppose that there are no females remaining in the same stage next year;

c) $c = 5$ (almost maximum available value of c to fulfil $\|A\| \leq 4$);

2. vectors e_j with accuracy $\epsilon = 10^{-5}$ and parameters μ_j, $j = \overline{1,p}$, are computed. As a result, after 3 iterations, a convergence of sequence of vectors e_j to set E is obtained. The ultimate result is $p = 3$, $(n \times p)$- array $E = \{e_1, e_2, e_3\}$ and array $U = \{\mu_1, \mu_2, \mu_3\}$ where $e_1 = (0.3333, 0.3333, 0.3333)'$, $e_2 = (0.2705, 0.1475, 0.5820)'$, $e_3 = (0.5559, 0.1409, 0.3032)'$, $\mu_1 = 2.0333$, $\mu_2 = 1.7275$, $\mu_3 = 1.5009$;

3. as $A^3 = \lambda^3 I$ then y, $\{f^m y\}$ and $\omega_f y$ are located in the same set J_3. Here $\lambda = 1.7404$ is the maximum eigenvalue of $A \geq 0$ and I is identity matrix. So, calculate $x = \sum_1^3 y_i = 0.3$;

4. given accuracy $\epsilon = 10^{-5}$ for the trajectory $\{(\psi_{\mu_3} \circ \psi_{\mu_2} \circ \psi_{\mu_1})^m x\}$ obtain $\omega_{\psi_{\mu_3} \circ \psi_{\mu_2} \circ \psi_{\mu_1}} x$ as a fixed point per 8 iterations,

$$\omega_{\psi_{\mu_3} \circ \psi_{\mu_2} \circ \psi_{\mu_1}} x = \{x^*\} \quad \text{where } x^* = 0.368;$$

5. for the trajectory $\{f^m y\}$

$$\omega_f y = \{x^* e_1,\ (\psi_{\mu_1} x^*) e_2,\ (\psi_{\mu_2} \circ \psi_{\mu_1} x^*) e_3\} = \{(0.1227; 0.1227; 0.1227)',$$

$$(0.1279; 0.0698; 0.2752)', (0.2394; 0.0607; 0.1306)'\}.$$

The final population state is

$$S^*(y) = \{\omega_f y, E\} \quad \text{where } E = \{e_1, e_2, e_3\}$$

and is shown in Figure 1b.

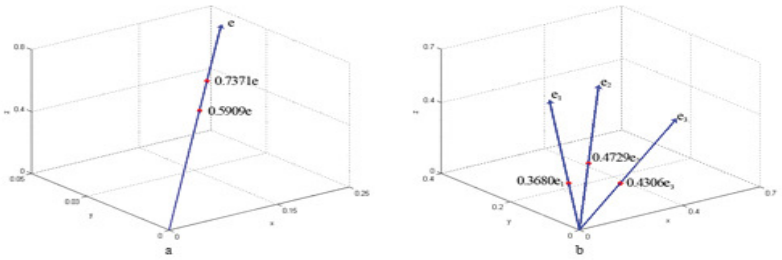

Fig. 1. Final states $S^*(y)$ of three-group populations with two different matrices $A \geq 0$ and the same initial vectors y

7.2 The dynamics of macro system composed of a large number of components

In the next two examples we demonstrate the advantages of the method of one-dimensional superposition in graphic visualization of the final macro system state at $n > 3$ and $p > n$. We briefly summarize the results obtained by the method. Assume that the macro system dynamics is described by the dynamical system $\{f^m, \mathrm{X}, Z_+\}$.

Example 3. Let $n = 10$ and A be (10×10)- matrix of a quasidiagonal form $\{A_1, A_2, A_3\}$ with matrices A_j on the main diagonal,

$$A_1 = \begin{pmatrix} 0 & 3.2 \\ 3.2 & 0 \end{pmatrix}, \quad A_2 = \begin{pmatrix} 0 & 2.56 & 0 \\ 0 & 0 & 3.2 \\ 4 & 0 & 0 \end{pmatrix}, \quad A_3 = \begin{pmatrix} 0 & 2.56 & 0 & 0 & 0 \\ 0 & 0 & 4 & 0 & 0 \\ 0 & 0 & 0 & 4 & 0 \\ 0 & 0 & 0 & 0 & 3.2 \\ 2.56 & 0 & 0 & 0 & 0 \end{pmatrix}.$$

(Matrix A is not a real matrix of the subsystems' relations, just some model matrix). Matrix A has 10 eigenvalues in modulus 3.2.

Enter $y = (0, 0.1, 0.1, 0.1, 0.1, 0.05, 0.05, 0, 0.3, 0.05)'$ and A as an input data.

As an ultimate result we get $p = 15$ and (10×15)- array E consisting of 15 vectors.

Given accuracy $\epsilon = 10^{-10}$ for the trajectory $\{(\psi_{\mu_{15}} \circ \psi_{\mu_{14}} \circ \ldots \circ \psi_{\mu_1})^m x\}$ its ω- limit set is a cycle of period 4.

For the trajectory $\{f^m y\}$ its ω- limit set $\omega_f y$ is a cycle of period $60 = 4 \cdot 15$.

The final macro system state is $S^*(y) = \{\omega_f y, E\}$.

We present graphic visualization of the part of $\omega_f y$ located in $\mathrm{J_p}$ along the vector e_1 i.e., four vectors with coordinates x^*, $(\psi_{\mu_p} \circ \ldots \circ \psi_{\mu_1})x^*$, $(\psi_{\mu_p} \circ \ldots \circ \psi_{\mu_1})^2 x^*$, $(\psi_{\mu_p} \circ \ldots \circ \psi_{\mu_1})^3 x^*$. In XY coordinate system four vectors with the same coordinates along the unit vector of the bisector of the first coordinate angle are drawn and their graphic image is shown in Figure 2a. The parts of $\omega_f y$ located in $\mathrm{J_p}$ along the vectors $e_2, \ldots, e_p$, are of the same type i.e., each of them consists of four vectors.

Example 4. Change the initial vector to $y = (0.1, 0.1, 0, 0.3, 0.1, 0, 0, 0, 0.3, 0.05)'$.

The ultimate result is $p = 30$ (the maximum possible value at $n = 10$), (10×30)- array E now consists of 30 vectors.

Given accuracy $\epsilon = 10^{-10}$ for the trajectory $\{(\psi_{\mu_{30}} \circ \psi_{\mu_{29}} \circ \ldots \circ \psi_{\mu_1})^m x\}$ we get non-stop iterative process when calculating its ω- limit set. It means that ω- limit set is irregular or a cycle of a very large period. In this case we agreed to accept the last 200 iterations when calculating the trajectory $(\psi_{\mu_{30}} \circ \psi_{\mu_{29}} \circ \ldots \circ \psi_{\mu_1})^m x$ as its ω- limit set.

Graphic visualization of 200 vectors which are the part of $\omega_f y$ located in $\mathrm{J_p}$ along the vector e_1, is presented in XY coordinate system by 200 vectors with the same coordinates, along the unit vector of the bisector of the first coordinate angle. The graphic image of these vectors is shown in Figure 2b.

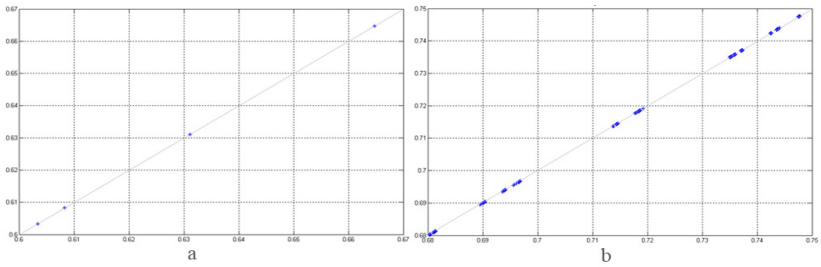

Fig. 2. Graphic visualization of the parts of $\omega_f y$ located along the vectors e_1 for two different initial vectors y

7.3 Outcomes of examples

The examples 1-2 show that in the first model the population structure is asymptotically stabilized and does not vary any more and population size, as well as age group sizes change periodically every two years. In the second model the structure of the population is stabilized and varies every three years along with the population size and age group sizes. Examining the dynamics of the population, one can see the mechanism of regulation or harvestable surplus of the population size without affecting long term stability, or average population size. Indeed, according to the second model all individuals of the third stage may be taken away after the childbearing period ($a_{33} = 0$) every year. In spite of the structure of the population, its size and age group sizes vary periodically, in this case the population remains persistent.

Stabilized periodic structure of macro system is determined by its initial structure and not its initial size. Indeed, by iterating the map F of the form (1) m times, we write out $F^m y = \Phi^{(m)}(y) A^m y$ where

$$\Phi^{(m)}(y) = \prod_{i=0}^{m-1} \Phi(F^i y),$$

$y \in$ X. Hence it follows that the directions of $F^m y$ and $A^m y$ coincide, $m = 1, 2, \ldots$ i.e., the directions of nonzero vectors of the trajectory $\{F^m y\}$ as $m \to \infty$ are defined by the linear part of the map F and are independent of the form of $\Phi(y)$.

Let all nonzero entries of the matrix A be equal to 3.2 in the examples 3-4. Then $\mu_1 = \ldots = \mu_p = \mu = 3.2$, $\psi_{\mu_p} \circ \ldots \circ \psi_{\mu_1} = \psi_\mu^p$. and $\omega_{\psi_\mu^p} x$ is a cycle of period 2 for any $x \in$ I [2, p. 26]. According to [20] there are more than one periodic attractors and therefore more than one different dynamics of the map $\psi_{\mu_p} \circ \ldots \circ \psi_{\mu_1}$, $p \geq 1$ at the fixed parameter values. So, if there is only one asymptotic regime of the map $\psi_{\mu_p} \circ \ldots \circ \psi_{\mu_1}$ in the interval I at the fixed $\mu_1, \ldots, \mu_p$, then macro systems with the same initial structure will have the same final state. If there are more than one asymptotic regimes of the map $\psi_{\mu_p} \circ \ldots \circ \psi_{\mu_1}$ in the interval I at the fixed $\mu_1, \ldots, \mu_p$, then macro systems with the same initial structure will have the same stabilized periodic structure and may have different sizes changed periodically (or not).

8 Conclusion

In this article we describe an approach we have developed to study multiparameter nonlinear dynamics. The advantages of applying the results of the qualitative theory and using the method of one-dimensional superpositions in a simulation of the dynamics are as follows:

1. The dynamical systems considered are nonlinear and thus very sensitive to the data entry errors. The proposed method simplifies computations of the ω- limit set of the system trajectory. Firstly, a stable cycle of rays of period p, which contains the ω- limit set, is identified using the system matrix of the n-th order. Secondly, the ω- limit set is obtained using the non-linear one-dimensional map. As a result, this leads to markedly reduced computing times, especially when the order n and the periods p are large.

2. In an n- dimensional case, $n > 3$ it is impossible to obtain a graphic image of ω- limit sets of the dynamical system, e.g. to realize their types. However, we can get graphic visualization of the part of ω- limit sets consisting of vectors along the first unit vector of the stable invariant set containing the ω- limit set. In an XY coordinate system, vectors along the unit vector of the bisector of the first coordinate angle which have the same coordinates can be easily plotted.

3. Theoretical results of the qualitative theory help us to correctly interpret the numerical results as well as to conduct an accurate computer simulation of the system dynamics. We specify the number of iterations to detect a stable cycle of rays containing the ω- limit set of the system as well as the number of iterations to compute the ω- limit set.

4. The determination of the dynamical parameters and the calculation of their number and values by the formulas provides the description of the system dynamics in stable cycles of rays containing ω- limit sets of the system and therefore, the identification of the regions with different dynamics. Their number may be very large, e.g. greater than the number of the system parameters.

However, one can see that this number cannot be reduced without the loss of accuracy of the system behavior description.

Acknowledgements

The work is supported by the grant 0292/GF3 of Ministry of Education and Science of the Republic of Kazakhstan.

References

1. A.N. Sharkovskii. Co-existence of cycles of a continuous mapping of the line into itself. *Ukrainian Math J*, 16:61-71, 1964.
2. A.N. Sharkovskii, Yu.L. Maistrenko, E.Yu. Romanenko. *Difference Equations and Their Applications*, Naukova Dumka, Kiev, 1986 (in Russian).
3. M. Feigenbaum. Quantative universality for a class of nonlinear transfomaions. *J Stat Phys*, 19:25-52, 1978.
4. R.M. May. Simple mathematical models with very complicated dynamics. *Nature*, 261(5560):459-467, 1976.
5. A.G. Radwan. On some generalized discrete logistic maps. *J Adv Res*, vol. 4, issue 2, 163-171, 2013.
6. G. Tiozzo. Topological entropy of quadratic polynomials and dimension of sections of the Mandelbrot set. *Adv in Math*, vol. 273, no. 19, 651715, 2015. doi:10.1016/j.aim.2014.12.033
7. M. Joglekar and J.A Yorke. Robustness of periodic orbits in the presence of noise. *Nonlinearity*, vol. 28, no. 3, 697-711, 2015. doi:10.1088/0951-7715/28/3/697
8. Z. Arai, W. Kalies, H. Cocubu, K. Mischaikow et al. A Database Schema for the Analysis of Global Dynamics of Multiparameter Systems. *SIAM J Appl Dyn Syst*, vol. 8, no. 3, 757-789, 2009.
9. I. Gohberg, P. Lancaster, L. Rodman. *Invariant Subspaces of Matrices with Applications*, Siam, 2006.
10. A. Kaw, E. Kalu, D. Nguyen. *Numerical methods with applications*, Univ of South Florida, 2009.
11. J. Sabuco, M.A.F. Sanjuan, and J.A. Yorke. Dynamics of partial control. *Chaos*, vol. 22, no. 4, 047507-1-047507-9, 2012.
12. A.S. de Paula, M.A. Savi. State space reconstruction applied to a multiparameter chaos control method. *Meccanica*, 50:207-216,2015. doi: 10.1007/s11012-014-0066-z
13. I.N. Pankratova, Cyclic Invariant Sets for One Class of Maps. *Siberian Math J*, vol. 50, no. 1, 107-116, 2009. doi:10.1007/s11202-009-0013-8
14. R. Muradore, R. Foroncelli and P. Fiorini. Statistical methods for estimating the dynamical parameters of manipulators. In: *Proc. of joint 48th IEEE Conf on Decision and Control and 28th Chinese Control Conf*, 6472-6477, 2009. doi: 10.1109/CDC.2009.5400194
15. I.N. Pankratova. Limit sets of manydimensional analogy of nonlinear logistic difference equation. *Differ Equ*, vol. 32, no. 7, 1006-1008, 1996.
16. P.H. Leslie. The use of matrices in certain population mathematics. *Biometrika*, 33:183-212, 1945.
17. D. O. Logofet. Projection matrices revisited: a potential-growth indicator and the merit of indication. *J Math Sci*, vol. 193, no. 5, 671-686, 2013.

18. I.N. Pankratova. On some properties of invariant subspaces of linear operator containing cycles of rays. In: *Conf Program and Book of Abstr of Conf MAT TRIAD*, Herceg Novi, Montenegro, 49-50, 2013. http://mattriad2013.pmf.uns.ac.rs/programme.php
19. R. Lamberson, R. McKelvey, B. Noon, C. Voss. A Dynamic Analysis of Northern Spotted Owl Viability in a Fragmented Forest Landscape. *Conserv Biol*, vol. 6, no. 4, 505-512, 1992.
20. J. Guckenhemer, G.F. Oster and A. Ipartchi. The Dynamics of Density Dependent Population Models. *J Math Biol*, 4:101-147, 1976.

The Complete Bifurcation Analysis of Switching Power Converters with Switching Delays

Dmitrijs Pikulins[1]

[1] Institute of Radioelectronics, Riga Technical University, Riga, Latvia
(E-mail: dmitrijs.pikulins@rtu.lv)

Abstract. The nonlinear dynamics of switching power converters has been actively studied during several last decades, proving the existence of extremely complex dynamical scenarios and uncommon routes to chaos in this kind of circuits. The main assumption in the majority of researches was that the control circuitry consisted of ideal elements, discarding all parasitics of feedback circuitry components. However, recently it has been shown that the inherently arising nonidealities, such as delays, could lead to the drastic changes in the overall dynamics of the system. This research is dedicated to the investigation of the effects of the delays on the global nonlinear behavior of switching DC-DC converters on the basis of complete bifurcation analysis, providing the most comprehensive information on the causes and consequences of all nonlinear phenomena in the systems under study.
Keywords: Bifurcations, chaos, non-smooth phenomena, switching power converters

Introduction

Active research performed during several last decades showed that the commonly used linearized models, describing the dynamics of switching power converters (SPC) are not capable of predicting the majority of instabilities, occurring in those systems [1,2]. Thus the classical models fail to provide reliable information for the feedback designers that would allow the development of stable control loops. The limited applicability of mentioned models has led to the development of some alternative approaches, based on non-linear models and analysis methodologies. While making the study of global dynamics of these systems more complicated, the latter approaches allow increasing the robustness and reliability of designed systems as the great amount of new unstable and potentially dangerous regimes could be detected.

The vast majority of researchers, working on the analysis of non-linear dynamics of SPC, have focused on the development of simplified models that could be used within their investigations. However, it has been shown that ignoring some unavoidable non-idealities of the control circuitry may lead to erroneous results and misinterpretation of analytically obtained data [3]. One of the most noticeable effects, that should be taken into account during the analysis

8th CHAOS Conference Proceedings, 26-29 May 2015, Henri Poincaré Institute, Paris France

of such feedback controlled systems, is the inherent delay of each component of the control loop. The delay of individual element in the analog feedback loop is not large enough to influence the global dynamics of the system. Though as all the delays are summed together, the time lag in the propagation of the control signal becomes essential.

The current paper studies the effects of the magnitude of the overall delay on the dynamics of one of the most widely used SPC – boost converter under current-mode control. It is assumed that the analog feedback loop is implemented and the appropriate values of delays are introduced. The analysis of bifurcation patterns is based on the discrete-time model of mentioned DC-DC converter and the Method of Complete Bifurcation Groups (MCBG).

The structure of the paper is as follows. Second section describes the principles of operation of the boost converter as well as presents the corresponding model. Third section provides the complete bifurcation analysis of SPC, changing the most relevant circuit parameters. The last section is dedicated to conclusions about the results obtained in Section 3, defining some common points and showing the perspective of future research.

2 Model of the boost converter with delays

The simplified schematic of the boost type SPC under current-mode control including delay is shown in the Fig.1. It consists of two active elements: capacitor *C* and inductor *L*; two switching elements: one of them marked as *S* could be a MOSFET transistor (the state of which is controlled by the voltage applied to the gate), the second one – *D*–is the diode (that is turned *ON* or *OFF* in accordance to the difference of voltages between its terminals). *R*, V_{in} and V_{out} represent accordingly simple resistive load, input and output voltages. Δt_d represents the total delay of all elements in the control loop.

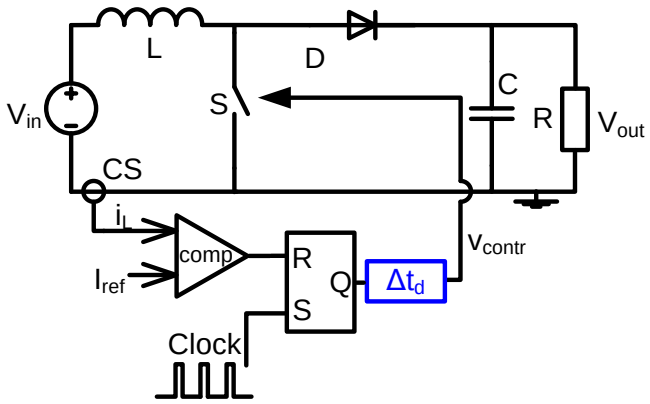

Fig.1. Simplified schematics of boost SPC under current-mode control

The control circuitry, shown above the main power plant, consists of current sensor (CS), comparator (comp), RS type flip-flop as well as clock element.

The principle of operation is as follows. When the switch *S* is in the *ON* (conducting) state, the energy is transferred to the inductor and the load is provided with the necessary amount of energy by the output capacitor. During the *OFF* interval the required output voltage is maintained by the input voltage and the energy released from the collapsing magnetic field of the inductor.

As it could be seen from Fig.1, the position of the switching element *S* is defined by the output signal of the control circuitry v_{contr}. In the case of ideal control loop with $\Delta t_d=0$, the switch is turned *ON* at the arrival of the next clock pulse and is switched *OFF* as the value of inductor current, obtained from the current sensor, reaches the reference value (see Fig. 2.a). However, real analog control loops include the non-zero delay, which is formed by the sum of current sensors', comparator', RS flip-flops' as well as MOSFET drivers' switching delays that are unified in the single block Δt_d in the Fig.1.

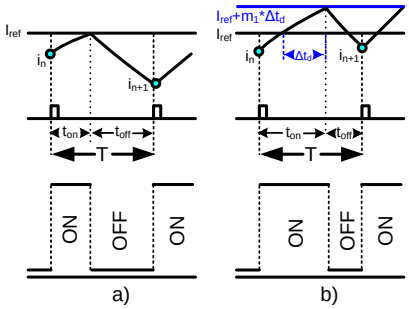

Fig.2. Waveforms of the inductor current and control signals: a) ideal case; b) including delay Δt_d

The delay causes the switch not to turn *OFF* at the moment the control parameter reaches some reference value defining new dynamical scenarios (see Fig. 2.b). The maximal value of sensed inductor current in this case is not limited by predefined reference I_{ref} and becomes dependent on the delay, reaching the value $I_{ref}+m_1*\Delta t_d$, where the slope of the rising inductor current $m_1=V_{in}/L$.

The dynamics of this type of energy converters could be described by systems of differential equations. However, the bifurcational analysis on the basis of this model would require great amount of computations. Another more effective approach is the use of discrete-time model in the form of iterative map that would allow obtaining exact values of inductor current and capacitor voltage samples at every switching instant without excessive effort [4]. The proposed model for the boost converter including the delay is as follows.

First, it should be noted that the overall dynamics of the converter is governed by the positions of the samples of inductor current in correspondence to the two

borderlines shown in Fig.3. The first borderline defines the case when the inductor current reaches the shifted reference value exactly at the arrival of next clock pulse (see Fig. 3.a). The second borderline represents i_n value for which the next sample i_{n+1} falls exactly to the I_{ref} for the falling inductor current (see Fig. 3.b).

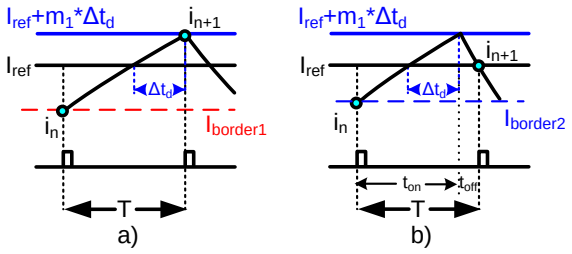

Fig. 3. Definition of borderlines and corresponding positions of inductor current samples: a) $I_{border1}$; b) $I_{border2}$

Thus the borderlines are:

$$I_{border1} = I_{ref} + m_1(\Delta t_d - T)\,, \tag{1}$$

$$I_{border2} = I_{border1} + m_1 \Delta t_d / \alpha\,, \tag{2}$$

where $m_1=V_{in}/L$, Δt_d - the value of delay, T– switching period, I_{ref}– reference current, L - value of inductance, R– load resistance; parameter α could be found using methodology proposed in [5] as the positive solution of this quadratic equation:

$$(1+\alpha)^2 V_{in}/R + \alpha V_{in} T/3L = I_{ref} + m_1 \Delta t_d\,. \tag{3}$$

Thus, taking into account (1)-(3), the discrete-time model is defined as:

1. if $i_n < I_{border1}$:

$$\begin{aligned} v_{n+1} &= v_n \exp(-T/RC) \\ i_{n+1} &= i_n + V_{in} T/L\,; \end{aligned} \tag{4}$$

2. if $I_{border1} < i_n < I_{ref}$:

$$\begin{aligned} v_{n+1} &= \exp(-mt_{off})\left[K_1\cos(\mu t_{off}) + K_2\sin(\mu t_{off})\right] + V_{in} \\ i_{n+1} &= \exp(-mt_{off})\begin{bmatrix}(K_1\cos(\mu t_{off}) + K_2\sin(\mu t_{off}))(1/R - mC) + \\ + \mu C(-K_1\sin(\mu t_{off}) + K_2\cos(\mu t_{off}))\end{bmatrix} + V_{in}/R\,; \end{aligned} \tag{5}$$

3. if $I_{ref} < i_n < I_{ref} + m_1 \Delta t_d$, then there are two possible scenarios, which are dependent on the value of the inductor current in the previous cycle:

3.1. if $I_{border1} < i_{n-1} < I_{border2}$, than the dynamics of the system between i_n and i_{n+1} is governed by:

$$\begin{aligned} v_{n+1} &= \exp(-mT)\left[K_3\cos(\mu T) + K_4\sin(\mu T)\right] + V_{in} \\ i_{n+1} &= \exp(-mT)\begin{bmatrix}(K_3\cos(\mu T) + K_4\sin(\mu T))(1/R - mC) + \\ + \mu C(-K_3\sin(\mu T) + K_4\cos(\mu T))\end{bmatrix} + V_{in}/R\,; \end{aligned} \tag{6}$$

3.2. if $i_{n-1}<I_{border1}$,than the dynamics of the system is governed by (5),

where: $p=1/\sqrt{LC}$; $\mu=\sqrt{p^2-m^2}$; $K_1=v_n\exp(-2mt_{on})-V_{in}$;

$K_2=\left((I_{ref}+m_1\Delta t_d)/C-m(v_n\exp(-2mt_{on})+V_{in})\right)/\mu$; $K_3=v_n-V_{in}$;

$K_4=\left(i_n/C-m(v_n+V_{in})\right)/\mu$; $t_{on}=(I_{ref}-i_n)/m_1+\Delta t_d$, $t_{off}=T-t_{on}$;

$m_1=V_{in}/L$.

Parameters of the system under investigation are as follows: V_{in}=3.3 (V); L=150 (μH); C=2 (μF); R=40 (Ω); I_{ref}= 0.2…0.7 (A); T=10 (μs); Δt_d=(0…0.2)*T (s).

3 Complete bifurcation analysis

The analysis of bifurcation patterns in this paper is based on the relatively new methodology – Method of Complete Bifurcation Groups – originally developed in the Institute of Mechanics of Riga Technical University for the analysis of complex dynamics of highly nonlinear mechanical systems [6]. This approach has been applied to the great variety of dynamical systems, including mechanical, biological and electrical ones [7-9]. The main distinctive feature of the MCBG is that the construction of bifurcation diagrams is not based on the widely used brute-force approach, when only stable periodic regimes are plotted using the process of simple iterations (also called natural transition). The mentioned brute-force method does not provide the complete information even about all existing stable regimes, not to mention unstable ones that are not taken into account in this approach. The MCBG is based on the numerical calculation of all stable and unstable periodic regimes (up to period of interest) in the system with following continuation of branches in the bifurcation diagram as some of the system's parameters are varied. This approach allows the construction of complete bifurcation diagrams, depicting even small regions of periodicity as well as unfolding unambiguous interconnections between different periodic as well as chaotic modes of operation.

On the basis of MCBG the complete bifurcation diagrams for the boost type converters with ideal feedback loop and for the system taking into account the delays in the control circuitry, have been constructed. The most obvious choice of the primary bifurcation parameter is the value of I_{ref} that could be changed during the operation of the SPC in order to preserve the desired output voltage.

The complete bifurcation diagrams obtained for the system with a various delays allow detection of some most distinctive changes in nonlinear dynamics of DC-DC converters as we vary the bifurcation parameter.

First, the complete bifurcation diagram for Δt_d=0 (i.e. in the ideal model without any delays) is constructed (see Fig. 4). Dark lines represent stable periodic regimes, light lines – numerically calculated unstable regimes, dashed lines depict the borderlines defined in (1) and (2), the shaded area represents the chaotic mode of operation.

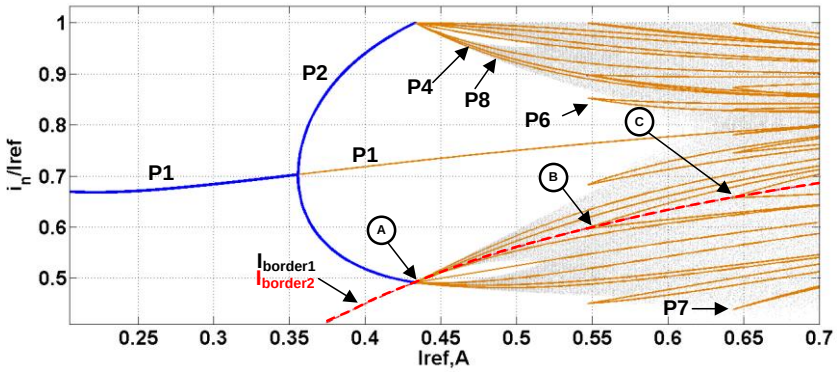

Fig.4. Complete bifurcation diagram of the boost converter with ideal control loop

The increment of reference current leads to the smooth transition from *P1* to *P2* operation through classical period-doubling bifurcation at I_{ref}≈0.36 (A). At point *(A)* the border collision (BC) with $I_{border1}$ and $I_{border2}$ appears (these borders overlap in the case of ideal system), leading to the formation of 4-piece chaotic attractor, converging to the robust chaotic area. The chaos is robust in the sense it is not interrupted by presence of stable periodic windows within the whole range of increasing bifurcation parameter. The MCBG allows the verification of the fact that in this case the great amount of unstable periodic orbits of *P4*, *P8*, *P16*, *P32* etc. appear at the point of the first BC (see Fig.4. point *(A)*, where only unstable branches of *P4* and *P8* are shown for the sake of simplicity). Thus the overall classical period doubling cascade is formed within the single point in the bifurcation diagram without the appearance of any stable subharmonic orbits. All the subsequent BC do not allow the formation of any stable orbits (see e.g. points *(B)* and *(C)* in the Fig.4.).

The structure of chaotic modes of operation and the mechanisms of transition to chaos noticeably change with the introduction of even slight delay in the control circuitry of DC-DC converter.

Fig.5 shows the bifurcation diagram of boost converter for Δt_d =0.05**T* (s). As it could be seen, the presence of delay does not affect the way the main *P1* mode of operation losses its stability – the classical period doubling bifurcation is observed. However, the following dynamics is formed by the non-smooth nature of collisions with two borderlines (see (1) and (2)), crossing the branches of bifurcation diagram.

$I_{border2}$ causes the appearance of discontinuity in the stable branch of $P2_1$ regime (see Fig. 5. point *(D)*) after which the next collision with the $I_{border1}$ (see Fig. 5. point *(E)*) changes the bifurcation sequence (in comparison to Fig.4) – the non-smooth transition to stable *P4* regime is observed. On the interval I_{ref} = 0.45…0.55 (A) the transition to robust chaos is defined not by the multiple piece

chaotic attractors, but by the sudden appearance and non-smooth transitions of subharmonic modes of operation caused by BC with both of the defined borders.

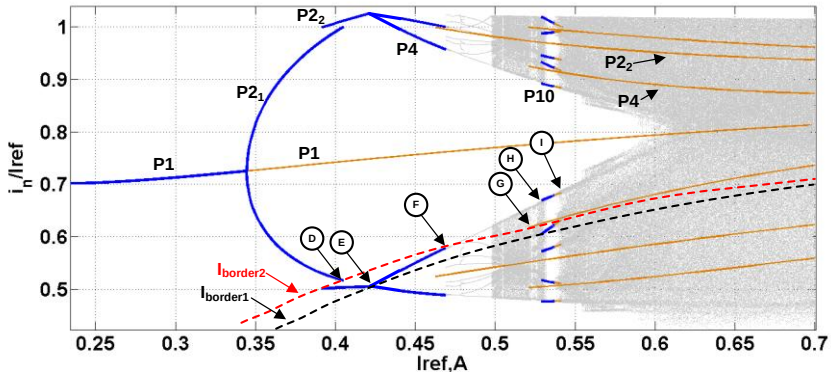

Fig.5. The complete bifurcation diagram of the boost SPC with Δt_d=0.05**T* (s)

One distinguishing feature of the diagram, shown in the Fig. 5, is that there is the region of coexistence of two stable *P2* regimes in the neighborhood of the first BC point (around I_{ref} = 0.4 (A)). Two different types of fixed points could be detected here – one is the attracting node with both characteristic multipliers real ($P2_1$), and the other – spiral attractor with complex conjugate characteristic multipliers ($P2_2$). Each of the regimes has its own basin of attraction. However, this bistability region is not important for practicing engineers, as it exists for very narrow range of bifurcation parameter, the periodicity of coexisting regimes is the same and the coordinates of fixed points are relatively close, so any excessive voltages or currents that could damage components of the switching power converter are not observed in this case.

As it could be seen from Fig.5, the $P2_2$ regime after the collision with $I_{border1}$ at point *(E)* does not just lose its stability, but disappears, meaning that the presence of stable or unstable period-2 regimes could not be detected to the right of the BC point with any numerical methods. However, the unstable branch of this regime is later detected in the vicinity of point *(F)*, where the *P4* regime disappears. The *P4* regime reappears at point *(G)*. The nature of the disappearance and sudden appearance of such periodic regimes in non-smooth systems up to author's knowledge is not yet clear and should be studied in details. In [10] this phenomena has been defined as "cutting border collision", as just after BC point no periodic orbit of the same periodicity is observed.

In the region between I_{ref} = 0.5…0.6 (A), the appearance of *P10* window is defined by both borderlines. The collision with $I_{border1}$ leads to the non-smooth transition from chaotic mode of operation to *P10* orbit (see Fig.5 point *(H)*). However, as the value of I_{ref} is further increased, the periodic window does not form classical period doubling route to chaos – the collision with $I_{border2}$ defines direct abrupt transition to chaotic mode of operation (see Fig.5 point *(I)*).

The described *P10* regime is the last periodic window within the chaotic region and all the following periodic orbits occur to be unstable, not causing the interrupts of robust chaotic operation as the bifurcation parameter is varied.

It should also be mentioned that the first relevant transition from the only practically acceptable stable *P1* operation to *P2* mode in this case appears almost at the same value as in the system without the delayI_{ref}≈0.36 (A). Thus, the introduction of relatively small delays do influence the dynamics of the system only after the first smooth period-doubling bifurcation.

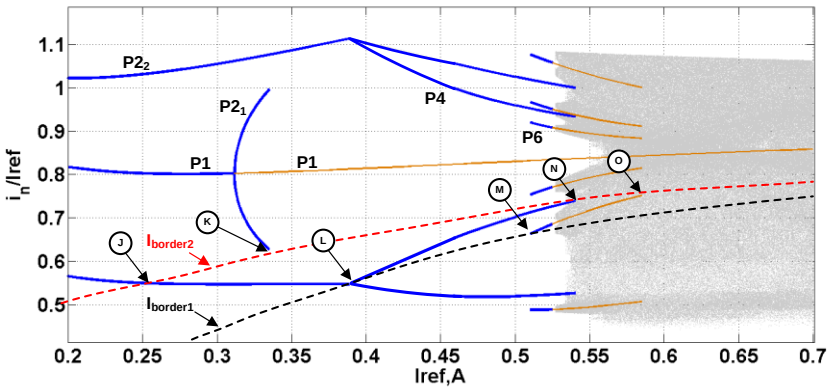

Fig. 6. The bifurcation diagram of the boost converter with Δt_d=0.2**T* (s)

The last complete bifurcation diagram (see Fig.6) depicts the case of Δt_d = 0.2**T* (s), when the complete structure of the bifurcation diagram drastically changes in comparison to Fig. 5. For small values of I_{ref} two coexisting regimes, namely *P1* and $P2_2$, define the dynamics of the SPC. In this case the system could not reliably operate in the required stable *P1* mode, as even small amount of noise (always present during the operation of SPC) could lead the system to operate in $P2_2$ regime with much higher voltages and currents. At I_{ref}≈ 0.32 (A) the smooth transition from *P1* to $P2_1$ regime occurs. However, no period-doubling route to chaos is observed for this branch of bifurcation diagram, as the $P2_1$ branch disappears just after the collision with $I_{border2}$ (see Fig. 6 point (K)). It is interesting to note that the collision of $P2_2$ regime with the same borderline does not change the topological structure of this branch (see Fig.6 point *(J)*). The BC at point *(L)* causes disappearance of $P2_2$ regime and transition to stable *P4* mode of operation that subsequently does not lead to the formation of chaotic region through period-doubling cascade, as it "cut off" at point *(N)*.

The subsequent chaotization of the system is governed by the appearance of *P6* orbit at point *(M)* that forms the chaotic attractor at I_{ref} ≈ 0.53 (A) and also disappears after the collision with $I_{border2}$ (see Fig.6 point *(0)*). The subsequent

chaotic region is robust, as the two borderlines do not allow the formation of stable periodic orbits or coexisting attractors.

4 Conclusions

This paper showed that the discrete-time model of the boost type SPC under current-mode control could be effectively improved, including the value of total delay in the control loop. The results of complete bifurcation analysis confirm that even small values of delay may drastically change the structure of bifurcation diagrams, causing the appearance of highly non-smooth events and uncommon routes to chaos. The most distinctive phenomena include the appearance of coexisting attractors even in the region of *P1* operation, as well as sudden disappearance and reappearance of stable and unstable periodic regimes after border collisions. The obtained results prove that it is not possible to provide reliable prediction of operating modes and their stability of SPC without taking into account time lag effects. It should be noted, that relatively small values of delays (up to 20% of switching period) were chosen, considering the analog control loops. However the typical values of delays in digital control circuitry could be much greater and the effects of these delays on the global dynamics of SPC will be addressed in the future research.

Acknowledgements

This research was funded by a grant (No. 467/2012) from the Latvian Council of Science.

References

1. E. R. Vilamitjana, E. Alarcon, A. El Aroudi. Chaos in switching converters for power management. New York: Springer, 2012.
2. C. K. Tse, M. Li. Design-oriented bifurcation analysis of power electronics systems, *Int. Journal of Bifurcations and Chaos*, vol. 21, no. 6, pp. 1523–1537, 2011.
3. S. Banerjee, S. Parui, A. Gupta. Dynamical effects of missed switching in current mode controlled dc-dc converter, *IEEE Trans. on circuits and systems*, vol. 51, no. 12, pp. 649–655, 2004.
4. D.C. Hammil, J.H.B. Deane, D.J. Jefferies. Modeling of chaotic dc/dc converters by iterative nonlinear mappings. *IEEE Transactions on Circuits and Systems Part I*, vol.35, no.8, 25-36, 1992.
5. S. Banerjee and G. C. Verghese (Ed.) . Nonlinear Phenomena in Power Electronics. Attractors, Bifurcations, Chaos, and Nonlinear Control, IEEE Press, 2001.
6. M. Zakrzhevsky, "Bifurcation theory of nonlinear dynamics and chaos. Periodic skeletons and rare attractors", Proc. 2 nd Int. Symposium (RA 2011), pp. 26–30, 2011.
7. M.V. Zakrzhevsky and D. A. Pikulin (Eds.). Rare Attractors in Discrete Nonlinear Dynamical Systems, Riga, Latvia, 2013.

8. D. Pikulins. Complete Bifurcation Analysis of DC-DC Converters Under Current Mode Control, *Journal of Physics: Conference Series „Physics and Mathematics of Nonlinear Phenomena 2013”*, Issue 1, Vol. 482, 2014.
9. D. Pikulins. Exploring Types of Instabilities in Switching Power Converters: the Complete Bifurcation Analysis, *Electronics and Electrical Engineering*, Kaunas, Lithiuania, Technologija, -No.5, pp. 76-79, 2014.
10. D. Pikulins. The Mechanisms of Chaotization in Switching Power Converters with Compensation Ramp. *CHAOS 2014 Proceedings 7th Chaotic Modeling and Simulation International Conference* , Portugal, Lisbon, 7-10 June, 2014. pp.367-375.

Fractional Chen Chaotic Network

Carla M.A. Pinto[1] and Ana R.M. Carvalho[2]

[1] School of Engineering, Polytechnic of Porto, and Centre for Mathematics of the University of Porto, Rua Dr António Bernardino de Almeida, 431, 4200-072 Porto, Portugal
(E-mail: cap@isep.ipp.pt, corresponding author)
[2] Faculty of Aciences, University of Porto, Rua do Campo Alegre s/n, 4169-002 Porto, Portugal
(E-mail: up200802541@fc.up.pt)

Abstract. We analyze a fractional order model of a network of one ring of three cells coupled to a 'buffer' cell. By cell we mean a nonlinear system of ordinary differential equations. The full network has $\mathbf{Z}_3$ symmetry group. We consider the Chen chaotic oscillator to model cells' internal dynamics. We observe interesting dynamical patterns, such as steady-states, rotating waves and chaos, for distinct values of the parameter c of the Chen oscillator and the derivative of fractional order α. The different patterns seem to appear through a sequence of Hopf and period-doubling bifurcations. Possible explanations for the peculiar patterns are the symmetry of the network and the dynamical characteristics of the Chen oscillator, used to model cells' internal dynamics.
Keywords: fractional Chen oscillators, $\mathbf{Z}_3$ symmetry, chaos.

1 Introduction

The theory of networks of coupled cells has taken a major breakthrough in the last few years, mainly due to the work of Golubitsky, Stewart, and co-authors [3,5,4]. These networks appear in many areas of science, from biology, economy, ecology, neuroscience, computation, and physics [11,1,14,6]. Particular attention has been given to patterns of synchrony [9], phase-locking modes, resonance, and quasiperiodicity [1,10].

Networks of coupled cells are schematically identif ed with directed graphs, where the nodes (cells) represent dynamical systems, and the arrows indicate the couplings between them.

In this paper, we study the dynamical features of the coupled cell systems associated to the network in Figure 1, for variation of the fractional order derivative $\alpha \in [0,1]$.

In Section 2, we summarize some concepts of the theory of coupled cell networks and bifurcation theory, for symmetric dynamical systems. In Section 3, we simulate the coupled cell system associated with the network in Figure 1. In Section 4, we state the main conclusions of the current work and sketch some future research.

8thCHAOS Conference Proceedings, 26-29 May 2015, Henri Poincaré Institute, Paris France

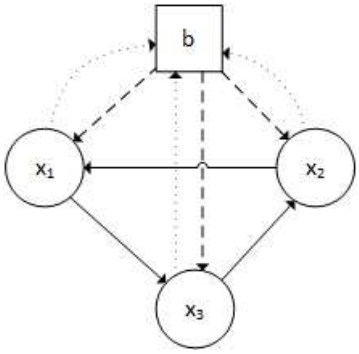

Fig. 1: Networks of one ring of cells coupled to a 'buffer' cell with $\mathbf{Z}_3$ exact (left) and interior (right) symmetry. Each node represents a cell or a dynamical system. The arrows indicate the couplings between them.

1.1 Summary of fractional calculus

The theory of fractional calculus (FC) had its start in 1695, when Leibniz exchanged letters with L'Hôpital about $D^{\frac{1}{2}} f(x)$. In FC the concept of the derivative operator $D^{\alpha} f(x)$ is generalized to fractional values of α, the order of the derivative. FC development is due to relevant contributions of mathematicians, such as Euler, Liouvulle, Riemann and Letnikov [8,12]. In the f elds of physics and engineering, FC is commonly associated with long term memory effects [2,7].

There are several def nitions of a fractional derivative of order α. The most adopted def nitions are the Riemann-Liouville, Grünwald-Letnikov (GL) and Caputo formulations. GL is def ned as:

$$ {}_{a}^{\mathrm{GL}}D_{t}^{\alpha} f(t) = \lim_{h\to 0} \frac{1}{h^{\alpha}} \sum_{k=0}^{\left[\frac{t-a}{h}\right]} (-1)^{k} \binom{\alpha}{k} f(t-kh), \, t > a, \, \alpha > 0 \tag{1} $$

where $\Gamma(\cdot)$ is Euler's gamma function, $[x]$ means the integer part of x, and h is the step time increment.

The fractional derivatives capture the history of the past dynamics, as opposed to the integer counterpart that is a 'local' operator.

The GL def nition inspired a discrete-time calculation algorithm, based on the approximation of the time increment h by means of the sampling period T, yielding the equation in the z domain:

$$ \frac{\mathscr{Z}\{D^{\alpha} f(t)\}}{\mathscr{Z}\{f(t)\}} = \frac{1}{T^{\alpha}} \sum_{k=0}^{\infty} \frac{(-1)^{k} \Gamma(\alpha+1)}{k!\,\Gamma(\alpha-k+1)} z^{-k} = \left(\frac{1-z^{-1}}{T}\right)^{\alpha} \tag{2} $$

where $\mathscr{Z}$ denotes the Z-transform operator.

In order to apply the previous equation (2), it is considered a r-term truncated series:

$$ \frac{\mathscr{Z}\{D^{\alpha} f(t)\}}{\mathscr{Z}\{f(t)\}} = \frac{1}{T^{\alpha}} \sum_{k=0}^{r} \frac{(-1)^{k} \Gamma(\alpha+1)}{k!\,\Gamma(\alpha-k+1)} z^{-k} \tag{3} $$

where, in order to have good approximations, is required a large r and a small value of T. This procedure is commonly known as Power Series Expansion (PSE).

Expression (3) represents the Euler, or first backward difference, approximation in the so-called $s \to z$ conversion scheme. Another possibility, consists in the Tustin conversion rule. The most often adopted generalization of the generalized derivative operator consists in $\alpha \in \mathbf{R}$.

2 Network

A network of cells is represented as a directed graph, where the nodes represent the cells and the arrows the couplings between them. Cells and arrows are classified according to certain types [5]. Cells of the same type have the same internal dynamics, and arrows with the same label identify equal couplings. Each cell is a dynamical system. The input set of a cell is the set of edges directed to that cell. Figure 1 depicts a coupled cell network, where the nodes are drawn as circles (cells in the rings) and squares ('buffer' cell). There are three different types of coupling (three distinct arrow types).

Coupled cell systems are dynamical systems consistent with the architecture or topology of the graph representing the network. Each cell c_j of the network has an internal phase space P_j. The total phase space of the network being the direct product of internal phases spaces of each cell, $P = \prod_{i=1}^{n} P_i$. Coordinates on P_j are denoted by x_j and coordinates on P are denoted by $(x_1, \ldots, x_n)$. The state of the system at time t is $(x_1(t), ..., x_n(t))$, where $x_j(t) \in P_j$ is the state of cell c_j at time t.

A vector field f on P is called *admissible*, for a given network, if it satisfies two conditions [4]: (i) the domain condition - each component f_j corresponding to a cell c_j is a function of the variables associated with the cells c_k that have edges directed to c_j; (ii) the pull-back condition - two components f_j and f_k corresponding to cells c_j and c_k with isomorphic input sets are identical up to a suitable permutation of the relevant variables.

In the current study, we consider an important class of networks, namely, the ones that possess a group of symmetries. A symmetry of a coupled cell system is the group of permutations of the cells (and arrows) that preserves the network structure (including cell-labels and arrow-labels) and its action on P is by permutation of cell coordinates. It is thus a transformation of the phase space that sends solutions to solutions. The network in Figure 1 is an example of a network with $\mathbf{Z}_3$ symmetry.

3 Numerical results

In this section we simulate the coupled cell system associated with the network depicted in Fig. 1. We consider the Chen oscillator to model the internal dynamics of each cell in the 3-ring and an unidimensional phase space for the 'buffer' cell. The total phase space is thus tenth dimensional. The dynamics of a singular ring cell is given by [13]:

$$\begin{aligned}\dot{u} &= a(v-u)\\ \dot{v} &= (c-a)u-uw+cv\\ \dot{w} &= uv-b_1 w\end{aligned} \tag{4}$$

where $a=35$, $b_1=3$ and c are real parameters. The unidimensional dynamics of the 'buffer' cell is given by [10]:

$$f(u)=\mu u-\frac{1}{10}u^2-u^3 \tag{5}$$

where $\mu=-1.0$ is a real parameter.

The fractional coupled cell system of equations associated with the network in Fig. 1 is given by:

$$\begin{aligned}\frac{d^\alpha x_j}{dt^\alpha} &= g(x_j)+c_1(x_j-x_{j+1})+db \qquad j=1,...,3\\ \frac{d^\alpha b}{dt^\alpha} &= f(b)\end{aligned} \tag{6}$$

where $g(u)$ represents the dynamics of each Chen oscillator, b is the 'buffer' cell, $c_1=-5$, $d=0.2$, and the indexing assumes $x_4\equiv x_1$. We consider that the coupling between all cells is linear and is done only in the f rst variable of each Chen oscillator.

We start with $c=15$ and increase c till $c=24.5$. Figure 2 depicts the patterns of the network for three values of the fractional derivative α and $c=15$. We observe an equilibria for all values of α.

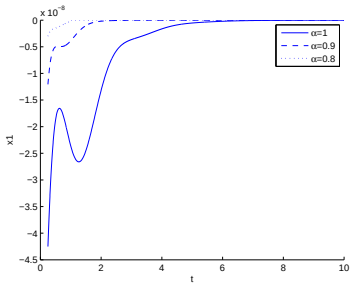

Fig. 2: Dynamics of the coupled cell system (6) for $c=15$ and three values of the fractional derivative $\alpha=\{0.8,0.9,1.0\}$.

In Figures 3- 5, are shown the dynamics of the fractional coupled system for $c=16$, and $\alpha\in\{0.8,0.9,1.0\}$. It is observed a Hopf bifurcation of the system as c is increased from $c=15$. The model depicts a rotating wave state, where the cells in the three ring are $1/3$ of the period out-of-phase (Fig. 4). This rotating wave state is explained by the symmetry of the network [1]. Moreover, one can distinguish another Hopf bifurcation as the fractional derivative α is decreased from $\alpha=0.9$ to $\alpha=0.8$. The periodic orbit at $\alpha=0.9$ has the same period as the one for $\alpha=1.0$ but smaller amplitude.

We increase c another time to $c=23$. Figures 6- 7 show the dynamical features of the system for $\alpha\in\{0.8,0.9,1.0\}$. The motion is quasiperiodic for $\alpha=1.0$. For $\alpha=0.9$,

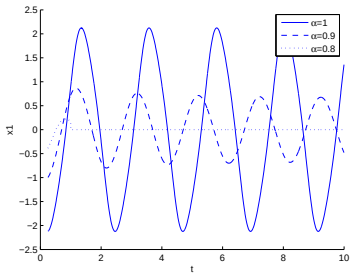

Fig. 3: Dynamics of the coupled cell system (6) for $c = 16$ and three values of the fractional derivative $\alpha = \{0.8, 0.9, 1.0\}$.

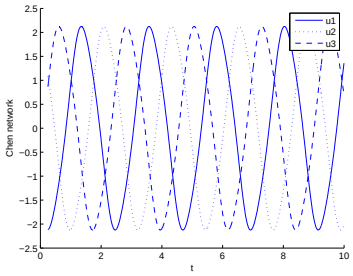

Fig. 4: Rotating wave of the coupled cell system (6) for $c = 16$ and $\alpha = 1.0$. A similar wave is observed for $\alpha = 0.9$ with smaller amplitude.

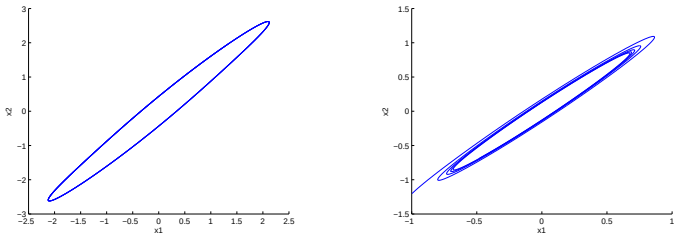

Fig. 5: Phase plot of a Chen oscillator of the coupled cell system (6) for $c = 16$ and $\alpha = 1.0$ (left) and $\alpha = 0.9$ (right).

the dynamics of system (6) is still quasiperiodic but is 'simpler' than for $\alpha = 1.0$. Moreover for $\alpha = 0.8$ we obtain an equilibrium of the coupled system 1.

In Figure 8- 9, we depict the motions of the fractional coupled cell system (6) for $c = 24.5$ and $\alpha = \{0.8, 0.9, 1.0\}$. For $\alpha = 0.8$ the system is at equilibrium. In addition, we remark that the dynamics of system (6) are less 'chaotic' as α is decreased from 1

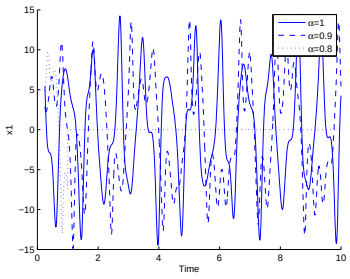

Fig. 6: Dynamics of the coupled cell system (6) for $c = 23$ and three values of the fractional derivative $\alpha = \{0.8, 0.9, 1.0\}$.

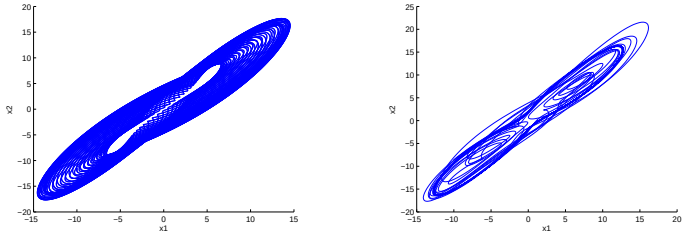

Fig. 7: Phase plot of a Chen oscillator of the coupled cell system (6) for $c = 23$ and $\alpha = 1.0$ (left) and $\alpha = 0.9$ (right).

(Fig. 9). For $\alpha = 1.0$ the system is chaotic, and at $\alpha = 0.9$ it seems to be at a periodic orbit of long period.

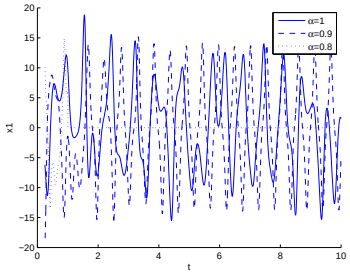

Fig. 8: Dynamics of the coupled cell system (6) for $c = 24.5$ and three values of the fractional derivative $\alpha = \{0.8, 0.9, 1.0\}$.

From the observation of the f gures in this section, one can conclude that there is a variety of curious phenomena exhibited by system (6), that is attributed to the variation

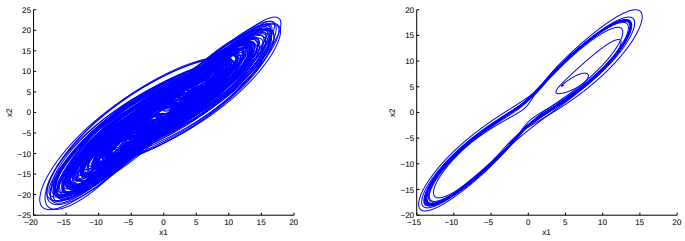

Fig. 9: Phase plot of a Chen oscillator of the coupled cell system (6) for $c = 24.5$ and $\alpha = 1.0$ (left) and $\alpha = 0.9$ (right).

of parameter c of the Chen oscillator, and is also due to the order of the fractional derivative α. This will be further studied in future work.

4 Conclusions

We analyze curious patterns arising in a fractional order network of one ring of three cells coupled to a 'buffer cell. We observe a broad range of dynamical features for increasing c and as α is decreased from 1. The exotic behaviors are explained by the symmetry of the network, the characteristics of the Chen oscillator, used to model cells' internal dynamics, and the fractional order derivative. Future work will focus on analyzing theoretically the role of the derivative of fractional order α as a bifurcation parameter of the network.

Acknowledgments

The author was partially funded by the European Regional Development Fund through the program COMPETE and by the Portuguese Government through the FCT - Fundação para a Ciência e a Tecnologia under the project PEst-C/MAT/UI0144/2013. The research of Ana Carvalho was supported by a FCT grant with reference SFRH/BD/96816/2013.

References

1. F. Antoneli, A.P.S. Dias and C.M.A. Pinto. Quasi-periodic states in coupled rings of cells. *Communications in Nonlinear Science and Numerical Simulations*, **15**, 1048–1062, 2010.
2. D. Baleanu, K. Diethelm, E. Scalas, J.J. Trujillo. *Fractional Calculus: Models and Numerical Methods*, Series on Complexity, Nonlinearity and Chaos, World Scientif c Publishing Company, Singapore, 2012.
3. M. Golubitsky, M. Nicol and I. Stewart. Some curious phenomena in coupled cell systems. *Journal of Nonlinear Science*, **14**, 207–236, 2004.
4. M. Golubitsky, I. Stewart. Nonlinear dynamics of networks: the groupoid formalism. *Bull Am Math Soc*, **43**, 305–364, 2006.
5. M. Golubitsky, I. Stewart, A. Török. Patterns of synchrony in coupled cell networks with multiple arrows. *SIAM J Appl Dyn Syst* **4**(1), 78–100, 2005.

6. X. Gong , D. Liu and B. Wang. Chaotic system synchronization with tridiagonal structure and its initial investigation in complex power systems. *Journal of Vibration and Control*, **3**(20), 447–457, 2014.
7. C.M. Ionescu. *The human respiratory system: an analysis of the interplay between anatomy, structure, breathing and fractal dynamics*, Series in BioEngineering, Springer-Verlag, London, 2013.
8. K.B. Oldham, J. Spanier, *The fractional calculus: theory and application of differentiation and integration to arbitrary order*, Academic Press, 1974.
9. A. Pikovsky, M. Rosenblum and J. Kurths. *Synchronization, A Universal Concept in Nonlinear Sciences*, Cambridge: Cambridge University Press, 2001.
10. C.M.A. Pinto and A.R.M. Carvalho. Strange patterns in one ring of Chen oscillators coupled to a 'buffer' cell. *Journal of Vibration and Control*, **text**, 1–29, published online 2014.
11. C.M.A. Pinto and M. Golubitsky. Central pattern generators for bipedal locomotion. *Journal of Mathematical Biology*, **53**, 474–489, 2006.
12. S.G. Samko, A.A. Kilbas, O.I. Marichev, *Fractional integrals and derivatives: theory and applications.* Gordon and Breach Science Publishers, 1993.
13. T. Ueta and G. Chen. Bifurcation analysis of Chen's attractor. *International Journal of Bifurcation and Chaos*, **10**, 1917–1931, 2000.
14. J. Zhu, J. Lu and X. Yu. Flocking of multi-agent nonholonomic systems with proximity graphs. *IEEE Transactions on Circuits and Systems*, **60**(1), 199–210, 2013.